D. van Dusschoten

Probing water motion in heterogeneous systems

A multi-parameter NMR approach

925700

Promotor: Dr. T.J. Schaafsma
hoogleraar in de moleculaire fysica

Co-promotor: Dr. H. Van As
universitair hoofddocent
vakgroep moleculaire fysica

NN08201, 2082

D. van Dusschoten

Probing water motion in heterogeneous systems

A multi-parameter NMR approach

Proefschrift
ter verkrijging van de graad van doctor
in de landbouw- en milieuwetenschappen
op gezag van de rector magnificus
dr. C.M. Karssen,
in het openbaar te verdedigen
op maandag 20 mei 1996
des namiddags te vier uur in de Aula
van de Landbouwuniversiteit te Wageningen.

ISN: 925700

BIBLIOTHEEK
LANDBOUWUNIVERSITEIT
WAGENINGEN

ISBN 90-5485-528-2

NN08201, 2082

Stellingen

1. De veel gebruikte uitspraak dat NMR de absorptie van electromagnetische straling door materie betreft is onzorgvuldig geformuleerd.
(bv. R.K. Harris, 'Nuclear Magnetic Resonance Spectroscopy', 1986)

2. Indien bij NMR imaging een ruimtelijke resolutie beneden 50 μm wordt ingesteld zijn de signaal afname curves niet door T_2 bepaald, zoals beweerd door Millard et al., maar door diffusie.
(M.M. Millard, O.B. Veisz, D.T. Krizek and M. Line, Plant, Cell and Environment 19, 1996).

3. Bij veel metingen moet niet de signaal:ruis verhouding voorop staan maar de informatie:ruis verhouding.

4. De combinatie van NMR relaxatiemetingen en NMR diffusiemetingen geeft een significante verbetering van de betrouwbaarheid van diffusieconstanten in heterogene systemen.
(Dit proefschrift, hoofdstukken 3 en 4.)

5. De temperatuur waarbij een glasovergang wordt waargenomen is afhankelijk van de tijdschaal van de moleculaire bewegingen waarvoor de gebruikte techniek gevoelig is.

6. De voorwaarden voor de toename van complexiteit in de moleculaire biogenese zijn onderling tegenstrijdig.

7. De grootte van de genetische pool die beschikbaar is voor selectie op basis van de *survival of the fittest* komt niet tot stand door selectiedruk.

8. De mens in het algemeen heeft het eerste, universele gebod van God, zijnde:" Weest vruchtbaar en wordt talrijk; vervult de aarde en onderwerpt haar, heerst over de vissen der zee en over het gevogelte des hemels en over al het gedierte, dat op de aarde kruipt." (Genesis 1:28), in de loop van de geschiedenis incorrect geïnterpreteerd.

9. De meeste argumenten betreffende de gevaren van verslavingen gaan in rook op, worden achterovergeslagen, weggespoten, gedelete of gezapped.

Dagmar van Dusschoten
Probing water motion in heterogeneous systems.
Wageningen, 20 mei 1996.

Contents

		page
	Voorwoord en dankwoord	i
Chapter 1.	Introduction	1
	1.1 General introduction	
	1.2 Some principal aspects of the NMR signal	
	1.3 NMR and translational motion	
	1.4 NMR in heterogeneous systems	
	1.5 Contents of this Thesis	
Chapter 2.	Experimental setup for probing motion	15
	2.1 Introduction	
	2.2 SNR requirements for probing motion	
	2.3 Flexible PFG NMR desensitized for susceptibility artifacts, using the PFG multiple-spin-echo sequence (D. van Dusschoten, P.A. de Jager and H. Van As, *J. Magn. Reson. A*, **112**, 237-240, 1995)	
Chapter 3.	Diffusion Analysis by Relaxation Time Separated PFG NMR.	33
	3.1 Extracting diffusion constants from echo-time-dependent PFG NMR data using relaxation-time information (D. van Dusschoten, P.A. de Jager and H. Van As, *J. Magn. Reson. A*, **116**, 22-28, 1995)	
	3.2 Unravelling diffusion constants in biological tissue by combining Carr Purcell Meiboom Gill imaging and Pulsed Field Gradient NMR. (D. van Dusschoten, C.T.W. Moonen, P.A. de Jager and H. Van As, Subm. to *Magn. Reson. Med.*)	
Chapter 4.	Water mobility in heterogeneous systems investigated by PFG NMR. A nuts and bolts approach	69
	4.1 Introduction	
	4.2 Diffusion and T_2 in heterogeneous samples	
	4.3 Materials and methods	
	4.4 Results and discussion	
	4.5 Conclusions	

Chapter 5. Flow measurements in phantoms and fish
5.1 Visualising the water flow in a breathing carp using NMRi, 107
(C. van den Berg, D. van Dusschoten, H. Van As, A. Terlouw, T.J. Schaafsma and J.W.M. Osse, *Netherlands Journal of Zoology*, **45**, 338-346, 1995)
5.2 Line scan flow measurements

Summary 135

Samenvatting 138

Curriculum Vitae 141

Voorwoord en dankwoord

Eén van de unieke eigenschappen van de mens is het vermogen om onbegrepen verschijnselen te onderzoeken en, met geluk en doorzettingsvermogen, te doorgronden. De mate van succes van dit proces is afhankelijk van de beschikbare (algemene) voorkennis. Verder is de vrijheid en mogelijkheid die de omgeving biedt voor onderzoek van essentieël belang. Door de steeds veranderende omgevingsfactoren, zoals de cultuur en de toenemende voorkennis, kunnen daardoor steeds weer nieuwe waarnemingen gedaan, onderzocht en soms verklaart worden. Gezien de drang van veel mensen om nieuwe ontdekkingen wereldkundig te maken is er door de eeuwen heen de mogelijkheid gerezen om dieper te graven in het functioneren van onze omgeving aangezien dit proces van ontdekking, verklaring en notificatie een steeds voortschrijdende frontlinie van kennis met zich mee heeft gebracht. Dit proefschrift is één van de gevolgen van het voortschrijden der wetenschap en draagt, naar ik hoop, zelf ook weer bij tot het proces zelf.

Om wetenschappelijk onderzoek te kunnen verrichten is het noodzakelijk om zowel de reeds bestaande kennis te vergaren en te structureren als ook de gereedschappen te ontwikkelen welke het vergaren van (nieuwe) kennis vereenvoudigd. Niet alleen hiervoor is onderwijs nodig maar ook voor het ontwikkelen van communicatievaardigheden. Onderlinge communicatie is noodzakelijk aangezien geen mens in staat is als het gebodene alleen te ontdekken en te begrijpen, zeker tegenwoordig. Dit proefschrift is dientengevolge niet het werk van een éénling, maar van verscheidene mensen die in onderlinge interactie elkaar helpend een klein deel van de wetenschappelijke integraal hebben opgelost en nieuwe randvoorwaarden voor verder onderzoek hebben ontdekt en geschapen. Het succes van het begrijpen van onze omgeving is aldus afhankelijk van de communicatievaardigheden van de betrokkenen gecombineerd met hun intellectuele vermogen. Alleen doordat zovele mensen met ieder een uniek karakter en specifieke vaardigheden mij geholpen, gestuurd, tegengewerkt, gekwetst en opgevrolijkt hebben ligt dit proefschrift hier. Ik wil hier die mensen bedanken waarvan ik denk dat deze een bewust positieve bijdrage hebben geleverd aan mijn vorderingen.

Allereerst wil ik mijn ouders bedanken, die mij altijd gestimuleerd hebben om door te leren en te werken en die met hun geduld, inzet en liefde meer aan mijn educatie in de breedste zin hebben bijgedragen dan wie dan ook. Bovendien was mijn vader zo vriendelijk om zijn tekenvaardigheid te demonstreren op de

omslag van mijn proefschrift. Henk Van As, met wie ik zoveel heb gepraat dat vaak onduidelijk was wie er met een idee kwam, omdat onze gedachten vaak langs dezelfde lijnen gingen. Zijn werkelijke bijdrage aan dit proefschrift is dus moeilijk te traceren, maar samenwerken met hem was en is voor mij een genoegen. Adrie de Jager, die zoveel informatie kan aanreiken dat het een kunst is om daaruit het noodzakelijke te halen, was net zo belangrijk voor dit proefschrift. Een belangrijke bron van hulp kwam verder van enkele studenten die een afstudeervak onder mijn begeleiding hebben doorstaan, namelijk, Jozien Goense, die me leerde op geoorloofde wijze met data om te gaan, John van Noort, die me dwong op mijn tenen te lopen, en Jacco de Zwart, die besloot om John daarbij te helpen. Elk van hen heeft een stuk werk afgeleverd dat in dit proefschrift is verwerkt. Een vergelijkbare bijdrage is geleverd door Hommo Edzes die op een belangrijk moment mij bij mijn onderzoek kon helpen. Coen van den Berg heeft geholpen mijn visie op vissen weer bij te stellen. Verder wil ik iedereen op de vakgroep Moleculaire Fysica bedanken, met name die mensen die (on)bewust hebben bijgedragen aan mijn algemene opvoeding. Aan het hoofd van hen staat Tjeerd Schaafsma, die mij de vrijheid gegeven heeft om te onderzoeken wat ik leuk vond en daarna mijn werkstukken zorgvuldig heeft nagepluist op allerlei ongerechtigheden en de kwaliteit van deze werkstukken aanmerkelijk heeft verbeterd. Iedereen, van harte bedankt. Als laatste ben ik Philips Medical Systems dankbaar voor het scheppen van de noodzakelijke financiële randvoorwaarden en de ruimte om deze aan te spreken.

Als laatste noot; de mogelijkheid om scheppend en creatief bezig te zijn is geschapen door een uitermate originele, creatieve en scheppende daad hieraan voorafgaand.

Dagmar van Dusschoten,
Wageningen, 13 maart 1995.

Chapter 1

Introduction

1.1 General introduction

Water is a complex liquid. In it several types of movement of the individual water molecules and the ensembles it forms can be distinguished. Scrutinizing the movements of the individual molecules is far beyond the human eye and just about beyond all measuring tools, but ensembles of water molecules are accessible to experiment. For an ensemble of water molecules we can distinguish between several types of motion some of which involve a net displacement of water when it moves from one region to another. Motion of molecules is considered coherent when the path and speed of the movement can be predicted. This path may either be a straight line or a tortuous path. The definition of incoherent or chaotic motion is used when it cannot be predicted along which path an ensemble of water molecules moves from region A to B. That is, the ensemble can choose between different , unpredictable, paths and, on inversion of the motion, the return to the starting point is uncertain. In a closed system which does not receive energy no net displacement of water is observed. Then, motion is purely chaotic, as is characteristic for diffusion. In how far we observe net displacement of water depends on the spatial and the time resolution as determined by the instrument characteristics. For example, a bottle with clear water can be placed on a heater. When visible light is used to study water motion none will be discerned even when using a microscope. By using a dye however, convective flow patterns may be discerned; on a scale smaller than the bottle itself net displacement of water is found, but on the scale of the bottle or larger no net water movement is observed. After several minutes the dye is spread out homogeneously over the bottle and water motion can no longer be followed.

Most living species minimise the net water transport. To maintain a robust water balance special organs regulate the uptake and removal of water. It is not only interesting to study these specialised organs like the intestines, kidneys, lungs and skin, but also how cells in general react on variable external conditions and how they maintain an equilibrium in which uptake of nutrients and discard of waste products is achieved. The medical sciences seem primarily interested in physiological abberations and their effects on the human body. E.g. blood flow measurements are often used for the indentification of occlusions (1). Flow

measurements in plants on the other hand, are used to indentify root uptake efficiency and the water evaparation speed of leaves (2,3). Flow measurements in the buccal cavity of a fish can be used to study the effectiveness of filter feeding (4). The measurement of flow is only a first step to study water balance. The study of diffusional processes, which drive exchange between compartments and other cells (5), is just as important. It is in this region that Nuclear Magnetic Resonance (NMR) has proven its fruitful potential.

Because the NMR technique uses very little energy, has a high penetration depth in living tissue and can be made very sensitive to translational motion, it is suitable for *in vivo* measurement of both flow and diffusion or diffusion-like processes. Soon after the first observation of NMR (6,7) it was discovered that flow could be measured using NMR (8) as could diffusion (9). Since then several authors have contributed to developing quantitative flow and diffusion measurements, both in an experimental and theoretical context (10-12). An important contribution was made by Steskjal and Tanner who developed the Pulsed Field Gradient Spin Echo technique and the theoretical framework to quantify diffusion both in homogeneous and inhomogeneous samples (13-16).

Whether a sample is considered homogeneous or heterogeneous depends strongly on the technique which is used to explore a sample. For NMR two boundary conditions can be defined which determine whether a sample can be considered homogeneous or not.

(*i*) During the time window of a NMR experiment an ensemble of molecules does not encounter differences in its environment. (*ii*) Within the region of interest no differences in composition exists which influence the NMR signal. Of course, both conditions are very much related. Using the above definitions a tube filled with pure water is homogeneous, a sample of apple parenchyma tissue is heterogeneous even when the cells within the sample are alike.

In recent years the theoretical background for a robust interpretation of experimental results has been enriched by the propagator or q-space formalism introduced by Kärger (17), Cory (18) and Callaghan (19), with several other authors contributing to this development (20-22). The spatial localization of diffusion by means of combining Magnetic Resonance Imaging and PFG NMR was demonstrated by Taylor et al. (23), Merboldt et al. (24) and Le Bihan (25). The last author was first to demonstrate *in vivo* applications of these measurements. The combination of flow and imaging was made several years before that of diffusion and imaging. The visualisation of the vascular system by means of MR angiography was developed by Moran (26) and Dumoulin (27). Here, the same pulsed field gradients as are used to measure diffusion by NMR, were used to

quantify flow. Introduction of an incremental increase of the flow sensitizing gradients was shown by Feinberg (28) which increases the flow resolution. The results of these measurements can be nicely displayed by Fourier transforming the NMR signals in the "flow domain", a procedure identical to the earlier mentioned q-space imaging which was developed later. Introduction of very fast MRI sequences like Echo Planar Imaging (EPI), by Mansfield (29) in principle allows real time flow measurements with a temporal resolution in the order of 100 ms, but this was only demonstrated many years after the introduction of this method because of stringent hardware demands for EPI (30,31).

Although the development of the theoretical framework for NMR diffusion measurements has continued over the years, the extension of PFG NMR sequences has been slightly slower. In this Thesis two new procedures are presented which enhance the resolving power and the accuracy of NMR diffusion experiments.

Technical advances concerning NMR flow measurements have been much more extensive than for diffusion measurements even though e.g. the PFG Spin Echo sequence is quite suitable to measure both flow and diffusion. A reason for this difference is the earlier recognition of the medical importance of NMR flow imaging which dates back to as early as 1960 (11). Despite these developments a sequence with a sufficiently high temporal (~30-40 Hz) resolution to quantitatively measure flow velocities in e.g. the aorta without the need to trigger the measurements has not been demonstrated on an average medical imager. In this Thesis a sequence is demonstrated which in principle can do this while retaining the capability to measure flow in regions which are difficult to access by NMR, e.g. the lungs.

1.2 Some principal aspects of the NMR signal

All nuclei having odd mass number possess the property of spin, the spin angelur momentum vector (I). A nucleus like the hydrogen atom (I=1/2) has two possible spin states, i.e. +1/2 and - 1/2. When a tube with water is placed in a magnetic field with strength B_0 (T) the ensemble of protons undergoes a polarization. In the magnetic field an small energy difference between the two spin states is created. This results in a population difference at thermal equilibrium, determining the magnitude of magnetization M_0:

$$M_0=N_s\gamma^2(h/2\pi)^2I(I+1)B_0/3kT_s \quad [1.1]$$

with

γ = gyromagnetic ratio; for protons: 2π. 4.2576 10^7 rad/sT
h = Planck's constant
k= Boltzmann's constant
T_s= sample temperature
N_s= number of magnetic moments per unit volume
B_0= magnetic field strength (T)
I= spin

The magnetization M_0 results in a small change of the magnetic field. In order to accurately measure the magnetization, transitions between the two spin states are induced by means of an oscillating magnetic field perpendicular to the static field B_0. The frequency of this oscillation should obey the resonance condition

$$\omega_0=\gamma B_0 \quad [1.2]$$

where ω_0 equals the so-called Larmor frequency (the precession frequency) of the spin system. Optimum detection of the longitudinal magnetization M_0 is obtained when the magnetization is rotated 90° relative to the z axis (the direction of the magnetic field) into the transverse plane (xy). This can be achieved by a short circularly polarised radio frequency (rf) pulse with strength B_1, generated within a rf coil surrounding the sample. This rf coil generally also serves as the detector for the transverse magnetization which induces a voltage in the coil proportional to the magnitude of the transverse magnetization as it develops and decays in time.

Molecules exhibit three different types of motion, internal vibration, translational diffusion and rotational diffusion, of which only the last is of importance to the decay of the NMR signal by dipolar interaction. The random Brownian motion of the water molecules, a combination of rotational and translational diffusion, causes very small local fluctuations of the magnetic field at the spins of nearby protons, by way of dipolar interaction, which restores the thermal equilibrium after the 90° pulse by spin-lattice relaxation, characterized by the relaxation time T_1. Also, these random motions cause a blurring of the two spin states resulting in loss of transverse phase coherence (not to be confused with motional coherence) after the 90° pulse, a process called spin-spin relaxation, with the characterstic relaxation time T_2. T_1 can be approximated by (32)

$$\frac{1}{T_1} = \gamma^2 \left(\overline{b_x^2} + \overline{b_y^2} \right) \left\{ \frac{\tau_c}{1 + \omega_0^2 \tau_c^2} + \frac{4\tau_c}{1 + 4\omega_0^2 \tau_c^2} \right\} \qquad [1.3]$$

and T_2 by

$$\frac{1}{T_2} = \frac{\gamma^2}{2} \left\{ \overline{3b_z^2} \tau_c + \left(\overline{b_x^2} + \overline{b_y^2} \right) \left(\frac{5\tau_c}{1 + \omega_0^2 \tau_c^2} + \frac{2\tau_c}{1 + 4\omega_0^2 \tau_c^2} \right) \right\} \qquad [1.4]$$

where τ_c is the correlation time of the tumbling molecules and signifies the decay time for a typical fluctuation (for rotational diffusion; the average time to rotate through one radian). The value of τ_c is dependent on complicated details of the molecular motion, but is roughly dependent on the viscosity of the fluid and the radius of the molecules; $\mathbf{b}_{x,y,z}$ are the components of the local fluctuating magnetic fields at the position of the magnetic moments .

As mentioned earlier molecules undergo a magnetic polarization when placed in a magnetic field and so become magnetic dipoles. The induced magnetic dipoles influence the local magnetic field strength and Eq.[1.2] should therefore be corrected for frequency offsets (β) relative to the Larmor frequency in vacuum:

$$\omega = \gamma B_0 (1 + \beta(r,t)) \qquad [1.5]$$

where $\beta(r,t)$ is a general term which encompasses several phenomena which influence the local magnetic field. By using phase sensitive detection at the Larmor frequency a signal with the Larmor frequency will appear as a DC signal. When $\beta(r,t)$ is non-zero off-resonance signals appear. The variation of the local magnetic field, expressed by $\beta(r,t)$, is mostly within a few tens ppm. It may comprise :(*i*) The shielding effect of the electrons of an atom or molecule, which is the source of chemical shift (σ). (*ii*) The effect of bulk diamagnetic susceptibility (χ_m): the electron orbits of diamagnetic atoms and molecules, which have no net atomic angular momentum, are polarised by the magnetic field which results in a small induced local magnetic dipole which perturbes the local magnetic field. (*iii*) The effect of an external (pulsed) (linear) magnetic field gradient (G(t).r) over the sample so spins on every location in the direction of this gradient have a different resonance frequency. All these effects influence the development and decay of the NMR signal but do not influence the intrinsic T_2. So, when a NMR experiment is performed the time-dependent signal is given by

$$S(t)=k\sum_n M_{0,n}\exp(-t/T_{2,n})\exp(-i\Delta\omega_n(\sigma,\chi_m,G.r).t) \qquad [1.6]$$

where $\Delta\omega$ denotes the frequency offset relative to ω_0, which can be caused by one or more of the above factors, n denotes the number of distinguishable ensembles and k represents the spectrometer constant. Fourier transformation of the signal shows a spectrum of frequencies which are present within the sample, each line of the spectrum broadened by $T_{2,n}$.

The versatility of NMR lies in the fact that a wide variety of NMR pulse sequences can and have been build which modulate the spin system in such a way that parameters like T_1 or T_2 can be extracted with little or no influence of other parameters. In Fig. 1.1 an example is given of a combination of an inversion recovery and a spin echo (IR-SE) sequence. The 180° pulse prior to the 90° pulse inverts the M_z magnetization which process is reversed by T_1 recovery during the τ_{IR} period. The 90° pulse creates the detectable transverse magnetization which loses phase coherence because of spin-spin relaxation and because of variations of the resonance frequency over the sample ($\beta(r,t)$). This phase coherence loss can be partially restored using a second 180° pulse which inverts the phase of the spins and causes those spins with a stable resonance frequency during 2τ to refocuss at 2τ, resulting in a NMR signal the so-called spin echo.

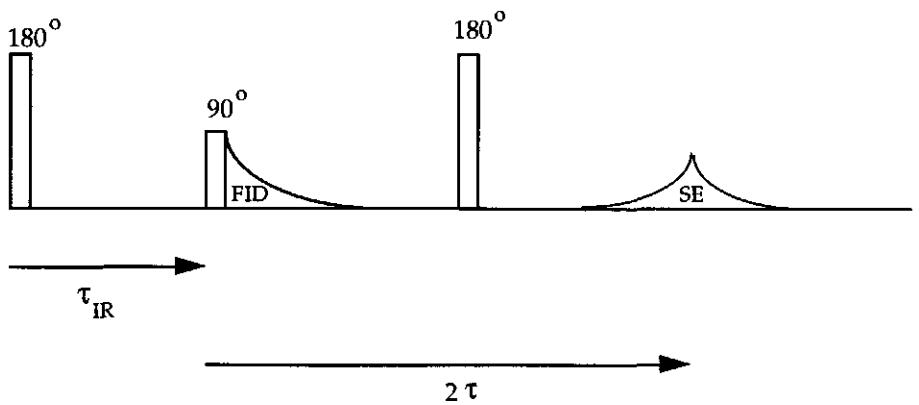

Figure 1.1 The Inversion Recovery Spin Echo sequence. T_1 relaxation occurs during τ_{IR}, whereas T_2 relaxation is only significant during 2τ. The spin echo occurs at 2τ (twice the 90°-180° pulse spacing), after the phase inversion of the 180° pulse. The curved lines represent the NMR signal; the length of the Free Induction Decay and the width of the spin echo is governed by T_2^*.

1.3 NMR and translational motion

When a tube with water is placed in a perfectly homogeneous magnetic field the decay of the magnetization starting from the 90 ° pulse is governed by T_2. When a magnetic field gradient (G [mT/m]) is superimposed on the homogeneous magnetic field by external gradient coils the phase coherence loss is accelerated due to the fact that spins at different locations along the gradient have different resonance frequencies. At the boundary between two regions with different bulk diamagnetic susceptibility *in situ* magnetic field gradients are present since the flux of the magnetic field through any closed surface vanishes (33). These gradients also cause an increase in the phase coherence loss. If water molecules were non-mobile this dephasing process could be corrected for by using a 180° pulse following the first 90 ° pulse while the gradient is kept constant. However, water molecules move around as a result of self-diffusion. A convenient way to understand molecular self-diffusion is to picture it as a succession of discrete uncorrelated hops (10). The time between these hops, τ_s, and the root mean square displacement per hop ξ determines the self-diffusion constant:

$$D=\xi^2/2\tau_s \qquad [1.7]$$

The r.m.s. displacement during a time interval t along one axis is defined by

$$\bar{x}^2=2Dt \qquad [1.8]$$

When a sample is placed within a linear magnetic field gradient, or when *in situ* field gradients (G_0) are present within the sample, and the transverse magnetisation is monitored using e.g. a spin echo sequence, the random hops of the molecules along the gradient cause a temporary fluctuation of the Larmor frequency. Each molecule therefore accumulates a phase shift during the period 2τ. This results in a decrease of the net magnetization in the xy-plane giving signal loss. The signal loss can be expressed for a linear gradient as (10)

$$S(G)=kM_0\exp(-2\tau m/T_2)\exp(-\gamma^2G^2Dm(2\tau)^3/3) \qquad [1.9]$$

In this equation m denotes the number of 180° pulses; for a SE experiment m=1 (Fig. 1.1). It can be seen from Eq.[1.9] that the signal attenuation due to diffusion along a magnetic field gradient increaseswith 2τ. In order to reduce diffusional losses m should be made very large and τ should be reduced. This technique was

first developed by Carr and Purcell (34) and later modified by Meiboom and Gill into the CPMG sequence (35) for correction of rf pulse errors. Diffusion through *in situ* field gradients results in fluctuations of the Larmor frequency, defined by $<\Delta\omega_0^2>$. The magnitude of $<\Delta\omega_0^2>$ is determined by a correlation time τ_d corresponding to the time it takes for a water molecule to diffuse over the distance associated with the local field variation. If $<\Delta\omega_0^2>\tau_d^2 >> 1$, i.e. if the distance scale of the susceptibility-induced frequency spread has dropped below 2 μm, this signal loss is partly reversible and follows Eq.[1.9]. If $<\Delta\omega_0^2>\tau_d^2 << 1$ this shows up as a reduction of the intrinsic T_2 (34). Effectively this means that the phase coherence of an ensemble cannot be restored when water molecules experience a large change of the local magnetic field (expressed by $\Delta\omega_0$) during a very short time (<< 1 ms). Since $\Delta\omega_0$ is linearly dependent on B_0 the phase coherence loss increases with B_0 in inhomogeneous samples, i.e. samples with regions which differ with regard to their chemical composition and (bulk) magnetic susceptibility (e.g. glass beads in water or plant cells). A similar effect on the echo amplitude occurs with chemical exchange, that is exchange of protons between different molecules (36).

Diffusion may be measured using a SE sequence in the presence of a constant linear gradient, but because of the rapid dephasing of the magnetization the width of the echo is small. The exact determination of the echo amplitude is therefore more difficult, especially in the presence of a strong magnetic field gradients. In order to circumvent this difficulty the field gradient may be pulsed, which still gives a signal attenuation related to diffusion, but does not reduce the width of the echo. Now Eq. [1.9] transforms into (13)

$$S(G)/S(0)=\exp(-\gamma^2G^2\delta^2(\Delta-\delta/3)D) \qquad [1.10]$$

Here δ equals the duration of the pulsed field gradients and Δ equals the separation between the rising flanks of the pulses, i.e. the "observation time" of the experiment. This period may be varied independently of 2τ with the restriction $\Delta < 2\tau$.

One of the interesting aspects of NMR is its capability to distinguish coherent from incoherent motion or even the transition between these two regimes if the transition falls within the time window of the NMR experiment (10^{-4} to 10 s). Because the correlation time of self-diffusion of water in various environments is very short (in the order of $10^{-8}$to 10^{-11} s), this type of translational motion may be considered chaotic or incoherent. Laminar flow through a long tube, on the other hand, may have a τ_c in the order of tens of seconds. Since for NMR experiments

the time window is less than 10 s (< 5 times T_2 or T_1), laminar flow through a tube can be considered coherent motion. In case of coherent flow during Δ a net phase shift develops which is linearly proportional to the flow velocity (26,37) whereas self-diffusion only gives a signal attenuation (Eq.[1.10]). An interesting situation arises when the correlation time of the motion falls within the time window of a NMR experiment itself, e.g. flow through a glass bead bed (38), intra voxel incoherent motion (25), or perfusion.

Whether translational motion can be considered as coherent or incoherent does not only depend on the time scale of the observation but also on the spatial resolution. For example, if we could zoom in on a single microcappillary with a diameter of 10 μm and a length of 100 μm before splitting up, coherent net flow is observed if the displacement of the water in the cappillary during the observation time is less than 100 μm. On a medical imager a resolution of 1x1x5 mm^3 is possible, which means that we will observe a number of cappillaries each of which follows an unpredictable path. When we now observe the water movement by NMR we observe incoherent motion if the average displacement of the water molecules is significantly larger than 100 μm during the observation time. For an average velocity of 1 cm/s during an observation time of 50 ms the travelled distance is 50 mm. In this case motion would appear totally chaotic.

1.4 NMR in heterogeneous systems

Sofar we have primarily discussed the NMR signal arising from a homogeneous sample. Although it is interesting to measure the flow velocity and profile in a pipe, or the diffusion constant of a wide variety of molecules using NMR, other techniques may serve as well to achieve the same goal. Judged on what is found in scientific literature and the work which has been performed at this laboratory it seems safe to conclude that the main thrust of NMR lies in biological samples, e.g. human beings, animals, plants etc.. It is here that the strength of NMR becomes evident, but also its complexity.

As an instructive example to explain some of the difficulties that arise when studying a heterogeneous sample by NMR, as all biological samples are, we take a plant cell,a schematic representation of which is given in Fig. 1.2. Three compartments may be recognised. (*i*) The vacuole which functions as a resevoir for sugar monomers and -polymers, (paramagnetic) ions and water. (*ii*) The cytoplasm, which contains many small sub-cellular compartments like the nuclues, ribosomes, endoplasmatic reticulum and sometimes chloroplasts or starch granules and water. As the vacuole the cytoplasm also contains (paramagnetic)

ions, polymeric sugars and proteins. (*iii*) The cell wall and extra-cellular space. The cell wall itself is a flexible structure made up of long chains of polysaccharides. Within the cell wall and around it water may be found, but also air.

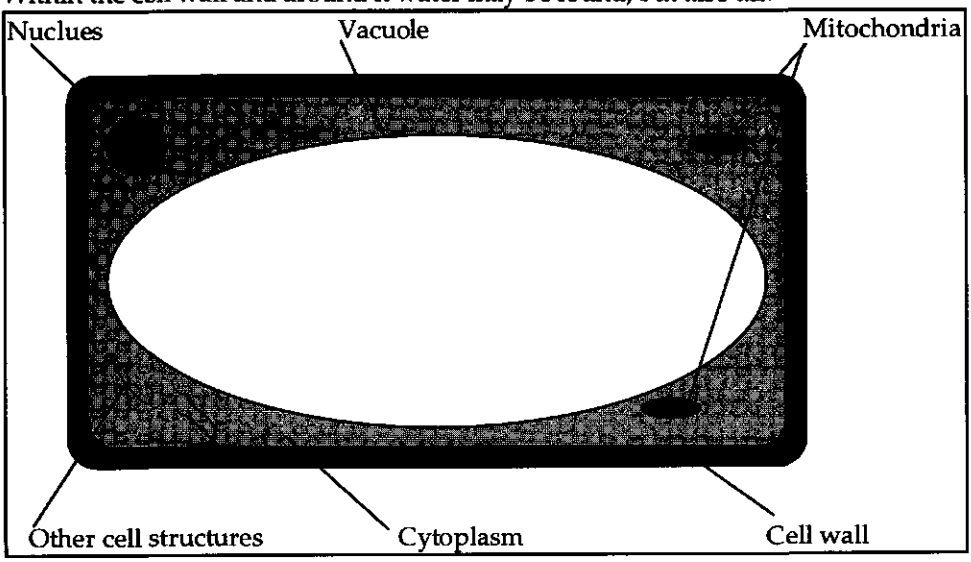

Figure 1.2 A schematic representation of a plant cell.

Firstly, we may focus on the cytoplasm alone and give a somewhat phenomenological description of magnetization coherence loss and translational diffusion within this compartment. Within the cytoplasm there are a wide variety of molecules and structures that have a significant effect on signal loss and translational diffusion.

Paramagnetic ions, with a net electronic spin (and possibly orbital momentum), produce large fluctuating dipolar magnetic fields which accelerate the nuclear magnetic relaxation for nuclei near these centers. Radicals exhibit similar effects on the relaxation process as does the paramagnetic O_2 molecule (32).

Proteins and polymeric sugars adsorb water. In the presence of surface charges (and even without these) both rotational and translational diffusion of the water molecules, which are electric dipoles, is inhibited. Hereby τ_c increases and the T_2 of the bound water may reduce to a few milliseconds (33). The adsorbed fraction is often loosely called bound water, whereas the non-adsorbed water is called free. The protons of the macromolecules themselves have a very short T_2 (< 100 μs). Interaction between the bound water protons and the macro molecular protons takes place via proton exchange, which causes an additional signal loss because the resonance frequency of the exchanging protons can be different. In order for proton (or chemical) exchange to take place the water molecule and the

macro-molecule must be in close contact. Neither the macro-molecule nor the water molecule need to move during this process. Exchange between the bound water and the free water is driven by diffusion. Diffusive exchange between bound and free water is very fast and results in a T_2 which is a weighted average of the intrinsic T_2's of the bound and free water (39,40). The exchange process is characterisez d by τ_{ex}, the lifetime of a water molecule in one of the exchanging fractions. When $T_2\tau_{ex} << 1$ for the shortest T_2 of the exchanging fractions the T_2's of both fractions mix completely and are not distinguishable, as is the case with diffusice exchange between bound and free water with an τ_{ex} in the order of 1 nano-second. For a diffusion constant of 1.10^{-9} m^2/s and a T_2 of 100 ms structures below 5 μm are not observable separately. If τ_{ex} is comparable with the intrinsic T_2's these are modufied and we obtain observed T_2's. When $\tau_{ex} >> T_2$ for the longest T_2 of the exchanging fractions the observed T_2's are identical to the intrinsic T_2's.

Because of the microscopic inhomogeneity of the cytoplasm the diamagnetic susceptibility within this compartment varies with position. Diffusion through the field gradients evoked by the local differences in magnetic environment also gives rise to an additional signal loss (Eq.[1.9]). Depending on the susceptibility difference and the size of the structures this signal loss may be recoverable using a CPMG or a similar sequence.

Finally, several structures like membranes in and around the cytoplasm may incorporate surface sinks, e.g. paramagnetic ions or some bound water. Diffusion of water near or into these sinks generates an acceleration of the relaxation process (41). Both diffusion through *in situ* field gradients and diffusion into surface sinks result in additional signal loss. It follows that relaxation and diffusion are coupled and the observed T_2 is dependent on the diffusion constant. The above mentioned membranes can accelerate relaxation and at the same time inhibit the self-diffusion of water. The likelyhood that a diffusing molecule encounters an obstructing membrane is proportional to the distance it travelles. This results in a smaller increase of the r.m.s. displacement with time than predicted by Eq.[1.8]. Furthermore, the displacement of water molecules near membranes or proteins can be inhibited because these molecules can be bound to the macro-molecules. Thus, within the cytoplasm alone many different conditions exist which affect the relaxation process and the r.m.s. displacement of molecules.. If one would be able to study the cytoplasm selectively parameters like T_2 and the diffusion constant represent an average value over the whole cytoplasm.

The other compartments also contribute to the NMR signal and interact with the cytoplasm. The membranes which separate the cytoplasm from the

vacuole (the tonoplast) and the extra-cellular spaces (the plasmalemma) are permeable for water molecules and a selection of other molecules. As a result, the magnetization pools of these two compartments become mixed during the observation period and the observed T_1 and T_2 are a mixture of the intrinsic relaxation times of the connected compartments. Because these compartments are larger than the sub-cellular structures in the membrane and they are separated by a semi-permeable membrane, diffusive exchange is associated with a longer τ_{ex}, resulting in a smaller difference between the intrinsic and the observed T_2's. Therefore these relaxation times may be observed separately. Fortunately the measured relaxation rates and diffusion constants can be analysed such that the exchange rate or membrane permeability and the compartment size can often be measured quantitatively (5,16,20,42).

The above review represents only a simplistic summary of the processes which occur within a plant cell, influencing the magnetization coherence. Both relaxation and diffusion are affected by the heterogeneity of the plant cell. In order to study the water balance, governed by diffusion, perfusion and flow within living tissue it is not only necessary to formulate theoretical models which describe the time-dependent NMR signal in heterogenous systems, but also, to develop methods which enhance the non-spatial resolution so as to extract the desired information like T_1, T_2 and the parameters characterising diffusion, perfusion and flow.

1.5 Contents of this Thesis

Chapter 2 deals with the NMR instrumentation used for most measurements reported in this Thesis . Some factors which influence the signal to noise ratio of diffusion and flow measurements are treated which are specific for the type of NMR spectrometer,used in the experiments.

Chapter 3 introduces the combination of T_2 relaxation measurements and pulsed field gradient diffusion measurements. It is demonstrated how this combination enhances the diffusion resolution and enables a better understanding of diffusion measurements in heterogenous systems.

Chapter 4 is an extension of Chapter 3. Here the introduction of 2D fitting of Pulsed Field Gradient Carr Purcell Meiboom Gill data is shown to improve both T_2 and diffusion measurements. The 2D or surface analysis approach in complex

systems is demonstrated for measurements on blood, apple parenchyma tissue and flow in a chromatographic column.

Chapter 5 reports on flow measurements in a living fish and real time flow measurements in phantoms with a time resolution below 20 ms. It is also shown that high temporal resolution or high flow velocity resolution are trade off parameters.

References

1. C.T.W. Moonen, P.C.M. van Zijl, J.A. Frank, D. Le Bihan and E.D. Becker, Science **250**, 53 (1990).
2. H. Van As, J.E.A. Reinders, P.A. de Jager, P.A.C.M. van de Sanden and T.J. Schaafsma, J. Exp. Bot. **45**, 61 (1994).
3. J.E.A. Reinders, Ph.D Thesis, Wageningen (1987).
4. C. van den Berg, Ph.D Thesis, Wageningen (1993).
5. T. Conlon and R. Outhred, Biochim. Biophys. Acta **288**, 354 (1972).
6. E.M. Purcell, H.C. Torrey and R.V. Pound, Phys. Rev. **69**, 37 (1946).
7. F. Bloch, W.W. Hansen and M. Packard, Phys. Rev. **70**, 474 (1946).
8. G. Suryan, Proc. Ind. Acad. Sci., Section **A33**, 107 (1951).
9. E.L. Hahn, Phys. Rev. **80**, 580 (1950).
10. H.Y. Carr and E.M. Purcell, Phys. Rev. **94**, 630 (1954).
11. J.R. Singer, J. Appl. Phys. **31**, 125 (1960).
12. D.E. Woessner, J. Phys. Chem. **67**, 1365 (1963).
13. E.O. Stejskal and J.E. Tanner, J. Phys. Chem. **42**, 288 (1965).
14. E.O Stejskal, J. Chem. Phys. **43**, 3597 (1965).
15. J.E. Tanner and E.O. Stejskal, J. Chem. Phys. **49**, 1768 (1968).
16. J.E. Tanner, J. Chem Phys. **69**, 1748 (1978).
17. J. Karger and W. Heink, J. Magn. Res. **51**, 1 (1983).
18. D.G. Cory and A.N. Garroway, Magn. Res. Med. **14**, 435 (1990).
19. P.T Callaghan, D. MacGowan, K.J. Packer and F.O. Zelaya, J. Magn. Res. **90**, 177 (1990).
20. J.E.M. Snaar and H. Van As, J. Magn. Res. **A 102**, 318 (1993).
21. B.P. Hills and J.E.M. Snaar, Mol. Phys. **76**, 979, (1992).
22. P.C. Lauterbur, Nature **242**, 190 (1973).
23. D.G. Taylor and M.C. Busheli, Phys. Med. Biol. **30**, 345 (1985).
24. K.D. Merboldt, W. Hanicke and J. Frahm, J. Magn. Res. **84**, 479 (1985).

25. D. Le Bihan, E. Breton, D. Lallemand, P. Grenier, E.A. Cabanis and M. Lavel-Jeantet, Radiology **161**, 401 (1986).
26. P.R. Moran, Magn, Res. Imag. **1**, 197 (1982).
27. C.L. Dumoulin and H.R. Hart, Radiology **161**, 717 (1986).
28. D.A. Feinberg, L.E. Crooks, P. Sheldon, J. Hoenninger III, J. Watts and M. Arakawa, Mag. Res. Med. **2**, 555 (1985).
29. P. Mansfield. J. Phys. C. **10**, L55 (1977).
30. D.N. Guilfoyle, P. Gibbs, R.J. Ordidge and P. Mansfield, Magn. Res. Med. **18**, 1 (1991).
31. K. Kose, Phys Rev. **A 44**, 2495 (1991).
32. A. Carrington and A.D. McLachlan, Introduction to Magnetic Resonance, Harper and Row (1967).
33. P.T. Callaghan, Principles of Nuclear Magnetic Resonance Microscopy, Oxford Science Publications (1991).
34. H.Y. Carr and E.M. Purcell, Phys. Rev. **94**, 630 (1954).
35. S. Meiboom and D. Gill, Rev. ci. Instr. **29**, 688 (1959).
36. B.P Hills and S.L. Duce, Mag. Reson. Imaging **8**, 321 (1990).
37. D.G. Nishimura, A. Macovski and J.M. Pauly, IEEE Trans. Med. Imaging **MI-5**, 140 (1986).
38. W. Palstra, H. Van As and T.J. Schaafsma, To be published.
39.J.R. Zimmerman and E.O. Brittin, J. Phys. Chem. **61**, 1328 (1957).
40. H.T. Edzes and E.T. Samulski, J. Magn. Res. **31**, 207 (1978).
41. K.R. Brownstein and C.E. Tarr, J. Magn. Res. **26**, 17 (1977).
42. J.E. Tanner, Arch, Biochem and Biophys. **224**, 416 (1983).

Chapter 2

Experimental setup for probing motion

2.1 Introduction

Because of its many advantages NMR is used in several distinct scientific research areas such as (bio)physics, chemistry, biology and medicine. As applications vary widely among these research areas so do the NMR spectrometers. Spectrometers with small permanent magnets and relatively simple electronics. like the Bruker Minispec, are made for e.g. off-line quality research of food products. Such a Bruker Minispec has been modified at our laboratory to investigate the waterbalance of plants *in vivo* and *in situ* (1,2,3). On the other side of the spectrum we have highly advanced medical imagers equipped to investigate humans. These two examples exemplify the need to modify the NMR equipment such that the relevant research parameters can be investigated. Below a more specific example is given of how relevant research parameters shape a NMR spectrometer.

Over the last 15 years great effort has been put into NMR measurements of water flow in large plants like cucumber and tomatoes in our laboratory (3). Not only flow in plants was investigated, but also flow through glass bead beds (4). Both these objects require good vertical access from both sides to the rf coil; a horizontal superconducting magnet is thus ruled out (vertical superconducting magnets with good access have only become available recently) limiting the choice to a ferrous core electromagnet. A gap of 14 cm between the pole shoes (10 cm between the shims), favourable for larger plant leaves, could be obtained for 0.5 T; the iron core gets saturated at higher fields at this dimension. In principle higher magnetic fields with non ferrous electromagnets with resistive coils can be obtained, but then the operational costs become prohibitive. Although this low magnetic field gives a limited signal amplitude it is advantageous when susceptibility differences within a sample exist or chemical exchange between sites with different chemical shift occurs (5). Furthermore, since probing and localising motion requires strong, high quality (preferably active shielded) gradients, which do not inhibit the access to the solenoïd rf coil, are required. These requirements have led to the configuration described in detail in Section 2.1.1.

2.1.1 The local NMR spectrometer.

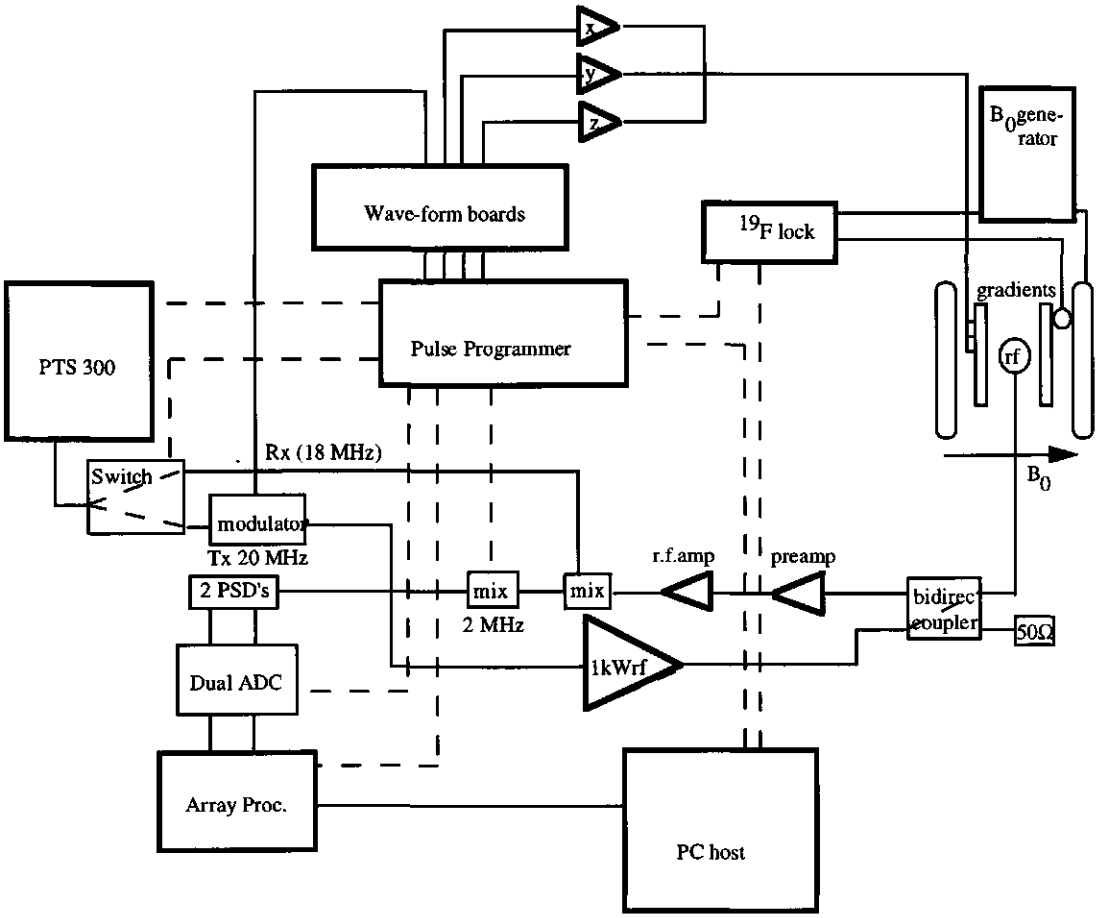

Figure 2.1 Schematic representation of the SMIS/Bruker NMR spectrometer as used for most experiments described in this Thesis. Throughout the text the function of most of the components is explained.

In Fig. 2.1 the experimental configuration was used for most experiments described in this thesis is depicted. As is usual for scientific research this setup has come into existence by several small improvements over the years. Most items are commercially available components which have been connected to form a spectrometer, only a few parts have been home made. The core of the system is a 0.5 T electromagnet with power supply (Bruker Spectroscopy, Karlsruhe, Germany), operated at 0.4780 T (20.35 MHz). This magnet is fitted with

a set of planar shims of which the x,y and z shims can be used as pulsed field gradients. However, this function has been taken over by a custom designed microscopy probe (Doty Scientific Inc., Columbia, USA) with active shielded gradients and a 3 cm I.D. glass tube sticking through the rf coil with full access from top and bottom (see Figure 2.2). The probe fits firmly in the 10 cm gap between the shims. Two amplifiers are used to drive the gradients: a single channel Techron 7570 and a Crown DG-300A dual channel (Elkhart, Indiana, USA). This setup gives a 370 mT/m z-gradient, a 175 mT/m y-gradient and a 360 mT/m x-gradient using a low (~5%) duty cycle.

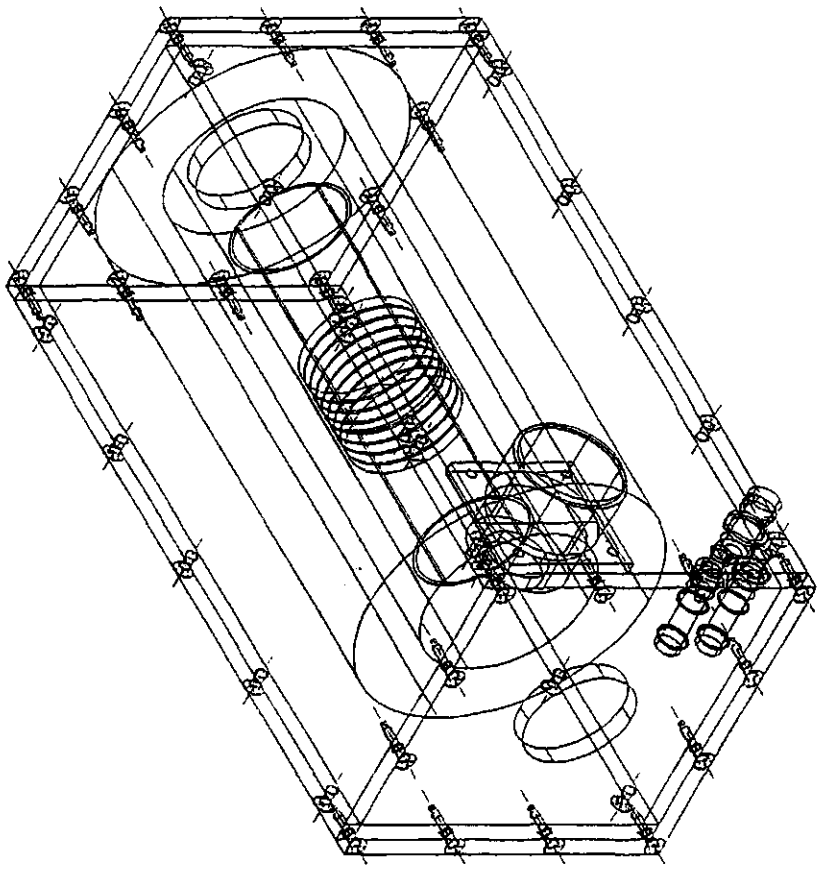

Figure 2.2 The Doty Microscopy probe. The gradients are not drawn, only the rf coil and the outer box.

The two gradient drivers and a 1 kW AN 8031 rf amplifier (Analogic, Wakefield, USA) are controlled by a SMIS console (Guildford, England). This

console consists of a 20 MHz 386DX PC serving as a host for a 10 MHz pulse programmer board, 3 waveform generator boards, a V32c array processor and a video board. The dual channel ADC is located in a seperate rf unit box (SMIS, Guildford, England),which gives a better noise figure than inside the PC. In the rf unit box two phase sensitive detectors operated in quadrature and one rf channel are also located. The ADC (16 bit output resolution at 1-100 kHz sampling rate and 12 bit at 200 and 400 kHz) receives its signals via a broadband LD-2L rf preamp (Doty Scientific Inc. , Columbia, USA) which is connected via the main line to the rf coil. The ADC directly sends its data to the array processor where digital filtering of the signal is applied. After each separate scan the data is transferred to the computer's disk. For high speed sequences a virtual disk can be created (MS-DOS). A PTS 300 (Programmed Test Sources Inc., Littleton, USA) is used to generate rf frequencies. The console now is broad band from 5 MHZ to 300 MHZ.

To achieve linearity of the rf modulation and transmitting system a CI604 -14 dB bi-directional coupler (Werlatone Inc. Brewster, USA) is placed in the rf chain, for both the soft shaped pulses and the hard pulses (generally 16 μs long for a 180° pulse at ~150 W input). For optimal functioning of this coupler all four ports should be terminated with 50 Ω. However, the preamp is 0.2 Ω during transmission and 150 Ω during the receiving phase, causing rf reflections during transmission. Minimisation of the reflections, resulting in phase glitches and incorrect 180° pulses, was obtained by placing a empirically determined length (not $\lambda/4$) of cable between the rf coil and the preamp.

Another characteristic of the SMIS system is the usage of an extra 2MHz mixer which allows the PTS 300 to be switched from 20.35 to 18.35 MHz during the non transmission phase. This switching procedure is phase coherent and achieves minimisation of the effect of rf leakage of the rf amplifier during the receiving phase which gives a lower noise figure.

A ^{19}F-lock, the home made rf coil of which is placed directly outside the microscopy probe close to the center of the magnet in a region with sufficient homogeneity (T_2^*>3 ms), monitors and adjusts the B_0-field and completes the whole setup.

2.2 SNR requirements for probing motion

Almost all NMR experiments comprise a definite set of scans, each of these scans using several rf pulses and pulsed field gradients. Even 1D experiments in which a FID or a CPMG curve is sampled normally consist of several averages. As a result the overall accuracy and reliability of these multi scan experiments is

not only determined by the signal to noise ratio (SNR) of the rf coil and the receive part of the spectrometer but also by the stability of the NMR spectrometer as a whole and its response to changes and disturbances in the environment of the equipment.

When we look at possible sources of noise four can be distinguished; the rf coil, the sample, the spectrometer itself and the environment. The first three possibilities can be considered constant and are caused by random thermal motion of electrons in the wire of the rf coil, in the sample and the spectrometer, mainly the preamp, whereas the fourth source is variable and often unpredictable. Also, these environmental disturbances (e.g. fluctuations of room temperature, airflow, voltage of the electricity grid) are picked up by the spectrometer and may affect the signal. The stability of the gradients, the magnet, the rf chain, the environment and the sample have to be included in a proper assessment of the fidelity of the NMR measurements.

2.2.1 The SNR of the rf coil

To determine the signal to noise ratio of a specific rf coil one needs to access both the NMR signal amplitude of a sample generated in a certain rf coil and the electro magnetic force (e.m.f) noise of the coil and the sample. Hoult and Richards (6) have developed a method, assuming certain characteristics of the rf coil and using the principle of reciprocity (6), to calculate both the signal amplitude which can be obtained using an 'ideal' rf coil and the thermal noise power generated by the same coil. The in-phase signal component is given by (6)

$$S_0=\omega_0 K(B_1/i)_{xy} M_0 V_s \cos\omega_0 t \qquad [2.1]$$

Here V_s denotes the volume of the sample, $(B_1/i)_{xy}$ is the transverse component of (B_1/i), the amplitude of the magnetic field generated at the centre of the rf coil, $K(B_1/i)_{xy}$ represents the integrated B_1 field and M_0 represents the amplitude of the transverse magnetisation (see Eq.[1.1]). The thermal noise power per unit frequency, $\Delta\nu$, is determined by the coil resistance and temperature. The time domain e.m.f. root mean square (rms) noise is thus given by (6)

$$\sigma_t = (4\kappa_b T_c \Delta\nu R)^{1/2} \qquad [2.2]$$

κ_b representing the Boltzmann constant, T_c being the coil temperature. R, the resistance of the rf coil is dependent on ω_0, and also the geometry of the coil (6,7). Assuming an ideal solenoid coil following the principles of Hoult and Richards,

and filling in all relevant parameters (^{1}H NMR at 25 ^{o}C of pure water) the SNR of such a coil can be calculated to be (7):

$$S_0/\sigma_t = 2.72 \times 10^{-3} V_s f_0^{7/4} r^{-1} F^{-1/2} \Delta\nu^{-1/2} \sigma^{-1/2} \qquad [2.3]$$

Here F is the the spectrometer noise figure and σ a factor correcting for the reduced skin depth at high frequencies because of the proximity effect. For example, at 20 MHz, after a single 90^o pulse the time domain SNR of a cube of 1 cm^3 of water molecules in a coil of 16 mm radius (r) the SNR will be about 1050 ($\Delta\nu$= 200 kHz, F=1 and σ=5). Application of a saddle coil results in a reduction of the SNR by a factor of 3. This is a considerable advantage of an electromagnet compared to supercons which can only use solenoids for some specific applications.

At 20 MHz, using samples with a diameter of a few centimeter, the rf-field losses, caused by insertion of a conducting sample, which constitute the e.m.f. noise of the sample, are dominated by the thermal e.m.f. noise of the coil and can therefore be ignored. If however, the sample sticks outside the rf shield which surrounds the microscopy probe, the sample itself can serve as an antenna and introduce rf signals which are overwhelmingly present in the air of a modern society. Especially our PC but also other parts of the spectrometer generate frequencies at and around 20 MHz. For this reason the magnetic field was fixed so that the resonance condition was laid at 20.35 MHz, a relatively quite frequency. Furthermore the large samples where connected to the conducting surface of the microscopy probe which reduces the leakage of external rf signals into the rf coil.

2.2.2 The gradients

Probing translational motion requires reliable gradient coils and gradient drivers. Nowadays the magnetic field linearity of commercial gradients is excellent and these do not limit the application of NMR in diffusion studies. Also, the input waveform for the gradient drivers is generally digitally controlled and therefore leaves little room for timing and amplitude errors, except perhaps when incorrect programming occures.

The results of the diffusion or flow measurements are mostly influenced by the noise on the gradients and the unfaithful reproduction of the input waveform by the gradients and the gradient amplifiers. The main source of the noise on the gradients is not the amplifier that drive the gradient, but the connection between the computer and the amplifier. If, at any point between the

analog output of the computer and the amplifiers, the wires are grounded so called groundloops are introduced which may cause severe variations of G. These variations give rise to non-Gaussian fluctuations of the echo amplitude and phase. A solution to the groundloops is application of a balanced input. Although the amplifiers are used to supply current at audio frequencies, signals at rf frequencies can be picked up by the gradient wires, enter the amplifiers, and also seriously distort the output signal. Therefore these cables were double shielded. The second problem, the low fidelity of the magnetic field gradient waveform, can be attributed to the inductance of the gradient coils and/or the mutual induction between the gradient coils and surrounding metal. This mutual inductance gives rise to eddy currents in the surrounding metal which may persist for several milliseconds after the input waveform has been switched of. Fortunately the electromagnet has a geometry which is unfavourable for these eddys, and in combination with active shielded gradients and a distance of several centimeters between the gradient coils and the pole caps, these eddys do not seem to exist in our system. However, the dual channel Crown amplifier could only be operated in constant-voltage mode. This results in a rise time of the gradient current (= magnetic field gradient) which is proportional to the inductance of the gradients divided by it's resistance. In table 2.1 the time constant, τ, of these gradients is given. The rise and fall time (0-100%) of the input waveform voltage was normally set to 200 μs (no pre-emphasis was used).

	Inductance (μH)	Resistance (Ω)	τ (μs)
x-gradient	750	4.7	160
y-gradient	350	4.3	80
z-gradient	40	0.8	50

Table 2.1 Values of the time constant of the gradients when driven in constant voltage mode.

The z-gradient, which is driven by the more powerful 7570 amplifier, is evidently faster, especially when driven in constant-current mode. However, it suffered from non-linear distortions when pulsed field gradients near maximum power where generated in constant-voltage mode (as it was initially used) using short pulse intervals. This was caused by the very low resistance of the gradient. Placing a 2 Ω resistance in series with the gradient reduced the distortion. When the non-linear distortion of the gradient driver occured this resulted in an effective mismatch of the two pulses which leads to an extra signal attenuation (8)

$$S(t,b)/S(t,0)=\sin(2r/\Delta k)/(2r/\Delta k) \qquad [2.4]$$

r being the sample diameter, Δk the mismatch of the surface below the pulsed field gradients ($\gamma g \delta$). When, in a diffusion measurement the pulse duration of 5 ms was long compared to the distance in between the pulses, 1 to 3 ms, this extra attenuation could rise to 10-15 % at full power. Mismatch of the gradient pulses therefore leads to a systematically enhanced diffusion constant. For imaging experiments, which are also based on pulsed gradients, mismatch of the gradients leads to timing errors and therefore distortion of images.

The errors discussed sofar in this section have dealt with errors within the gradient chain itself. A different type of noise is generated by pickup of rf frequencies by the cables connecting the gradient drivers with the probe. The rf signals are directly transmitted by the gradient coils to the rf coil (in our setup the rf shield was removed to prevent eddy currents from arising in this shield). By careful grounding of a thin sheet of aluminium wrapped around the cables this source of noise was minimised. Prior to this grounding several lines in the phase direction appeared in images and caused a SNR reduction by a factor ~8.

2.2.3 The magnet

An electromagnet is not as stable as a superconductive magnet which is one of the reasons it is less suitable for (2D) chemical shift spectroscopy measurements. Two types of noise of the main field should be considered, short term hum at 50 Hz and higher harmonics of this frequency due to leakage of small fluctuations in the AC supply of the power supply into the main field, and long term drift of the main field in the order of seconds to minutes mainly because of temperature fluctuations of the cooling water. The first type of noise is not corrected for (no flux stabilisor) and seriously affects SE measurements when echo times are an exact multiple of 2.5 ms. Echo times exceeding 20 ms especially suffer from this type of noise. The second type, which may change the Larmor frequency up to 100 or 200 Hz when the cooling water temperature rises by as little as 0.05 °C, is corrected for by the ^{19}F lock unit which limits the main field drift to within 5 Hz. The effect of these field drifts on the results strongly depend on the type of measurement. When averages are necessary the phase shift caused by the main field drift should be small compared to π, otherwise the phase sensitive detected averages do not properly add up. However, if only the echo top is sampled like in CPMG experiments and some PFG SE experiments these phase shifts are not relevant and larger field drifts are allowable. In general it can be

said that the field fluctuations, expressed in $\Delta\omega$, should be smaller than $1/((TE/2).SNR)$. So, if the time domain SNR=250 and fluctuations of $\Delta\omega$ should not influence the measurements, τ should be smaller than 0.8 ms, at a SNR of 10 (normal for imaging experiments) TE/2 should not exceed 20 ms.

2.2.4 Software

As is obvious from the above, and is found to be generally so, the local NMR spectrometer is not perfect. The time lag of the gradients causes a time shift of the echo in a spin echo experiment, the small fluctuations of the B_0 field cause first order phase errors of the same echo. To arrive at acceptable results it is therefore essential that the software which controls the experiment is flexible and accurate. One of the assests of the current spectrometer is the timing control. Phase coherency during the NMR experiments can be ensured by setting the resonance frequency to 20.35 MHz and synchronising the pulse program with this frequency and 100 kHz, the clock frequency of the ADC, whereby rf pulses have absolute constant phase and amplitude (every 20 μs the ADC and the spectrometer have the same phase). This significantly reduces the effect of errors like the main field drift (e.g. when the exact top of the echo is sampled first order phase shifts have no effect on the acquired signal) and allows for data acquisition in both imaging and non-imaging mode to be purely real or imaginary in stead of modulus, a property which is essential for multi exponential analysis of the data.

2.2.5 The SNR of diffusion and T_2 experiments

The spectral bandwidth used in the diffusion and T_2 experiments described in this thesis has, in general, been set to 200 kHz. This broad bandwidth allows for very short echo times, down to 500 μs, in non imaging mode, which is important for measurements in heterogeneous samples. Given a sample volume of 0.67 ml of $CuSO_4$ doped water (4mM) a SNR of 460 was obtained compared to 700, which the theoretically reachable value. This SNR number was obtained by dividing the amplitude of the Free Induction Decay after a 90° pulse by the root mean square noise of the last 128 data points of the F.I.D. where no signal was found. 200 Repititions of this experiment yielded a standard deviation of the initial point of the F.I.D. of 2.5 promille. Measuring diffusion of the same sample with 8 repetitions using the PFG MSE sequence (see chapter 2.3) with 16 gradient steps yielded a diffusion constant which rose from 2.26 10^{-9} m^2/s to 2.29 10^{-9} m^2/s, but only after 5 scan which were reproducable within 5 promille did this rise of D occur. These 8 repetitions of the PFG MSE experiment took 10 min The

cause of this upward drift of the diffusion constant was the room temperature which fluctuates around 24.5 °C, generally with about 1 °C. This room temperature fluctuation poses a upper limit to the accuracy of NMR diffusion measurement if the SNR exceeds 100. Optimisation of the room temperature control would facilitate diffusion measurements with a standard deviation less than 1 %. Other factors like the field drift or noise on the gradient amplifiers may pose another upper limit to the maximum accuracy of diffusion measurements if the temperature control is improved.

The reproducibility of the T_2 measurements was tested with a somewhat larger sample (1.4 ml) using the same solution. The SNR was determined by dividing the height of the first echo by the rms noise of the last 128 data point of the 8196 echoes (2τ=TE=0.6 ms). Using 7 repititions we found a T_2 of 288 +/- 0.6 ms, a S(0) of 7080 +/- 14 a.u. and a rms noise of 6.2 a.u. (SNR=1150). Up to a 2τ of 2 ms this reproducibility was maintained. The reduction of the spectral bandwidth however, not only reduced the noise level but also introduced extra slow fluctuations of successive echoes (~ 5 times the rms noise) because of the already mentioned magnetic field drifts during the CPMG rf pulse train. Currently this poses a upper limit to the reproducibility of the T_2 measurements but this upper limit lies 5 times higher than for diffusion measurements.

References

1. J.E.A. Reinders, H. Van As, T.J. Schaafsma, P.A. de Jager and D.W. Sheriff, J. Exp. Bot. **39**, 1199-1210 and 1211-1219 (1988).

2. J.E.A. Reinders, Ph. D. thesis, Wageningen (1987).

3. H. Van As, J.E.A. Reinders, P.A. de Jager, P.A.C.M. van de Sanden and T.J.Schaafsma, J. Exp. Bot. **45**, 61 (1994).

4. W. Palstra, H. Van As and T.J. Schaafsma, to be published

5. B.P. Hills and S.L. Duce, Magn. Reson. Im. **8**, 321 (1990).

6. D.I. Hoult and R.E. Richards, J. Magn. Reson. **24**, 71 (1976).

7. P.T. Callaghan, Principles of Nulcear Magnetic Resonance Microscopy, Clarendon Press, Oxford (1991).

8. M.I. Hrovat and C.G. Wade, J. Magn. Reson. **44**, 62 (1981).

2.3 Flexible PFG NMR desensitized for susceptibility artefacts using the PFG Multiple Spin Echo sequence[1] .

Pulsed Field Gradient (PFG) NMR has proven to be a versatile technique for examining diffusional processes in a wide variety of systems (*1*). Its popularity arises from the fact that the observed signal attenuation is proportional to the Einstein diffusion constant (D) and three adjustable NMR parameters, the amplitude (G), the duration (δ) and the interval (Δ) of the magnetic field gradient pulses. The natural logarithm of the signal attenuation vs. $\gamma^2G^2\delta^2(\Delta-\delta/3)$, the *b*-factor, results in a Signal Attenuation Plot (SAP). Given a homogeneous sample in a homogeneous magnetic field, the slope of this plot represents the diffusion constant of the sample (*2,3*). The exponential relation between the signal amplitude S(t,b) and *b*D is perturbed in case of restrictions in the diffusion pathway. The restrictions may consist of (im)permeable membranes with or without relaxation sinks (3). In well-defined systems the free diffusion path length can be quantitatively determined in the presence of these barriers, using q-space or translational motion imaging (*4,5*). However, there is another phenomenon that perturbs the exponential relation between the signal amplitude and *b*D which is a spatial variance of the magnetic susceptibility within the sample, causing *in situ* magnetic field gradients. The *in situ* field gradients occur in various kinds of samples for which considerable interest exists such as plant material, porous media and zeolites. The amplitude of these gradients is dependent on the magnetic field strength.

Assuming that the internal field variations can be approximated by a constant linear external background gradient (G_0), application of PFG NMR for diffusion measurements in such systems yields (*2*):

$$S(t,b)=S(0,0).\exp(-2n\tau/T_2).\exp(-\gamma^2D[G^2\delta^2(\Delta-\delta/3)+G_0^2(2/3)n\tau^3- \mathbf{G_0}\cdot\mathbf{G}\delta\{(t_1^2+t_2^2)+\delta(t_1+t_2)+(2/3)\delta^2-2\tau^2\}]) \qquad [1]$$

where the symbols are defined in Fig 1. Eq. [1] holds for a PFG Spin Echo experiment with the number of π-pulses n=1. It expresses two features of a diffusion experiment in the presence of a background field gradient. Firstly the background field gradient reduces the echo amplitude resulting in a limited range

[1] Reprinted from J. Magn. Reson A 112, 237-240 (1996)

over which Δ can be varied because of signal to noise ratio (SNR) limitations and, secondly, the cross term $\mathbf{G_0 \cdot G}$ changes the SAP. A diffusion constant derived from this SAP slope no longer represents the self diffusion constant. As both restricted diffusion and *in situ* field gradients affect the observed SAP curvature there is no straightforward relation between Δ and the signal attenuation, a necessary condition for q-space imaging. In order to relate diffusion constants with spatial information it is necessary to reduce or nullify the effects of *in situ* field gradients.

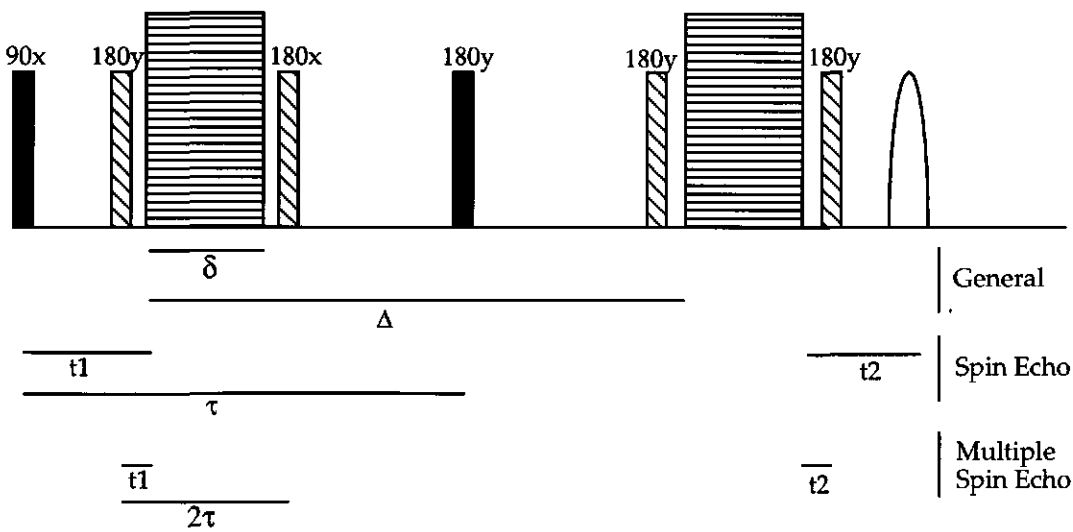

Figure 1. Figure depicting both the PFG SE and MSE sequence. The black rf pulses and the gradients are used in both sequences, the additional, shaded, rf pulses are only used for the MSE sequence. The consequence of the addition of extra rf pulses on t_1, t_2 and τ is explained in the lower part of the figure.

Therefore, instead of the PFG SE the PFG STimulated Echo sequence has been used (*6*). Although during the middle period t_m, between the second and third 90° pulse, only T_1 relaxation causes signal loss, the stimulated echo is still affected by diffusion through *in situ* field gradients. The overall effect on a PFG STE diffusion measurement is expressed as (*6*):

$$S(t,b)=(1/2).S(0,0).\exp(-t_m/T_1-2\tau/T_2).\exp(-\gamma^2 D[G^2\delta^2(\Delta-\delta/3)+G_0^2\tau^2(t_m+2\tau/3)- \mathbf{G_0 \cdot G}\delta\{(t_1^2+t_2^2)+\delta(t_1+t_2)+(2/3)\delta^2-2(t_m+\tau)\tau\}]) \qquad [2]$$

Normally the SAP obtained by the PFG STE is less sensitive to background field gradients than the SAP obtained by the PFG SE since at prolonged echo times (τ(SE) >> τ(STE)) the term $(2t_m+\tau)\tau$ in Eq.[2] is considerable smaller than $2\tau^2$ in Eq.[1] , these factors determining the influence of the crossterm $\mathbf{G_0}.\mathbf{G}$. To avoid T_2 attenuation τ is kept short and constant. Increasing Δ, and thus t_m, automatically introduces a T_1 dependence of the SAP in a multi compartment sample. This causes an alteration of the relation between the SAP slope and Δ, yielding an incorrect interpretation of the acquired diffusion data (*7*). Because of mixing T_1 and diffusion information and because of the sensitivity to diffusion through background field gradients, albeit this effect is considerably smaller than for the PFG SE sequence, the PFG STE method is not optimally adapted for diffusion measurements in inhomogeneous samples and thus for q-space imaging.

It is well known that the application of a CPMG sequence with small values of τ minimises the destructive effect of random fluctuations of the precession frequency with time. By intertwining two PFG's and a CPMG sequence not only the SNR, but also the reliability of the diffusion constant can be improved (*8,9*) when *in situ* field gradients occur in a sample. This has been demonstrated by Williams *et al.* (*8*) who adapted the basic method developed by Packer *et al.* (*9*). Packer left the phase of the π-pulses between the PFG's unchanged. This can result in a considerable signal loss when *b* becomes non-zero since a temporary change of the precession frequency can not be compensated by a train of π-pulses with identical phase and small pulse errors. By alternating the phase of contiguous π-pulses this problem is only partially solved. Since the method of Williams *et al.* is based on increasing the number of π-pulses between the PFG's, hence increasing Δ, incomplete refocusing of the xy-magnetisation gives an increase of the apparent diffusion constant. Furthermore the method can not be used for samples with a short T_2 since Δ needs to be increased over a certain number of π-pulses. For the above mentioned reasons the original sequence of Packer *et al.* was adapted by changing the phase scheme between the PFG's. The XY-8 variant phase scheme$(xyxyyxyx)_m$ (*10*), which allows extending the number of π-pulses up to 1000 or more, turned out to work well; other phase schemes like MLEV-16 should give similar improvements. The number of π-pulses between the diffusion gradients is not limited to $8m$+1 but can be increased in pairs, keeping the total number uneven, although a number of $8m$+1 gives a few percent higher signal amplitude.

In Fig. 1 the PFG Multiple Spin Echo (PFG MSE) pulse sequence in its final form is depicted. To calculate the effect of a linear background gradient Eq. [1] can be used, n denotes the total number of π-pulses, other symbols are explained in Fig. 1. The echo time TE equals $2n\tau$. From this equation it is evident that careful setting of τ and δ can eliminate the effect of background and *in situ* field gradients. This occurs when $(2/3)\delta^2 \approx 2\tau^2$, which can be achieved since the PFG's are placed between two π-pulses (during the period 2τ) and not between the 90° pulse and a π-pulse (during the period τ). Because of the flexibility of this sequence it is quite suitable to evaluate the apparent diffusion constant as a function of both TE and Δ. TE is varied by placing extra π-pulses before the PFG's, keeping m between the PFG's constant, Δ is varied by changing m, while keeping n constant.

The PFG MSE sequence was tested and compared to the PFGS(T)E sequences using a NMR spectrometer consisting of a 0.5 T Bruker electromagnet (Karlsruhe, FRG), a SMIS imaging console (Guildford, UK) and a Doty microscopy probe (Columbia, USA). The three PFG NMR techniques were compared regarding their sensitivity to an artificially introduced linear background field gradient of + and - 3 mT/m in the same direction as the gradient used for the diffusion measurement. A tube with a diameter of 7 mm filled with demi-water served as a sample. The spacing between the first 90° pulse and the final echo was set to 200 ms for all sequences (δ=5 ms). The results are presented in Fig. 2 with all curves normalised to the same scale to facilitate visual comparison. Compared to a measurement in the absence of the background gradient the initial echo amplitude S(t,0) of the SE drops by 50 % and the STE by 5 %, whereas no changes occur for the MSE sequence. The SAP slope of the MSE does not change upon application of the background field gradient either (τ=2 ms, $D=2.28*10^{-9}$ m^2/s, T=25 +/- 1 °C), in contrast to the SAP slope of the STE, which fluctuated by ≈ 8 %. The sign of this change is dependent on the direction of the background field gradient with respect to the direction of G. Clearly the SAP slope of the PFG SE sequence can not be determined accurately in the presence of a background field gradient. Assuming that a symmetrical distribution of positive and negative *in situ* field gradients occurs within a sample, in the same direction as the PFG, the deviations of the SAP slope do not cancel. The net result would be a reduction of the SAP slope, arising from the fact that $0.5(e^{-x}+e^{x}) > 1$ (e.g. for a value of x=0.3 this is 1.1). When $\mathbf{G}^2\delta^2\Delta$ is comparable to $\mathbf{G}.\mathbf{G}_0\delta\tau^2$ and *in situ* field gradients in both directions exist, a reduction of at least 10 % of the expected attenuation will be

observed. A decrease of the SAP slope can also be expected with higher order gradients.

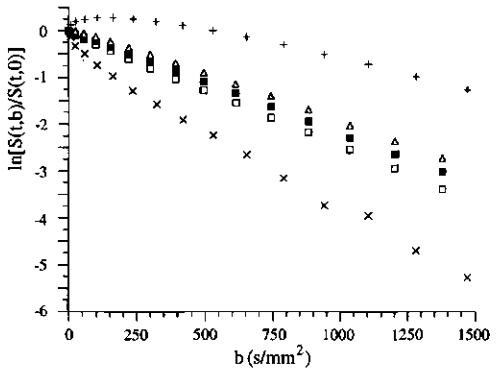

Figure 2. Signal Attenuation Plots (SAP) of water in a glass tube (ϕ=7 mm) obtained by the PFG SE, STE and MSE sequences as a function of a linear background gradient of 3 mT/m along the pulsed gradient direction (echo time=200 ms, δ=5 ms). PFG SE with a background gradient of -3 mT/m (+) and +3 mT/m (x). PFG STE with a background gradient of -3 mT/m (Δ) and +3 mT/m (□). (■) PFG MSE (τ=2 ms) with and without background gradient and the PFG S(T)E curves without background gradient.

The above mentioned predictions for NMR diffusion measurements have been verified in a model for porous systems: A homodisperse glass bead water system, with a bead diameter of 80 μm. All three PFG NMR techniques were used to evaluate diffusion in this sample. The average T_2 of this sample was measured with a CPMG sequence and found to be 0.36 sec (τ=2 ms). This relatively long T_2 indicates that magnetisation loss at the glass water interface, reducing the observed diffusion constant (*3,11*), does not have to be taken into account. Because of the *in situ* field gradients the measured T_2 depends on τ and therefore deviates from the expected value of 2.2 s found for bulk water. The spin echo amplitude at 30 ms (τ=15 ms) has been observed to be similar to that of an echo following a CPMG train of 540 ms (τ=2 ms). By consequence the application of the PFG SE sequence was limited to $\Delta \leq 20$ ms because of the SNR. Also the observed value of D, $1.29*10^{-9}$ m^2/s, for Δ=15 ms indicates that the SAP slope has decreased because of *in situ* field gradients.

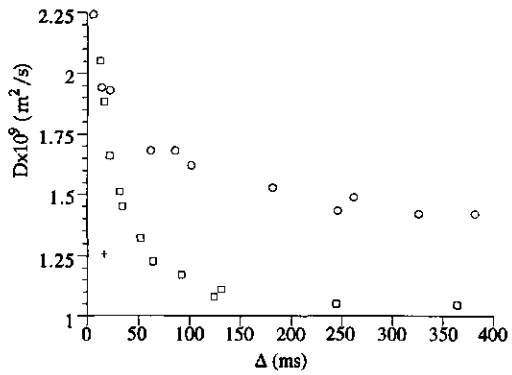

Figure 3. Diffusion of water in a glass bead system (bead diameter of 80 μm), measured for different values of the gradient interval Δ. □ Depicts the Δ dependency of the PFG STE sequence (echo time varying between 20 and 380 ms, δ=5 ms), O depicts the Δ dependency of the PFG MSE sequence (TE=416 ms, τ=2 ms). + depicts D of the PFG SE sequence (TE=20 ms).

A similar PFG MSE measurement (τ= 2 ms, n=7) gave a diffusion constant of $2.23*10^{-9}$ m^2/s indicating that the lower value found using the PFG SE sequence is not due to restricted diffusion. For comparison of the STE and MSE sequences the TE of the MSE was set to 416 ms for a range of Δ values. The echo time of the STE had to be varied from 20 ms to 380 ms to be able to measure with a comparable range of Δ values. The stimulated echo amplitude at 380 ms was half that of the spin echo of the MSE sequence at 416 ms. Fig. 3 shows the influence of the gradient interval time Δ on the observed diffusion constant and also what a difference in sensitivity to *in situ* magnetic field gradients makes. Because in a glass bead system no full restriction of motion occurs (5) the data presented in Fig. 3. cannot be fitted to a finite compartment size. The difference between the two curves can only be explained by *in situ* magnetic field gradients, as wall relaxation is minimal and the diffusion coefficient is independent of TE.

The advantage of the PFG MSE sequence not only holds for samples known for their relatively large susceptibility variations. Some preliminary restricted diffusion studies in apple, using the PFG MSE, have shown its capability to measure diffusion with TE=4 s (2τ=4 ms). This long echo time is necessary to study the effect of restricted diffusion in large cells without the perturbing effect of *in situ* field gradients.

We conclude that the PFG MSE sequence is fairly insensitive to diffusion through *in situ* field gradients and results in a higher accuracy for D and a higher SNR even for $T_1>T_2$. From the above results it can also be concluded that in the presence of *in situ* field gradients the compartment sizes, calculated from PFG SE and STE measurements, are underestimated. Furthermore the SAP can be evaluated against Δ while keeping TE constant which is an advantage when the sample has several T_2's. Also the SAP can be evaluated against TE with constant τ and Δ to explore these T_2 differences (*7*). These advantages make the PFG MSE a powerful new tool for diffusion measurements in heterogeneous systems.

Acknowledgements:
The authors wish to thank Philips Medical Systems, Best, The Netherlands, for their financial support of this work. Also we wish to thank T.J. Schaafsma for critical reading of the manuscript.

References:

1. J. Kärger, H. Pfeifer and W. Heink, Advances in Mag. Reson. **12**, 1 (1988).
2. E.O. Stejskal and J.E. Tanner, J. Chem. Phys. **42**, 288 (1965).
3. J.E.M. Snaar and H. Van As, J. Mag. Reson., A **102**, 318 (1993).
4. D.G. Cory and A.N. Garroway, Mag. Reson. Med. **14**, 435 (1990).
5. P.T. Callaghan, A. Coy, D. MacGowan, K.J. Packer and F.O. Zelaya, Nature **351**, 467 (1991).
6. J.E. Tanner, J. Chem. Phys. **52**, 2523 (1970).
7. D. van Dusschoten, H. Van As, 10th SMRM Works in Progress, 1135 (1991).
8. W.D. Williams, E.F. Seymour and R.M. Cotts, J. Mag. Reson. **31**, 271 (1978).
9. K.J. Packer, C. Rees and D.J. Tomlinson, Mol. Phys. **18**, 421 (1970).
10. T. Gullion, D.B. Baker and M.S. Conradi, J. Mag. Reson. **89**, 479 (1990).
11. K.R. Brownstein and C.E. Tarr, Phys. Rev. A **19**, 2446 (1979).

Chapter 3

Diffusion Analysis by Relaxation Time Separated PFG NMR

3.1 Extracting Diffusion Constants from Echo-Time Dependent PFG NMR Data Using Relaxation Time Information[1] .

Summary

Heterogeneous (bio)systems are often characterised by several water containing compartments that differ in relaxation time values and diffusion constants. Because of the relatively small differences among these diffusion constants non optimal measuring conditions easily lead to the conclusion that a single diffusion constant suffices to describe the water mobility in a heterogeneous (bio)system. This paper demonstrates that the combination of a T_2 measurement and diffusion measurements at various echo times (TE), based on the PFG MSE sequence, enable the accurate determination of diffusion constants which are less than a factor 2 apart. Several examples show that this new method gives errors of the diffusion constant below 10% in the case of 2 fractions being present, while the standard approach of a bi-exponential fit to the diffusion data under identical circumstances gives larger (>25%) errors. Applying this approach to water in apple parenchyma tissue the diffusion constant of water in the vacuole of the cells ($D=1.7\ 10^{-9}\ m^2/s$) can be distinguished from that of the cytoplasm ($D=1.0\ 10^{-9}\ m^2/s$). Also, for mung bean seedlings the cell size determined by PFG MSE measurements increased from 65 μm to 100 μm when the echo time increased from 150 to 900 ms demonstrating that the interpretation of PFG SE data used to investigate cell sizes is strongly dependent on the T_2 values of the fractions within the sample. Because relaxation times are used to discriminate the diffusion constants we propose to name this approach Diffusion Analysis by Relaxation Time Separated (DARTS) PFG NMR.

Introduction

The transient displacement of molecules, which can be quantified with Pulsed Field Gradient NMR, is a process of fundamental importance to comprehend physiological and physical processes at the microscopic level. Rather

[1] Reprinted from J. Magn. Reson A 116, 22-28 (1995).

than measuring the distance and frequency of successive and individual molecular jumps, PFG NMR samples the *average* displacement in a specified direction of an ensemble of molecules over a limited, specified time range (*1,2*). An ensemble is defined here as a group of identical molecules that experience a similar physical and chemical environment during the observation time of an experiment. From this average displacement (over a time range typically of 1 to 4000 ms) the Einstein self diffusion constant (D) can be determined. In a heterogeneous sample containing a set of barriers, e.g. membranes, the measured displacement yields information about distances between these barriers and their mutual arrangement, and about the permeability of the membranes (*2,3,4*). Knowledge of these parameters is essential for making an accurate assessment of various physiological processes, e.g. cellular growth, activity, orientation and function. For this reason much effort has been put into the development of theoretical models and experimental improvements related to diffusion measurements using PFG NMR (*5,6,7*).

A Spin Echo NMR signal of a heterogeneous region of interest (a voxel) is a superposition of the signals of different ensembles of molecules in a particular physical and chemical environment. Because of the relative insensitivity of NMR the number of distinguishable ensembles is limited. These ensembles are not necessarily coupled to spatial co-ordinates. Rather, a number of comparable compartments, e.g. a set of vacuoles or cytoplasm's of several different plant cells or water filled voids in a porous medium, constitute an ensemble and contribute to the NMR signal of the voxel. By consequence the measured diffusion constant of a specific ensemble represents an average value for these comparable compartments. An overall diffusion constant from a PFG NMR experiment of a heterogeneous voxel therefore comprises a broad spectrum of mobility's when it consists of several ensembles.

For diffusion measurements of a heterogeneous voxel to have any practical value it is necessary to further decompose the information contained in the echoes. Two well known examples of resolving diffusion constants are based on dissecting each individual echo in a NMR diffusion experiment. These methods are: (*i*) the combination of spectroscopy with PFG NMR (*8*) and (*ii*) the combination of imaging and PFG NMR (*9*). The use of spectroscopy is limited to those samples in which there are differences in the chemical shift of the molecules under investigation. The combination of PFG NMR and imaging is a valid approach for separating diffusion constants within a sample if the spectrum of molecular mobility's correlates with spatial co-ordinates. Heterogeneity below the resolution of the image causes the measured diffusion constant of the voxel to be an average

of several D's resulting in an apparent D, D_{app}. If neither method (*i*) or (*ii*) is applicable only widely different diffusion constants can be extracted from the data.

Unfortunately, many samples have compartments which are too small to image, have identical chemical shifts and small differences between diffusion constants. Because of lack of resolution a single D_{app} is often observed which is than erroneously interpreted as a single physical parameter. Due to this oversimplified interpretation of the PFG NMR data changes in D_{app} due to varying experimental or sample conditions are obscured and difficult to explain, e.g. the echo time (TE) dependence of D_{app} cannot be correctly interpreted (*10*). When it is assumed that the PFG NMR data can be described by a single exponential the TE-dependence of D_{app} arises from a different relative weighing of the ensembles with TE due to T_2 differences between the ensembles in combination with different D values. Instead of treating the TE-dependence of PFG SE measurements as an artefact (*10*), we have used this phenomenon to resolve the diffusion constants even when the differences between the D's are small. This goal can be achieved by T_2-analysis of a CPMG measurement and, using this information, subsequent analysis of the variation of D_{app} with TE. This procedure can be described as Diffusion Analysis by Relaxation Time Separated (DARTS) PFG NMR.

To test the performance of DARTS PFG NMR we have applied this procedure to heterogeneous samples of increasing complexity, i.e.

i) two separate tubes, one containing $CuSO_4$ doped water the other poly-ethylene glycol (PEG) or cyclohexane, respectively;

ii) a sample of apple parenchyma tissue;

iii) a sample of mung bean seedlings.

Theory

When the PFG SE sequence is used to study diffusion in a sample or voxel containing a set of distinguishable ensembles the echo time dependent signal amplitude is a superposition of these ensembles. The echo amplitude depends on the gradient factor $b = \gamma^2G^2\delta^2(\Delta-\delta/3)$ and TE as is described by:

$$S(TE,b)= \Sigma_n S_{0,n}\exp(-TE/T_{2,n}).\exp(-bD_n) \qquad [1]$$

where **n** denotes the number of distinguishable ensembles, G denotes the gradient pulse strength, δ the gradient pulse duration and Δ the gradient pulse separation, often equated with the observation or labelling time. Eq. [1] is an extension of the

conventional expression (*1*) of S(TE,*b*) which does not take multi-exponential T_2-relaxation into account. Plotting the natural logarithm of S(TE,*b*)/S(TE,0) versus *b* gives a Signal Attenuation Plot (SAP).

Diffusion constants and signal amplitudes of the different ensembles under investigation can be extracted by fitting the data to a multi-exponential function using a non linear least square (NLLS) fitting routine, generally based on a Marquardt-Levenberg algorithm (*11*). The reliability of the outcome of such a fit is determined by a set of factors: (*i*) the Signal to Noise Ratio (SNR; initial signal amplitude devided by the root mean square noise level) and the number of data points compared to the number of free fit-parameters, (*ii*) the duration and number of decades of the sampled decay curve compared to the ratio of the decay rates, (*iii*) the amplitude ratio of the ensembles and (*iv*) the presence of (non)-exponential artefacts. This last problem may arise from instrumental errors like dc fluctuations, field drifts or temperature changes, or sample induced errors, e.g. motion, *in situ* field gradients and the effects of restricted diffusion when prolonged observation times are used.

Assuming these artefacts absent some general SNR requirements can be defined. Kroeker and Henkelman (*12*) have extensively treated the accuracy of a non linear least square (NLLS) bi-exponential fit to T_1 and T_2 data. They noted that the required threshold SNR for a accurate fit, that is a fit with standard deviations (SD) of the fitted parameters below 10%, decreases with the ratio of the decay rates. For example; for a bi-exponential relaxation curve sampled over 3 decades with 200 data points, the threshold SNR increases from 20 to 2500 when the relaxation rate ratio of the two fractions drops from 10 to 2. Furthermore the threshold SNR is inversely proportional to the square root of the number of data points (*13*) and if one of the fractions is relatively small the threshold SNR also increases (*14*). In most diffusion experiments less than 20 data points are collected using *b*-factors which do not attenuate the spin echo more than a factor of 10 whereas a factor of at least 100 would be preferable to sample the baseline. Because of the stringent SNR demands which can only be met in some exceptional cases, generally a multi-exponential analysis of PFG NMR data is not a realistic option, especially in imaging mode.

A NLLS mono-exponential fit of the data to Eq. [1] results in a D_{app}. D_{app} is a weighed average of the present ensembles as can be shown by using two Taylor expansions, namely $e^x \sim 1+x$ and $\ln(1+x) \sim x$, of Eq. [1]:

$$S(TE,b)/S(TE,0) \sim \Sigma_n f_n(TE)[1-bD_n] \quad [2a]$$

$$\ln[S(TE,b)/S(TE,0)] = \ln\{\Sigma_n f_n(TE)[1-bD_n]\} \sim -\Sigma_n f_n(TE).bD_n = -bD_{app} \quad [2b]$$

$$f_n(TE) = S_{0,n}.\exp(-TE/T_{2,n})/S(TE,0) \quad [2c]$$

$\Sigma_n f_n(t)$ equals 1 for every echo time. When all diffusion constants are equal Eq. [2b] is not an approximation. The accuracy of the above approximation decreases with the ratio of the diffusion constants and the magnitude of bD_{app}. In practice it turns out that a NLLS mono-exponential fit of a bi-exponential curve is a good approximation when $bD_{app}<1.5$ and the diffusion constant ratio lies below 2. Higher ratios force the acceptable limit of bD_{app} downward.

From Eq. [2b] it is clear that D_{app} is determined by D_n as well as by the relative amplitudes, $f_n(TE)$, of the ensembles. As these relative amplitudes are a function of the echo time, so is D_{app}. Without exact knowledge of $f_n(TE)$ the behaviour of D_{app} with the echo time cannot be quantitatively solved. For this reason diffusion data for heterogeneous systems frequently can not be compared because the influence of TE on D_{app} was incorrectly ignored and therefore not reported. The first step in eliminating this problem is by determining the number of ensembles **n** and determining $f_n(TE)$ from a multi-exponential fit to data of a standard, separate, CPMG T_2-measurement. The second step is performing k PFG (M)SE measurements at k different TE's (k>**n**). We now have a set of D_{app} values at k echo times (Eq.[2a-c]). Since at every echo time the relative amplitude $f_n(TE)$ of the **n** fractions can be calculated, we arrive at a set of k linear equations (Eq. [2b]) relating the known coefficients ($f_n(TE)$) with k D_{app} values. This set of linear equations can be solved to obtain the values of D_n with e.g. a Singular Value Decomposition routine (SVD) (*11*). The number of diffusion constants which can be extracted is limited to the number of fractions which can be discriminated using a CPMG measurement. In principle the above procedure can also be performed using T_1 data and PFG NMR measurements with variable T_1 weighing.

Using the PFG STE sequence the problem of heterogeneity is less severe since T_1 values tend to have a smaller distribution than the T_2 values. This, however, does not eliminate the complication that water in different compartments may have different mobility's. Furthermore the apparently more homogeneous T_1 behaviour has been demonstrated to be partly the result of a fitting problem and exchange (*16*). The disadvantage of the PFG STE sequence is that a change in the observation time, Δ, to investigate restricted diffusion, is automatically followed by a change of the time at which the stimulated echo appears, since the middle

interval between the second and third 90° pulses, t_m, changes. This results in a different weighing of relevant compartments which can alter D_{app}. Hereby, alteration of the transient D, D(Δ), of an ensemble due to restricted diffusion can be masked or amplified by the difference in T_1 weighing of the relevant ensembles when changing Δ and t_m.

The loss of xy-magnetisation coherence is not only a function of the T_2 relaxation but also of chemical exchange and the presence of *in situ* field gradients. These factors cause a signal loss which depends on the time interval τ between the 90° and 180° pulses. Since the CPMG measurements are performed with relatively short pulse intervals the PFG NMR experiments should have a similar pulse interval. Using the PFG Multiple Spin Echo (MSE) sequence as described in reference (*15*) ensures that $f_n(TE)$ is at least comparable for both the CPMG experiment and the diffusion measurements. TE and 2τ are no longer identical, rather TE equals m*2τ, where m is the number of 180° pulses.

Experimental

All measurements were carried out on a spectrometer equipped with a 0.5 T Bruker electromagnet (Karlsruhe, Germany). The experiments were controlled by a S.M.I.S. console (Guildford, England) operating at 20.35 MHz. A microscopy probe, (I.D. 3 cm), with active shielded gradients was specially designed for this electromagnet by Doty Scientific (Columbia, USA) to fit firmly in the 10 cm air gap of the magnet. Gradients could be applied up to 375 mT/m for the **x** and **z** direction and up to 180 mT/m in the vertical **y** direction. Except for the **x** gradient which had a settling time of 800 μs the settling time of the gradients was about 100 μs. This allows studies with short gradient pulses and rf pulses close to these gradient pulses. The rf pulses were hard with a duration of 16 μs. The sample temperature was stabilised at 25 +/- 1 °C. For all measurements two averages were used with DC correction. Every experiment was repeated at least two times.

For CPMG experiments 2τ ranged from 0.8 to 2 ms. Larger pulse spacings caused small non gaussian fluctuations of the signal due to B_0 noise of the electromagnet. These fluctuations especially influence the reliability of a multi-exponential fit, as was done with the CPMG data, in contrast to the mono-exponential fits of the diffusion experiments. When necessary the number of echoes of the CPMG measurements could be extended to 64K, depending on the longest T_2, with a standard of 8K echoes. The TE/2 period of the PFG STE experiments was fixed at 6 ms with a variable middle period (t_m). In this period a

t_m crusher of 2 ms was used perpendicular to the direction of the diffusion experiment to avoid spurious echoes.

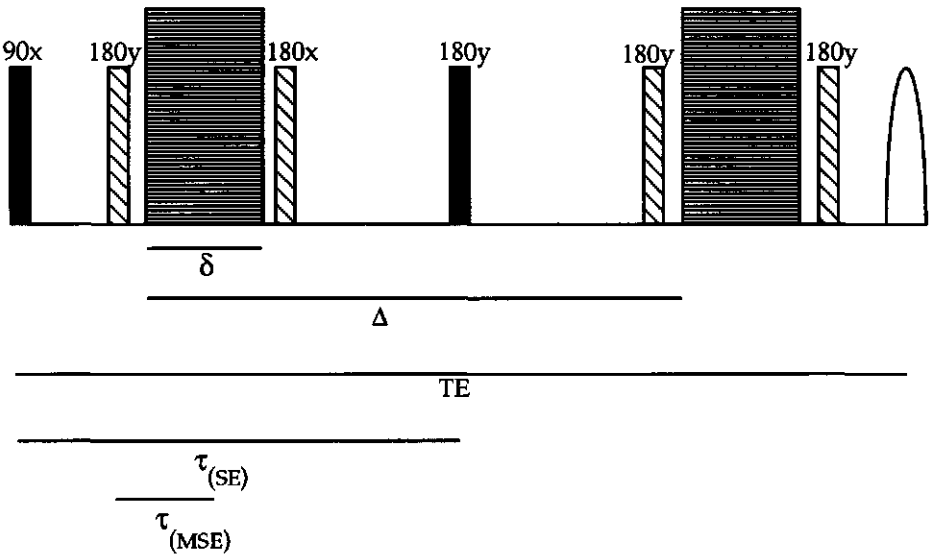

Figure 1. The PFG SE and PFG MSE sequences. Black bar rf pulses and gradient pulses are used in both sequences; the additional shaded rf pulses, which may vary in number, are only used for the MSE variant.

The PFG MSE sequence was used as described before in (*15*) and is depicted in Fig. 1, with 2τ normally set to 4 ms. In the experiments described below the pulsed field gradients were placed at the end of the train of π-pulses. The second of the two gradient pulses, each of 5 ms, was placed just in front of the last π-pulse. Depending on the required labelling time, Δ, the first gradient pulse can be placed anywhere in the train of π-pulses as long as the number of π-pulses between the gradient pulses is odd. The echo time can be modified by changing the number of π-pulses before the two gradient pulses. This approach has the advantage that Δ can be modified without affecting the TE. If the gradient pulse duration δ exceeds 2τ, the two periods in which the gradient pulses are given are set to $2\tau = \delta + 1$ ms. Because of the symmetry of these two periods refocussing of the magnetisation still occurs at τ ms after the last π-pulse. Thus 2τ may be modified independently of δ.

Setting 2τ to 4 ms was done as to reduce signal loss due to imperfect signal recovery of the XY-8 phase cycle scheme (*17*). When using large numbers of π-pulses, about 1K, between the two gradient pulses ($\Delta > 1$s) an extra signal loss (< 40 %) was found compared to experiments with the same TE (4 s) but with a single π-pulse (Δ=6ms) between the gradient pulses. The T_2 values of the investigated

objects did not show a 2τ dependence with 2τ between 0.8 and 2 ms. Setting 2τ of the PFG MSE sequence to 4 ms was not found to affect the described DARTS PFG NMR procedure. Shorter values of 2τ have been used but this cannot be combined with long observation times ($\Delta > 500$ ms) unless a better and more complex phase cycle scheme is used. With $2\tau > 10$ ms the B_0 noise diminishes the reliability of the diffusion measurement. To obtain a stable echo a small gradient of about 0.5 mT/m was applied perpendicular to the direction of the Pulsed Field Gradient (*18*). This small gradient was also applied during the CPMG measurements. The effect of this gradient on the T_2 is insignificant.

The fitting routines used to analyse the data were written using Interactive Data Language (RSI, Boulder, USA) and were based on the Marquardt-Levenberg algorithm (*11*).

Results

Using the PFG MSE sequence diffusion measurements were performed on a sample consisting of two tubes. One tube was filled with a 25 % PEG-2,000 solution and one with $CuSO_4$ doped water, respectively. Diffusion measurements on the individual solutions gave a diffusion constant for water of 2.25 10^{-9} m^2/s for the $CuSO_4$ doped water and 0.54 10^{-9} m^2/s for water in the PEG solution.

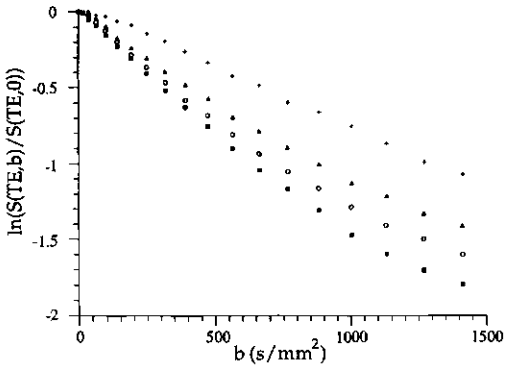

Figure 2. The SAP's of a two tube sample; one containing $CuSO_4$ doped water, one containing a 25% PEG solution, sampled at 4 different echo times using the PFG MSE sequence . TE= 54 (+), 108 (▲), 300 (□) and 600 ms (■). $\delta = 5$ ms, $\Delta = 18$ ms, $2\tau = 6$ ms.

The Signal Attenuation Plot (SAP) of Fig. 2 displays measurements at TE= 54, 108, 300 and 600 ms with 2τ=6 ms and Δ=18 ms. Because the T_2 of the PEG solution is

longer (T_2=0.81 s) than that of the $CuSO_4$ doped water (T_2=0.18 s) and D of the PEG-solution is lower, D_{app} decreases with TE. Although, in this case, the SAP's are visibly not single exponential a bi-exponential fit to the data did not yield accurate (SD~25%) diffusion constants. The data set was then analysed following the above mentioned DARTS PFG NMR procedure. That is, the first 8 gradient steps for all 4 echo times were fitted to a single exponent and $f_n(TE)$ was calculated on basis of a bi-exponential analysis of a separate CPMG measurement. The four linear equations, resulting from Eq. [2b], were then solved using a SVD routine.

	PEG solution (SD)	$CuSO_4$ doped water (SD)
$f_n(0)$	0.29 (4%)	0.71 (5%)
T_2 (s)	0.81 (5%)	0.18 (3%)
D (10^{-9} m^2/s) (DARTS)	0.5 (10%)	2.2 (8%)
D (10^{-9} m^2/s) (individual)	0.54 (3%)	2.25 (2%)

Table I. The relative amplitude $f_n(0)$ and T_2 values of $CuSO_4$ doped water and a 25% PEG solution determined with a CPMG measurement. Furthermore the diffusion constant determined with the DARTS PFG NMR procedure is compared with that of individual measurements on the two separate tubes. The standard deviation SD is given in percentages between the parenthesis.

The results of these calculations together with the CPMG data and the individual diffusion measurements are presented in Table I (SNR~250). Evidently, the calculated values for D using DARTS PFG NMR agree well with the D values obtained from the separate solutions, albeit with a somewhat lower accuracy. The accuracy however, can be increased by performing more diffusion measurements at a larger set of TE's.

The same PFG MSE experiment was performed on another two tube sample consisting of a tube filled with cyclohexane and a tube filled with $CuSO_4$ doped water, yielding a D of 2.3 10^{-9} m^2/s for the doped water and 1.4 10^{-9} m^2/s for cyclohexane (SNR~250), agreeing with measurements on the separated tubes, and values in literature (*19*). Results from PFG STE measurements, with constant TE, of the same sample at several Δ's suggested the presence of restricted diffusion since D_{app} decreased with increasing Δ (Fig. 3). Since the tubes were 6 mm in diameter restricted diffusion should not be observable on this time scale. The cause of this drop of D_{app} with Δ and thus t_m, is that the fraction with the longest T_1, cyclohexane, has the lowest diffusion constant. In the limit of t_m ---> ∞ D_{app} is expected to equal D for cyclohexane, being the fraction with the longest T_1.

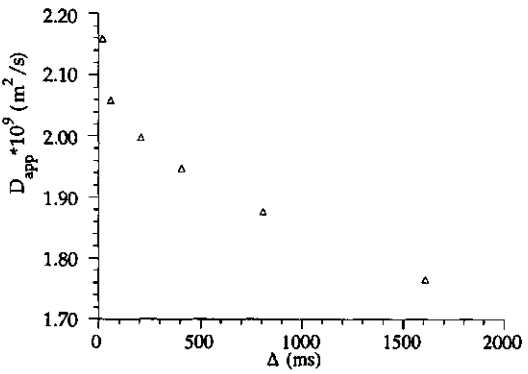

Figure 3. The dependency of D_{app} on the observation time Δ and the middle period t_m using the PFG STE sequence on a two tube sample with $CuSO_4$ doped water and cyclohexane. TE/2 = 6 ms, δ = 5 ms.

After testing the DARTS PFG NMR procedure on samples with known diffusion constants the studies were extended to samples without this additional check possibility, i.e. apple parenchyma tissue (Granny Smith) and mung bean seedlings respectively. A cylindrical part of a Granny Smith of 1 cm diameter and 1 cm length was cut out of the outer shell of the apple which contains cells which are relatively homogeneous in size and metabolically inactive. In this case, coupling between the T_2 values and actual compartments has been demonstrated by Snaar and Van As (*20*). For these measurements 2τ=1.6 ms, δ=5 ms, Δ=12 ms and the repetition time was set to 8 s for all measurements. The echo time was incremented in 8 steps from 20 to 1200 ms, three of these measurements are depicted in Figure 4 (TE=20,150 and 1200 ms). For this range of TE's the value for D_{app} increased from 1.51 10^{-9} m^2 /s to 1.71 10^{-9} m^2 /s (SNR=250, SD=1%) . These results combined with the results of a bi-exponential fit of CPMG data enabled the calculation of two diffusion constants, presented in Table IIa. The same CPMG data of the apple tissue could also be analysed using three, in stead of two, exponentials which lowers the χ^2 of the fit but increases the standard deviation of the fit-parameters (Table IIb). Using the three-exponential fit the shortest T_2 can be assigned to cell wall water and extra-cellular water, the middle T_2 to the cytoplasm and the long T_2 to the vacuole (*20*). The standard deviation of the three diffusion constants using the DARTS PFG NMR procedure however, now exceeds 20 %.

IIa.	Fraction 1 (SD)	Fraction 2 (SD)
$f_n(0)$	0.19 (5%)	0.81 (4%)
T_2 (s)	0.20 (3%)	1.21 (5%)
D (10^{-9} m^2/s)	1.0 (10%)	1.7 (9%)

IIb.	Fraction 1 (SD)	Fraction 2 (SD)	Fraction 3 (SD)
$f_n(0)$	0.08 (12%)	0.15 (8%)	0.77 (6%)
T_2 (s)	0.05 (10 %)	0.38 (7%)	1.3 (5%)
D (10^{-9} m^2/s)	1.4 (22%)	1.0 (25%)	1.7 (15%)

Table II a,b. The T_2 and relative amplitude values of Granny Smith determined using a) a bi-exponential analysis, b) a tri-exponential analysis of CPMG data, and the values of D determined using these values combined with diffusion measurements at 8 echo times, 2τ= 1600 μs, Δ =12 ms.

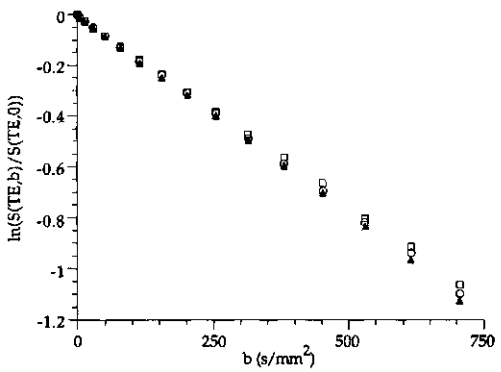

Figure 4. The dependency of D_{app} of apple parenchyma tissue on the echo time. TE= 20 ms (□), 150 ms (O) and 1200 ms (▲), TR=8 s, δ=5 ms, Δ= 12 ms and 2τ=1.6 ms.

Subsequently, we investigated parts of mung bean seedlings which display a wide spread of cell sizes, in contrast to the apple tissue. The aim of these experiments is to demonstrate the importance of the influence of the echo time on the determination of the size of cell compartments and how this problem can, to some extend, be circumvented. By analysis of the CPMG data three T_2's, namely 30 ms ($f_1(0)$=0.15), 210 ms ($f_2(0)$=0.55) and 550 ms ($f_3(0)$=0.30), were distinguished. Because of the large spread in cell sizes these T_2's could not be attributed to specific compartments, but the longest T_2 represents the T_2 of the larger vacuoles, as is supported by T_2 images of the mung beans (H.T. Edzes, H. Van As and D. van Dusschoten, unpublished results). At echo times of 150, 400 and 900 ms the Δ dependence of D_{app} was investigated with the PFG MSE sequence (Fig. 5). This

dependence can be analysed using equations derived by Tanner and Stejskal (*21*) or Snaar and Van As (*3*) which include two or more parallel impermeable walls. Using this geometry is not unreasonable since mung bean cells are cylindrical and only a small correction factor for the different geometry is required (*21*). Based on the two above models and assuming impermeable membranes the apparent compartment diameter at TE=150 ms was calculated to be 65 μm but at 900 ms this value had increased to 100 μm. Microscopic inspection suggested a diameter of the largest complete cells of about 120 μm.

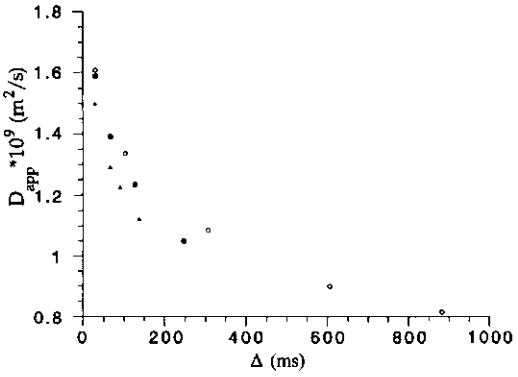

Figure 5. The Δ dependency of the apparent diffusion constant D_{app} in mung bean seedlings at a echo time of 150 (▲), 450 (■) and 900 (□) ms. δ = 5 ms, 2τ = 4 ms.

Evidently the compartment size determined at TE=150 ms, where all fractions contribute to the NMR signal ($f_1(150)$=0.5%, $f_2(150)$=55%, $f_3(150)$=45%), results in a compartment size which reflects an average value of all compartments contributing to the echo at that time. At a prolonged echo time the small cell compartments contributing to the NMR signal have decreased in amplitude ($f_2(900)$=11%, $f_3(900)$=89%) giving a value of the cell size which corresponds with the larger compartments which normally have the longer T_2 values.

Discussion and conclusions

Extracting accurate diffusion constants based using DARTS PFG NMR is not so much dependent on the accuracy of the (mono-exponential) fit of the diffusion measurements itself, but especially on the accuracy of the (multi-exponential) fit of the CPMG data. As goes for diffusion measurements, the reliability of a multi-exponential fit on CPMG data depends on the ratio of the decay constants. However, the number of data points obtained by CPMG experiments can be

extended to several orders higher than with a diffusion experiment without increasing the experimental time: a typical CPMG experiment may consist of 8000 echoes instead of the 20 or less *b*-increments which are normally used in a PFG NMR diffusion measurement. The above procedure breaks down when the T_2's of the ensembles differ less than a factor 2, still depending on the SNR, since this prevents accurate extraction of $f_n(TE)$. If for two compartments the T_2's are similar and the diffusion constants differ only slightly these constants cannot be resolved without additional changes to the condition of the sample e.g. by changing one of the T_2's by means of a relaxation agent.

A similar problem arises when three ensembles best describe the CPMG data but this does not give an acceptable accuracy for the diffusion constants as observed for the apple parenchyma tissue (Table II). For example, fitting with two exponentials gives standard deviations below 10% for the diffusion constants, but this fit causes a larger uncertainty in the interpretation of the source of the diffusion constants. However, judging from the results presented in Table II a and b, it seems that the contribution of the cell wall fraction, because of it's small amplitude and relatively short T_2, is small and has little effect on the calculated values of the other two diffusion constants. Therefore it seems reasonable to assign the largest D to the vacuole and the smaller one to the cytoplasm. The fact that the D of the fraction with the shortest T_2, when using the three compartment model, is higher than that of the cytoplasm seems surprising if one assumes a correlation between the T_2 and the translational diffusion. However, when one considers that the fraction with the shortest T_2 is a mixture of cell wall water and extra-cellular water (*20*) and these two fractions are in fast exchange this could explain the relatively short T_2 and the intermediate, average D.

It could be argued that it is better to fit the CPMG data to a continuous distribution of relaxation times. For apple parenchyma tissue this was done by Snaar and Van As (*20*), who obtained 3 distinct narrow peaks. On basis of these results they concluded that the three-exponential fit describes the data as well as the continuous distribution. Also, the continuous distribution fit is much more sensitive to the SNR (*22*) than the discrete fitting approach. In order to couple the relaxation times of the continuous distribution with diffusion constants belonging to the relaxation times a considerable increase of diffusion measurements at different echo times is required, since k should exceed **n**. This is, with the current experimental approach, time consuming. When a broad distribution of relaxation times is found, the best way to zoom in on the transient diffusion constant of the fraction with the longest T_2 is to use long echo times.

The effects of restrictions in the diffusion pathway have been mentioned to hamper a multi-exponential analysis of the diffusion data. These perturbations become more pronounced with larger *b*-factors and longer observation times. In samples with more than a single type of compartment contributing to the NMR signal methods like q-space imaging (*4*) become problematic. However, it suffices to measure the initial slope of the SAP at a set of different Δ's to extract the compartment dimensions (*6*). In heterogeneous samples this can be repeated for a set of TE's to encompass the problems posed by the multi-compartment behaviour of the sample. The combination of DARTS PFG NMR and Δ-dependent studies thus, in principle, allows zooming in on the water mobility of individual compartments .

An additional remark needs to be made: the signal decay per compartment ($f_n(t)$) calculated on basis of the CPMG data ignores exchange between compartments. In the presence of exchange $f_n(TE)$ determined by fitting to CPMG data does not truly represent the actual signal loss per ensemble. The coefficients used to solve the linear equations (Eq. [2b]) are modulated by exchange and the values of D_n become a mixture of those of the exchanging ensembles. The magnitude of this error depends on the exchange rate and does not dominate the results in case of slow or intermediate exchange as is the case in apple (*20*).

In conclusion, based on an accurate T_2 analysis it is possible to extract diffusion constants of a multi compartment sample with acceptable accuracy as has been demonstrated above. The interpretation of diffusion measurements in heterogeneous systems can thus be significantly improved by combining T_2 information from CPMG experiments with diffusion measurements at a set of different echo times. Using standard equipment a SNR of 200 is sufficient to discriminate diffusion constants which differ less than a factor 2, within half a hour. The effect of T_2 inhomogeneity over a voxel, which is often neglected, is therefore not a cumbersome artefact but a means by which water displacement in heterogeneous samples can be quantified and better understood.

Acknowledgements

The authors wish to thank Philips Medical Systems, Best, The Netherlands, for their financial support of this research. Also we wish to thank Prof.. T.J. Schaafsma for useful comments and critical reading of the manuscript.

References

1. E.O. Stejskal and J.E. Tanner, J. Chem. Phys. **42**, 288 (1965).
2. J.E. Tanner, J. Chem. Phys. **69**, 1748 (1978).
3. J.E.M. Snaar and H. Van As, J. Magn. Reson. A **102**, 318 (1993).
4. D.G. Cory and A.N. Garroway, Magn. Res. Med. **14**, 435 (1990).
5. D. Le Bihan, Magn. Res. Med. **14**,283 (1990).
6. J. Kärger, H. Pfeifer and W. Heink, Adv. in Mag. Reson. **12**, 1 (1988).
7. P.T. Callaghan, Principles of Nuclear Magnetic Resonance Microscopy, Clarendon Press, Oxford (1991).
8. P. Stilbs, Progress in NMR Spectr. **19**, 1 (1987).
9. K.D. Merboldt, W. Hanicke and J. Frahm, J. Magn Reson **64**, 479 (1985).
10. W. Heink, J. Kärger and H. Pfeifer, Z. für Phys. Chem. **170**, 199 (1991).
11. W.H. Press, S.A. Teukolsky, W.T. Veterling and B.P. Flannery, Numerical Recipes in C, Cambridge University Press (1992).
12. R.M. Kroeker and R.M. Henkelman, J. Magn. Reson. **69**, 218 (1986).
13. R.J.S. Brown, J. Magn. Reson. **82**, 539 (1989).
14. J. Pekar, C.T.W. Moonen and P.C.M. van Zijl, Magn. Res. Med. **23**, 122 (1992).
15. D. van Dusschoten, P.A. de Jager and H. Van As, J. Magn. Reson. **A112**, 237 (1995).
16. J.E.M. Snaar and H. Van As, J. Magn. Reson. **98**, 139 (1992).
17. T. Gullion, D.B. Baker and M.S. Conradi, J. Magn. Reson. **89**, 479 (1990).
18. M.I. Hrovat and C.G. Wade, J. Magn. Reson. **44**, 62 (1981).
19. M. Holz and H. Weingärtner, J. Magn. Reson. **92**, 115 (1991).
20. J.E.M. Snaar and H. Van As, Biophys. J. **63**, 1654 (1992).
21. J.E. Tanner and E.O. Stejskal, J. Chem. Phys. **43**, 3597 (1968).
22. R.J.S. Brown, G.C. Borgia, P. Fantazzini and E. Mesini, Magn. Reson. Imaging **9**, 687 (1991).

3.2 Unravelling Diffusion Constants in Biological Tissue by Combining Carr Purcell Meiboom Gill Imaging and Pulsed Field Gradient NMR[1].

Summary

A diffusion-weighted multi-spin-echo pulse sequence is presented which allows for simultaneous measurement of T_2, the fractional amplitude and the diffusion constant of different fractions. Monte Carlo simulations demonstrate an improvement of this sequence with respect to the accuracy of diffusion constant and fractional amplitude for slow exchange. Examples are shown for a simple phantom containing two fractions. In addition, experiments on cat brain in healthy condition and following occlusion of the middle cerebral artery show that the fractional amplitude and the diffusion constant of cerebral spinal fluid and normal brain tissue can be analysed within each pixel with acceptable accuracy.

Introduction

The unperturbed *in vivo* observation of the physiological state of cells or cell structures is an important objective of NMR Imaging. Several deviations of the normal physiological state of an organ or part of an organ can be evaluated by NMR, e.g. cancer, ischemia, multiple sclerosis, flow irregularities etc. (1). Detection of these deviations is of significant medical diagnostic value.

Resolution on a standard clinical MR imaging machine is insufficient to discriminate different cell types within one voxel or pixel. The NMR signal of a voxel is an integration over many cells and depends on different parameters. The translation of the NMR signal to a particular physiological state may therefore sometimes prove difficult. The introduction of specific NMR contrast mechanisms may clarify why the signal intensity of a particular structure deviates from its surrounding tissue. Given a particular water content the NMR signal intensity is modulated by T_1, T_2, magnetization transfer, translational diffusion and flow. By careful manipulation of the NMR magnetization these parameters can be studied independently. Carr Purcell Meiboom Gill (CPMG) sequences can be used yielding water content and T_2 information (2-4). Inversion Recovery sequences can be used to measure T_1 values or suppress fractions with long T_1 values like cerebral spinal fluid (CSF). Measurement of blood flow can be obtained in many different ways (5-7). Bolus injections with Gd-DTPA allow the determination of the regional cerebral blood volume (rCBV) (8,9).

[1] Submitted to Magn. Reson. Medicine.

By means of pulsed field gradient spin echo (PFG SE) or stimulated echo (PFG STE) experiments, translational diffusion and the effects of barriers on the diffusion process (10) have enabled the study of ischemia (11-13). However, the NMR signal in such experiments is a superposition of different ensembles. For example, in diffusion imaging of acute stroke, voxels contain intra and extra cellular water, some CSF and blood. In order to extract the diffusion constants of the different ensembles, an increase of the signal to noise ratio (SNR) or the number of gradient steps, in addition to relaxation measurements is often essential (14,15,16). The reliable determination of diffusion constants and fractional amplitudes may give a better understanding of the pathological processes.

In a recent improvement a combination of T_2 measurements with independent diffusion measurements at a set of echo times was performed (16). This method, *d*iffusion *a*nalysis by *r*elaxation *t*imes *s*eparated (DARTS) PFG NMR allowed even small differences of diffusion constants to be resolved on the basis of T_2 differences among the ensembles (16). The method was demonstrated for plant tissue. In order to use T_2 differences among animal tissues (17-19) we have adapted this method to include imaging and multi spin echoes. Here, we demonstrate the principles of the method in theory, in simulation and in *in vivo* experiments on cat brain.

Theory

In a spin echo experiment all ensembles with a net magnetic moment in the xy-plane contribute to the echo. When this initial spin echo is followed by a train of 180° pulses phase coherence is partially restored and the decay of the amplitude of each successive echo is governed by the T_2's of all the ensembles. In a PFG SE experiment only the initial echo is used. In separate scans the echo amplitude is reduced by displacement of water molecules in the presence of pulsed field gradients. Since an ensemble can be described by an initial amplitude S_0, a T_2 relaxation rate and a diffusion constant D, the spin echo amplitude of a voxel at the echo time TE can be described in case of no or slow exchange by:

$$S(TE,b) = \sum_n S_0^n . e^{\left(-TE/T_2^n\right)} . e^{\left(-\gamma^2 G^2 \delta^2 (\Delta - \delta/3) D^n\right)} \qquad [1]$$

,with the superscript n indicating the ensemble number, G the gradient strength, δ the gradient duration and Δ the observation or labelling time. The term $\gamma^2G^2\delta^2(\Delta-\delta/3)$ is often called the *b* factor.

In order to obtain a clear picture of water mobility in a heterogeneous voxel it may be necessary to extract the n diffusion constants from the data. The main problem with standard PFG S(T)E experiments is the reliable extraction of D^n and S_0^n since this requires the use of a multi-exponential non linear least square (NLLS) analysis of the data. The reliability of such a fit depends on the signal to noise ratio (SNR), the number of data points, the fraction ratio and the ratio of the diffusion constants (14,15,20-22).

It has been shown (16) that the accuracy of diffusion measurements can be enhanced when diffusion measurements at different echo times are combined with CPMG measurements which sample the T_2 of the different fractions within a voxel. This is not only caused by an increase of the effective SNR because of the extra diffusion measurements, but also because the T_2 values of these fractions serve as a label to discriminate the diffusion constant of the relevant fractions. Thus, the CPMG sequence serves to determine T_2^n and S_0^n. The diffusion constants D^n are determined by the pulsed field gradient measurements at different echo times (TE). However, this methodology (16) is not very time efficient since diffusion experiments have to be repeated at several echo times to ensure the desired extraction of D^n. Also, a separate T_2 measurement is required. Instead, we propose here that the first spin echo is followed by a train of 180° pulses like in a CPMG sequence, whereby the diffusion weighted magnetization of all ensembles is sampled directly at a set of echo times in a single scan. Doing so, diffusion and T_2 are sampled concurrently without loss of experimental time and the magnetization of an ensemble is now sampled in both the echo time domain and the *b* domain. The PFG CPMG measurements thus yield a 2D data set per pixel which can be described correctly with Eq.[1] for slow exchange. A 2D multi-exponential fit of the data can be performed using Eq.[1].

The extension of the initial diffusion weighted spin echo by a train of 180° pulses gives a pulsed field gradient CPMG (or CPMG-like) Imaging sequence. Because the number of data points is increased an increase in the effective signal to noise ratio is obtained (23) even when T_2 differences can not be used to unravel the diffusion constants. By echo summation the increase in SNR, η, is given by

$$\eta = m^{-0.5} \Sigma_i \exp(-iTE/T_2), \qquad [2]$$

with m being the total number of echoes and i=1,2.....,m. The optimal SNR increase is achieved when echoes are summed up to $iTE/T_2=1.26$ (23).

For the data of a PFG CPMG imaging sequence to be useful all subsequent echoes should experience the same initial diffusion weighting. Therefore all

coherences other than the multiple spin echoes should be avoided. Stimulated echoes, and other unwanted coherences, can arise which have not been properly diffusion weighted. These spurious echoes not only disturb the diffusion measurements, but also give rise to artefacts within the spin echo images. To prevent the spurious echoes it is necessary to select a unique coherence pathway of the spins, which should be **p**=[0,1,-1,1....] for a CPMG sequence (24). Several approaches can be used to reach this objective. Two possible solutions have been pointed out (25,26), i.e. phase cycling and the employment of gradient crushers. If gradients are used the reduction of the intensity of the unwanted echoes is dependent on the pixel size and the crusher gradient strength. The suppression factor f, can be expressed as (27):

$$\frac{1}{f} = \left| \frac{1}{(r_2 - r_1)} \int_{r_1}^{r_2} e^{-i\gamma G r t_1} dr \right| \qquad [3]$$

, with r_2-r_1 being the pixel size, t_1 the gradient pulse duration and G the gradient pulse strength.

It should be noted that it is assumed that exchange between the ensembles is absent or slow with regard to the longest T_2. For intermediate exchange magnetization between the ensembles is partially mixed causing the T_2 values, fractional amplitudes and diffusion constants to mix partially also. The ensembles can, however, still be discriminated. For fast exchange the ensembles are indistinguishable unless the average exchange time is still long with regard to Δ and the diffusion constant of the ensembles are distinguishable. The mathematical treatment of (hindered) exchange is beyond the scope of this paper and the effects of exchange are ignored for this reason.

Methods

In Figure 1 a schematic is presented of the new PFG CPMG sequence. Every 180° pulse is sandwiched between one, two or three pairs of sine shaped crusher gradients in different directions with adjustable gradient strength. In total 27 combinations of the net gradient vector were selected in this way thereby effectively preventing refocussing of unwanted magnetization when repetition of

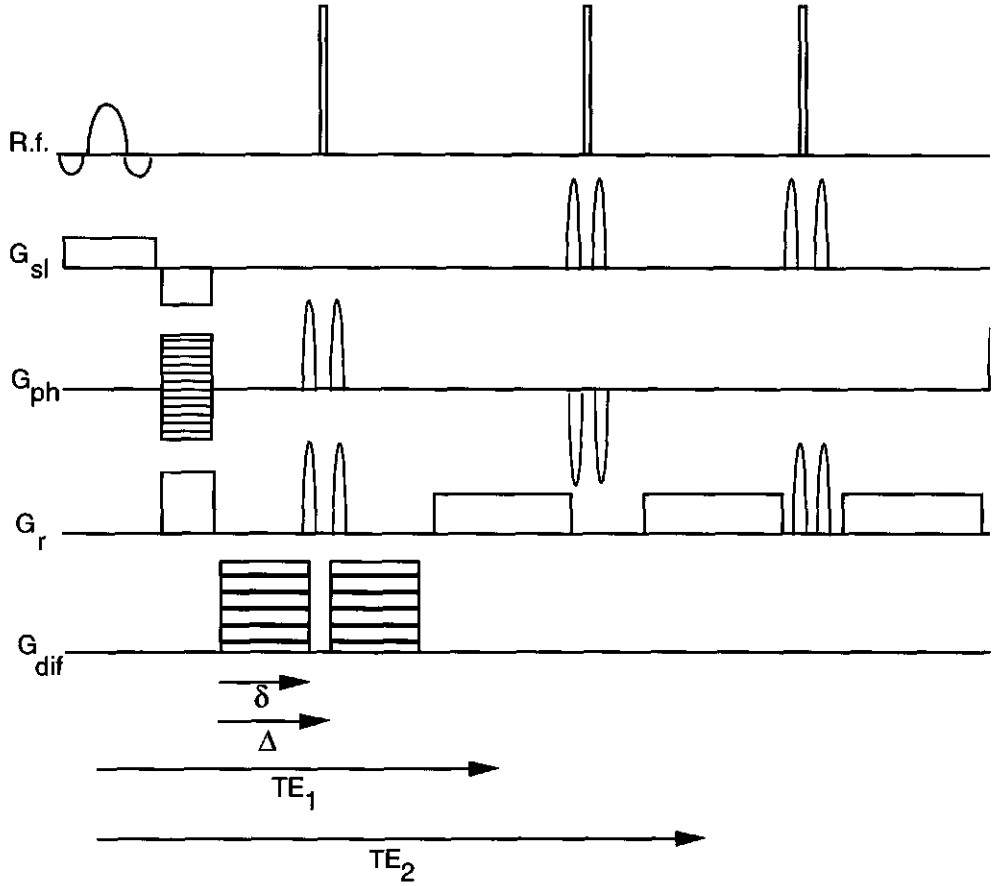

Figure 1. Schematic presentation of the Pulsed Field Gradient CPMG Imaging sequence. The sine shaped figures represent the gradient crushers which are used in all directions and are interlaced with the read gradients. The crusher gradients are placed in pairs around the hard 180° pulses (the thin beams of the top line). In all experiments δ = 8 ms and Δ = 15-30 ms. The pulsed field gradients were normally used in the slice direction.

identical or similar crusher gradient pairs does occur (27). Using sine shaped crushers with t_1=2 ms, Δ=3 ms and G= 30 mT/m the *b* factor of these crusher gradients is almost negligible, namely 0.5 s/mm^2. The suppression factor f, however, equals about 80 (*cf.* Eq[3]). The read gradients also cause a small signal reduction because of diffusion. For a field of view of 70 mm and a 128x128 data matrix a *b* factor of 1 s/mm^2 for the first echo is obtained which increases with every subsequent echo. This causes a reduction of the apparent T_2 of a few percent. However, the calculated values of the diffusion constants are not affected when the effect of the read gradients and the crusher gradients is included in the calculations.

The minimum echo time of a diffusion experiment is to a large extend determined by the maximum gradient strength of the NMR spectrometer and the lowest diffusion constant. Since a signal reduction of about 90% compared to the non diffusion weighted echo amplitude is normally advisable for accurate bi-exponential analysis of the diffusion data a b factor of about 2000-3000 s/mm^2 is desirable when D equals 0.4×10^{-9} m^2/s. Using a maximum gradient of 160 mT/m the minimum echo time is approximately 25 ms ($D_{min}=0.4 \times 10^{-9}$ m^2/s, δ=8 ms, Δ= 15 ms). The spacing between the subsequent echoes can be reduced since no further pulsed field gradients are required. This ensures adequate sampling of the ensembles with a short T_2. Fractions with a T_2 shorter than 15 ms are not measured with this particular implementation of the PFG CPMG sequence.

The phase of the soft 90^o pulse and of the receiver is alternated every phase encoding step. This ensures that DC artefacts are shifted to the edge of the image.

Using the PFG CPMG sequence a set of images is acquired, which, when analysed on a pixel by pixel basis, yield amplitude, diffusion and T_2 maps. The 2D data set per pixel, with diffusion and relaxation information, can be analysed in several ways. Here we only report the use of a 2D fitting routine, with two ensembles in Eq.[1]. This was by far the most robust and reliable method (unpublished results).

One of the problems with fitting the actual data was the generation of the initial guess. This requires the generation of 6 parameters per pixel, excluding a baseline. Since the PFG CPMG sequence is used to discriminate diffusion constants which cannot easily be extracted using a 1D bi-exponential fit of the diffusion data the initial guess generated in this way is unreliable, not robust and often gives useless starting points. The same sometimes holds for the T_2 fit. Therefore two separate single-exponential fits, one in the echo time domain and one in the b domain, were performed and of these average values the other T_2, D and amplitude values were guessed on basis of fixed ratios (T_2^a / T_2^b=0.25, D^a/D^b=0.25 and S_0^a/S_0^b=3.33) between the fit parameters . Even when this initial guess is far off (>50%), this generally had little effect on the outcome of the fit.

All experiments were carried out on a CSI 4.7 T instrument (GE, USA) at the NIH equipped with shielded gradients. The accuracy of the DARTS PFG CPMG Imaging sequence and the 2D fitting routine was first tested on a sample consisting of two plastic spheres. One was filled with tap water, the other with a 20 % w/w gelatine solution. These spheres were imaged, using a birdcage rf coil, at 17^o C. Furthermore five cats were studied to examine whether the overall apparent diffusion constant is dependent on TE and, if so, whether the source of this change can be indicated. For these experiments a surface coil was used for

transmission of the rf and reception of the NMR signal. A middle cerebral artery (MCA) occlusion was successfully performed in three of these cats so that ischemic regions in the brain could be pointed out on diffusion maps. NMR experiments were performed between one and twelve hours after the MCA occlusion. The animals were anaesthetised with ketamine/acepromazine and maintained on isoflurane using a ventilator. Reduction of motion artefacts was achieved by placing the cat head in a stereotaxic head holder and firmly fitting a surface coil (diameter 5 cm) on top the head (28).

Simulations

To investigate the accuracy of the PFG CPMG and the 2D analysis of the data Monte Carlo simulations (MCS) were performed, comparable to those of J. Pekar et al. (14). Here we focus on a CSF-like fraction to investigate whether this fraction could be quantitatively analysed with acceptable accuracy. Making Monte Carlo simulations for the PFG CPMG Imaging sequence with two compartments per voxel leaves room for varying 6 NMR parameters plus the SNR, the number of data points and the distribution of these data points over the decay curve. Therefore the parameters were limited in such a way that the data set compares with those from actual NMR experiments on cat brain. One fraction, a, was taken to represent brain tissue and its relative amplitude was fixed at 90 %. The other, b, was taken to represent CSF with a relative amplitude of 10 %, a shorter T_2 and a lower diffusion constant. The ratio of the diffusion constants, the T_2 ratio and the SNR were varied for these Monte Carlo simulations. The SNR represents the signal-to-noise ratio of the first echo, dividing the echo amplitude by the root mean square noise. The outcome of the fits was considered acceptable when the standard deviation (SD), determined for a number of simulations was below 20%. Determining these relatively large standard deviations with acceptable accuracy does not require many simulations. Therefore the number of simulations was set to a minimum of 100.

The distribution of the data points over the two decay curves was such that TE=20*i+40 ms (i=0,....,31) and b=k*16^2 s/mm^2 (k=0,.....,8). For comparison with standard PFG SE measurements an echo time of 40 ms was used with the same b values as were used in the PFG CPMG simulations. For the simulations of the PFG SE experiment we assumed D^{csf} =2.0x10^{-9} m^2/s, D^{brain}=0.5x10^{-9} m^2/s, S_0^{CSF}=0.1 and S_0^{brain}=0.9.

The generation of the initial guess for the 6 parameters was achieved by performing bi-exponential fits in both the TE and b-domain, in contrast to the

initial guess generation for the imaging experiments. This is necessary to make a fair comparison between the 1D fit in the *b*-domain and the 2D fit over the whole data plane. Both 1D fits generate initial guess values for S_0^n, but only the values acquired with the fit of the artificial CPMG data were used as such. The Monte Carlo Simulations (MCS) and the fit routines, based on the Marquardt-Levenberg search algorithm, were programmed using Interactive Data Language (IDL) from RSI (Boulder,USA).

Results

Monte Carlo Simulation

First a standard PFG SE experiment was simulated. A total of 250 simulations were used to compare the reliability of the standard PFG SE with the PFG CPMG experiments. For an acceptable result the SNR had to be increased to 450, a result very similar to that found by Pekar *et al.* (15) even though somewhat different parameters where used in the latter study.

When bi-exponential analysis of the diffusion measurements becomes difficult, the use of T_2 information is advantageous for discriminating the different fractions. The improvement in the determination of D of the CSF-like fraction is illustrated in Figure 2. The fitted D for the first 100 MCS runs of both the 1D and the 2D fit routine are depicted. The dashed line connects the results of the 1D fit and the solid line those of the 2D fit. Here T_2^a=60 ms and T_2^b=240 ms, with the other parameters identical to the PFG SE simulations. The SD of D^b reduces from 54 % to 7 %. Furthermore the average diffusion constant obtained by the 1D bi-exponential fits is 18 % too low. Note also that the number of outliers drops to zero when using the 2D fit routine. The values for D_n of the 1D fit were used as initial guess values for the 2D fit routine. In Table Ia the accumulated results are given of 200 MCS runs where the SNR of the first data point was set to 80, the T_2 ratio was fixed at 0.25 (fast T_2 of 60 ms) and the diffusion constant ratio was decreased from 0.5 to 0.2, with the lower D^a (large fraction with the short T_2) fixed at 0.5×10^{-9} m^2/s. Only the SD values of the amplitude and the diffusion constant of the smallest fraction are given since these have SD values almost 10 times higher than those of the major fraction. Clearly, the reliability of the fits increases when the diffusion constant ratio diverges from one. However, the reliability of the 2D fit is not only dependent on the diffusion constant ratio, but also on the ratio of the two relaxation times.

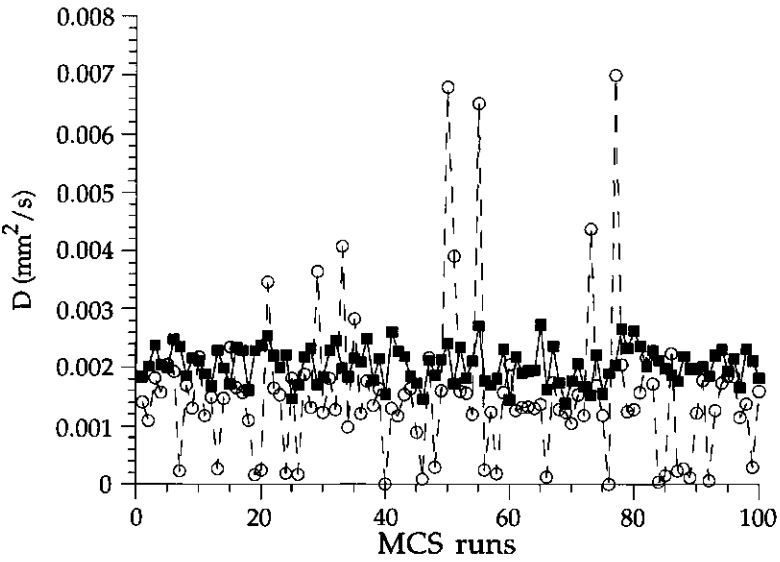

Figure 2. Fit results of 100 Monte Carlo Simulation runs for the diffusion constant of a CSF-like fraction. Input parameters: D^a=0.0005 mm^2/s. D^b=0.002 mm^2/s,T_2^a=60 ms, T_2^b=240 ms, S_0^a=90, S_0^b=10. The dashed line connects the results for D^b (○) for each successive MCS run using a standard bi-exponential fit routine. The solid line connects the results of each MCS run using a 2D bi-exponential fit routine (■) The outcome of the standard bi-exponential fit was used as the initial guess value for the 2D bi-exponential fit routine. SNR level of 80 at TE=40 ms.

In Table Ib. the accumulated results of 200 MCS runs with variable relaxation time ratios but with fixed diffusion constants are presented. When the T_2 ratio becomes smaller than 0.333 and the diffusion constant ratio equals 0.25, a 2D data set with a SNR of 80 can be analysed with sufficient reliability. In Figure 3 the SD values of all parameters of the second, smaller fraction are given as a function of the T_2 ratio (D^a/D^b=0.25). The fact that the SD of D^b decreases when the T_2 ratio diverges from one is caused by the coupling of the T_2 and the diffusion constant by the initial amplitude. Since a large difference in relaxation times increases the reliability of S_0^n, the fit routine has less freedom in finding a value for D^n. Consequently the SD of the diffusion constants also diminishes. The increase of the standard deviation of T_2^b with increasing T_2 ratio is caused by insufficient sampling of its T_2 decay curve. This increase can easily be avoided by modifying the distribution of the echo times over the decay curve, that is, using longer TE

values (TE=(i+1)*40). This causes the SD for T_2^a to increase slightly from 1.8 to 2.1 %, but since this value is one order of magnitude lower than the SD for the minor CSF-like fraction this does not affect the overall accuracy of the measurement. This example demonstrates that the choice of the NMR experiment parameters should be such that the smallest fraction is optimally measured since this gives the best overall accuracy of the fits. However, this optimisation only works when the values of the fitted parameters have a low correlation (15), which is the case for these 2D fits.

A.	SD,S_0^b(%)	SD,D^b (%)
D^a/D^b=0.5	25.5	11.6
D^a/D^b=0.333	22.6	13.1
D^a/D^b=0.25	17.8	13.5
D^a/D^b=0.2	15.9	13.8

B.	SD,S_0^b(%)	SD,D^b (%)
T_2^a/T_2^b=0.5	24.1	18.2
T_2^a/T_2^b=0.333	19.8	14.6
T_2^a/T_2^b=0.25	17.6	13.5
T_2^a/T_2^b=0.2	14.6	9.3

Table I. (a) The standard deviation of the fit results of the diffusion constant and the fractional amplitude of a small (10%) CSF-like fraction, after 100 MCS runs as related to the diffusion constant ratio. Here the T_2 ratio equals 0.25, other parameters as described in the text. (b) The same as in (a) but now related to the T_2 ratio. The diffusion constant ratio is set to 0.25.

The 2D fitting routine also calculates SD values per fitted parameter. The magnitude of these SD values are only slightly smaller (10 to 20%) than those calculated from the spread of the fitted results. This is contrary to the 1D analysis of the diffusion data or relaxation data alone where the internally calculated SD values are more than 2-3 times lower than the overall SD values (14). So, the statistics calculated within the fitting routine can now be used to assess the reliability of the fit, assuming that the noise is Gaussian.

An attempt was made to investigate the limits within which a perfusing fraction of 10% could be measured. Although the SNR demands for successful separation of the blood perfusion fraction are almost identical to that for separating a CSF-like fraction and brain tissue it was found that by introducing a very small CSF fraction such a separation is not feasible. Even a CSF fraction as low as 1% reduces the fitted perfusion constant from 20×10^{-9}, the input value, to

$10x10^{-9}$ m^2/s. With a 3% CSF fraction the measured diffusion constant of the second fraction begins to approach the diffusion constant of CSF (data not shown).

Rf pulse errors were simulated by an additional signal attenuation of $(1-\cos\Phi)^i/2^i$, where Φ is the pulse angle and i the number of the echo. This reduced the T_2, primarily that of the longest T_2. However, even a pulse error of 20% showed no significant reduction of the reliability of the fit of the diffusion constants and S_0^n.

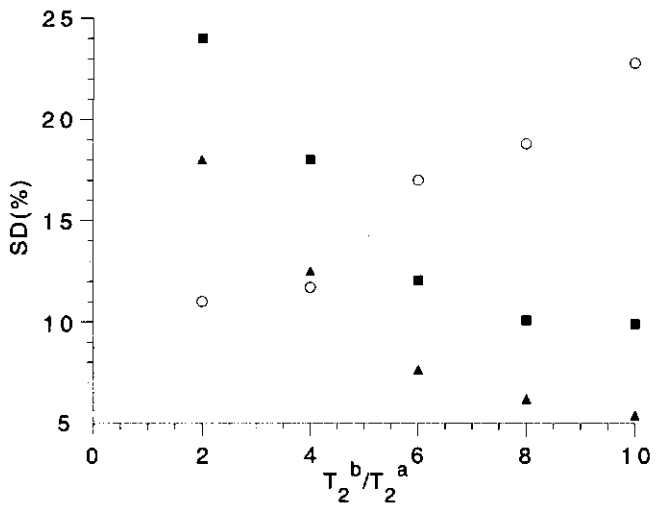

Figure 3. Dependency of the standard deviation of different parameters for the 2D bi-exponential fit routine on the T_2 ratio. Other parameters as described in the text and in the caption of Figure 2. The shortest T_2 was fixed at 60 ms; only the long T_2 was varied. The SD of the parameters was calculated on basis of 100 MCS runs for each T_2 ratio. SNR level of 80 at TE=40 ms. (■) SD of S_0^b, (▲) SD of D^b and (○) SD of T_2^b.

In vitro NMR

The PFG CPMG sequence was first used on a phantom in imaging and projection mode. The first was done to measure the T_2 and D of each sphere separately, as an external reference, the second to mimic a bi compartment voxel. Nine diffusion steps were taken, *b*-values ranging from 0 to 2000 s/mm^2, each with 24 echoes, TE ranging from 40 to 400 ms. The results of the 2D bi-exponential fit of the projections are presented in Table II and are compared with the results of the individually imaged spheres. Despite the fact that the diffusion constant ratio lies well below 2, the standard deviation of the diffusion constants is

approximately 4%. It is important to note that in this case the T_2 ratio equals 10 which simplifies the fit. Even at a SNR of 500 this precision is much better than can be expected for such a small diffusion constant ratio for a normal bi-exponential fit routine. Since the standard deviation is inversely proportional to the SNR it can be calculated that for a SNR of about 100 acceptable results from the fit of this particular data may be obtained. Using the 1D fit routine in the *b*-domain the standard deviation exceeds 25% and the fitted diffusion constants are 10% too low. This error arises from the fact that absolute images were used giving a baseline at the noise level. The 1D fit routine is very sensitive to the presence of a baseline, whereas the 2D fit routine is not.

	Imaging mode (SD)	Projection mode (SD)
T_2 water (s)	1.18 (0.03)	1.14 (0.08)
T_2 gelatine (s)	0.124 (0.003)	0.122 (0.006)
D water (10^{-9} m^2/s)	1.78 (0.04)	1.71 (0.07)
D gelatine (10^{-9} m^2/s)	1.21 (0.03)	1.20 (0.05)

Table II. Comparison of independent single exponential fits in the TE and b-domain of separate spheres in imaging mode and 2D bi-exponential fits of an overlapping region in projection mode. One sphere contained doped water, the other a 20 % gelatine solution. Parameters were: TE=30 +i*20 ms, δ=8 ms and Δ=15 ms.

In vivo NMR

Cats were studied using the same sequence and fitting routine as described above. In Figure 4a and 4b D_{app} maps at TE = 40 and 80 ms are depicted, obtained by a single-exponential fit of all pixels above an arbitrary signal limit just above the noise level. Negative values, which occurred in less than 1% of all instances due to low signal amplitude, for D were ignored. Figure 4c displays a subtraction image of Figure 4a and 4b. Because of the slice thickness of 4 mm some voxels also sample the upper part of the ventricles, which are filled with CSF.

Figure 4. Maps of D_{app} using a single exponential fit of normal cat brain at TE=40 ms (a) and TE=80 ms (b), δ=8 ms, Δ= 20 ms. Figure (c) is a subtraction image of (b) and (a). (d) Represents the fractional amplitude S_0^n of those fractions with a fitted T_2 exceeding 250 ms. Diffusion gradients in the slice direction, perpendicular to the image

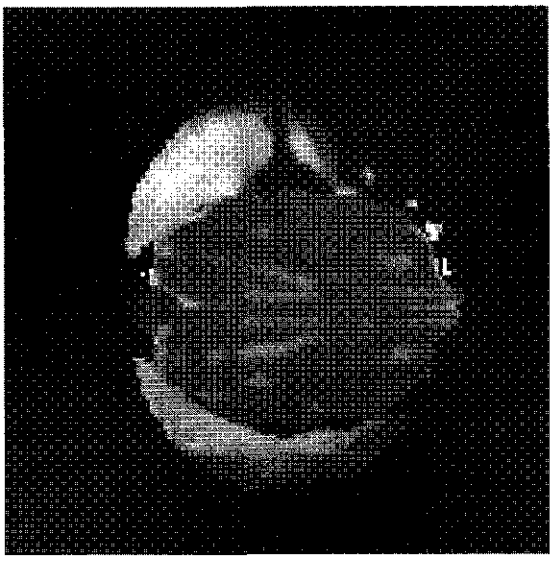

A

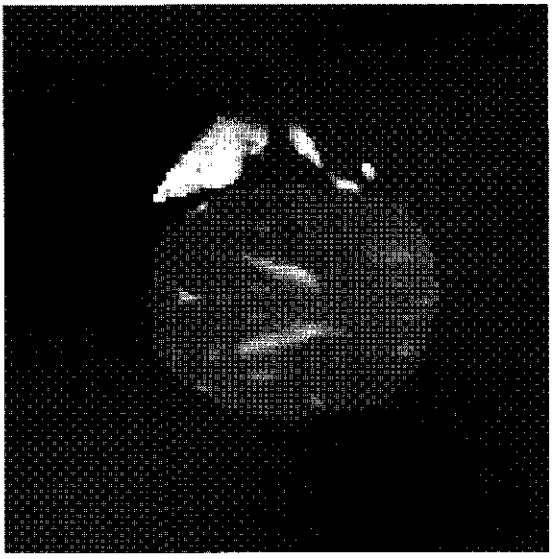

B

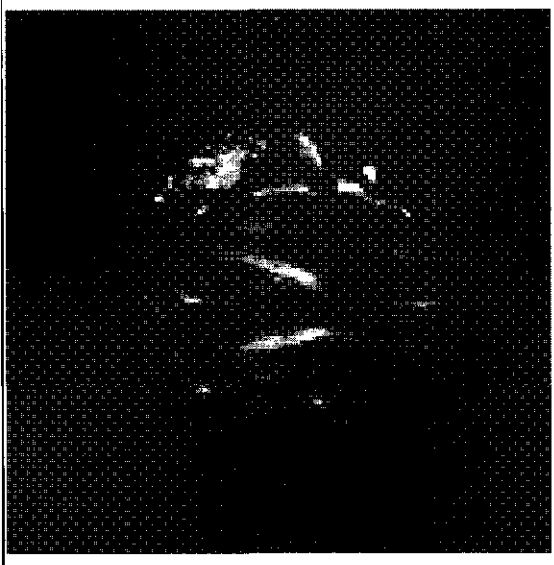

C

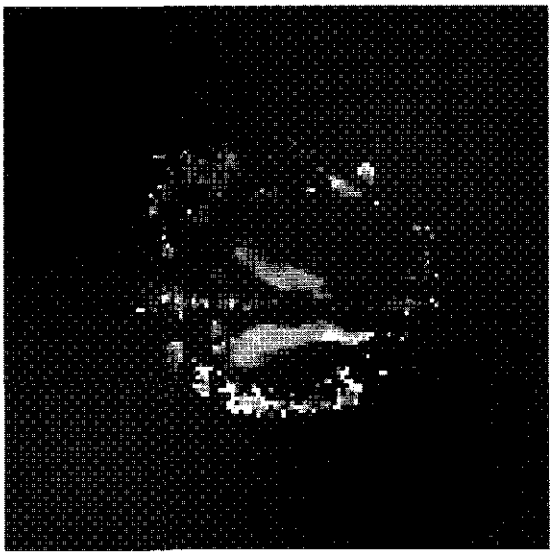

D

A

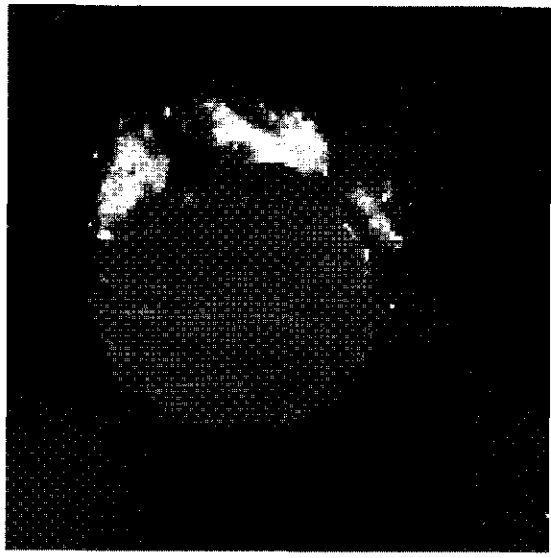

B

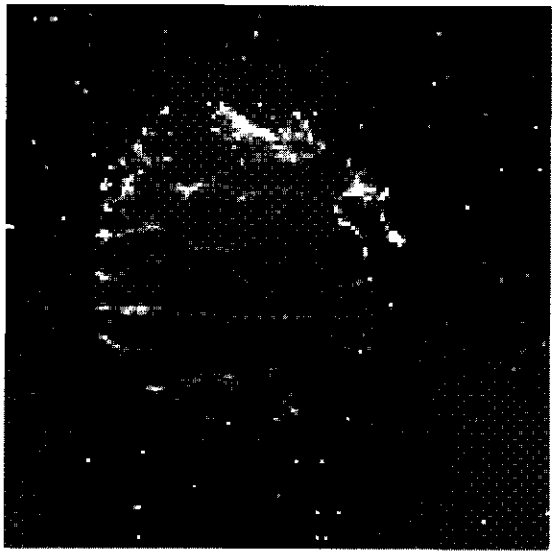

C

D

It is in these voxels where the largest increase of D_{app} with TE occurs, on average from 0.75 at TE=40 ms to $1.3x10^{-9}$ m^2/s at TE=340 ms. In other voxels, the dark ones in Figure 4c, D_{app} increases from 0.55 to $0.65x10^{-9}$ m^2/s. Figures 5a and 5b show a cat brain with a ischemic region in the left brain (upper half of the image), obtained with TE values at 40 and 100 ms, respectively. The increase of D_{app} in the ischemic region follows a similar pattern to that of the regions without the ischemia. Here, D_{app} increased with TE from 0.35 to $0.60x10^{-9}$ m^2/s. From the images at prolonged echo times, it is clear that the tissue at the edge of the cat brain has lost intensity because of rf inhomogeneity.

To quantify the contributions of CSF, blood, and brain tissue, to D_{app} the 2D bi-exponential fit routine was used for all pixels within the brain. Six fit parameters per pixel were generated. Since voxels can be homogeneous, having only one fraction, it sometimes happens that two or three parameters are not physically reasonable and have a large standard deviation. Therefore, only those pixels with a calculated SD for all parameters below 50%, positive values for all parameters and a comparable relatively low chi-square (χ^2) were accepted. This resulted in 5% of the pixels being disregarded. These were primarily pixels with a very low CSF content (mostly white brain tissue). The chi-square never converged to 1, because of rf pulse errors and small motion artifacts.

In Figure 4d and 5d spin density images of all ensembles with a T_2 exceeding 250 ms are depicted. Since the T_2's, diffusion constants and amplitudes are coupled by Eq.[1] it is possible to make a selection of pixels on the basis of e.g. the T_2 and display the spin density of those fractions with the selected relaxation time range. Although the selected regions in Figures 4d and 5d overlap with most of the brighter regions in Figures 4c and 5c the agreement is not perfect. One reason for the mismatch is the use of a surface rf coil not being perfectly parallel with the image plain. This induces shorter T_2 values for right half of the brain (lower part of the image) where the B_1 field was lower (Figure 5d), thus making a proper T_2 selection criterion more difficult. On the basis of Figure 4d it may be concluded that the fractions with a long T_2 mostly agree with regions where we expect CSF (the ventricles).

Figure 5. Maps of D_{app} using a single exponential fit of a cat brain with an ischemic region in the left brain (upper half) at TE=40 ms (a) and TE=100 ms (b). Same experimental parameters as in Figure 4. Figure (c) is a subtraction image of (b) and (a). (d) Represents the fractional amplitude S_0^n of those fractions with a fitted T_2 exceeding 250 ms. Diffusion gradients in the slice direction, perpendicular to the image.

In Figure 6 a histogram of the D values of those voxels with two fractions is given. Three peaks are evident, the 'normal' D (0.5×10^{-9} m^2/s), the D (0.3×10^{-9} m^2/s) of the ischemic region and a fast D (2.9×10^{-9} m^2/s). The latter fraction is attributed to CSF, since *1*) this values is very close to that of free water at 37 °C, 2) it is primarily found in the ventricles and 3) the T_2 lies around 350 ms (this relatively short value for CSF being caused by accumulative rf pulse errors). The large spread of the diffusion constant of CSF is caused by contribution of the CSF fractions smaller than 5%, making a positive identification of CSF or perfusing blood very difficult. These small fractions have larger standard deviations because of their low amplitude and therefore cause a broad range of diffusion constants in Figure 6. In none of the images any evidence of perfusion could be found. In the ischemic region no evidence was found of T_2 changes of the brain tissue fraction. Neither could an increase of the CSF fraction be detected in the ischemic regions.

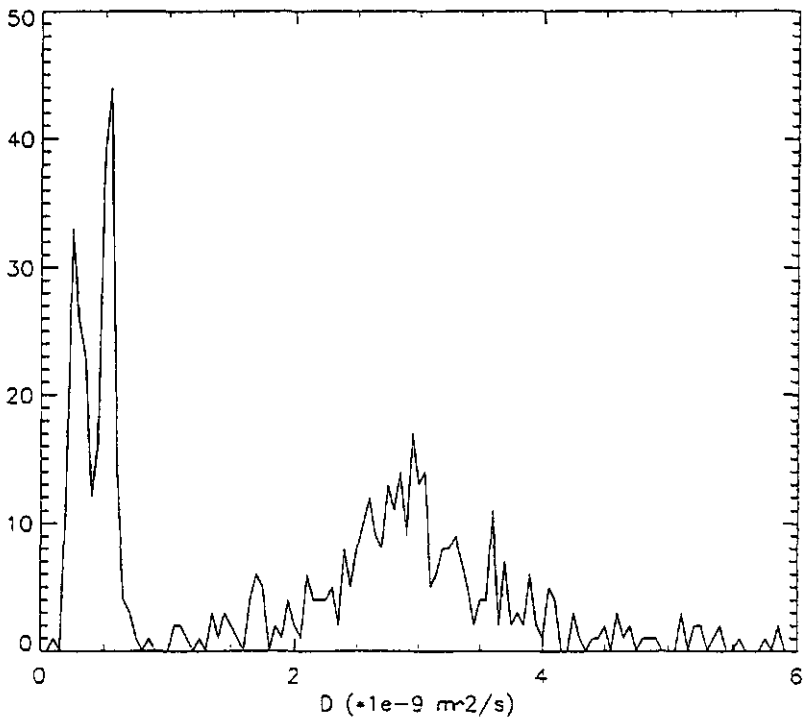

Figure 6. Histogram of the diffusion constants of the total cat brain as fitted with the 2D bi-exponential fit routine of the ischemic cat brain depicted in Figure 5.

Discussion and conclusions

Both the Monte Carlo simulations and test experiments have shown that the PFG CPMG imaging sequence allows separation of diffusion constants and fractional amplitudes in the case of slow exchange with an adequate reliability. The diffusion constants and fractions can be found using this sequence under conditions where the standard PFG SE approach no longer gives reliable results. The phantom experiment shows that even small differences among the diffusion constants may be separated given an adequate difference of the T_2 values among two ensembles. In case of a fractional ratio of 9 and a D ratio of 0.25 the PFG SE experiment requires an SNR of about 450. Because echo summation can be used when working with the PFG CPMG sequence the threshold SNR can be lowered in this way. The optimum SNR threshold reduction for 24 echoes is 4.9 ($T_2=\infty$). However, in practice the SNR threshold reduction is somewhat lower. In case of a T_2 of 100 ms and TE values of 40 +i*20 ms, only 5 echoes can be used to lower the SNR threshold. The use of images obtained at echo times larger than 126 ms leads to SNR deterioration. Therefore, based on Eq.[2] the SNR threshold can be reduced to only 300 in the above example. However, upon using the T_2 difference the SNR threshold can be decreased to 80, for a T_2 ratio of 4. In principle even lower SNR figures suffice to analyse a bi-compartment system of the mentioned composition by shortening the TE values and increasing the number of echoes.

In the cat studies CSF could be discriminated from brain tissue using both the T_2 and D differences. This analysis is more reliable than hitherto possible using separate measurements. A SNR in the order of 60 to 80 suffices to discriminate CSF from the brain tissue. Improvement is possible since a surface coil was used generating rf pulse errors that lower the measured T_2 of the CSF fraction. Reliable evidence of perfusion could not be found in any of the cats. Possible reasons are: (i) small CSF fractions cause a relatively large spread of D's making discrimination between CSF and blood difficult. (ii) Because of the rf pulse errors, really long T_2 values could not be measured and therefore, the T_2 could not optimally be used for discrimination of blood and CSF . (iii) When CSF and blood are present, the fitted D may be rather similar to that of CSF. The higher diffusion constant than represents a mixture of blood and CSF.

Using the PFG CPMG sequence in combination with the 2D bi-exponential fitting routine enhances the reliability of both PFG NMR diffusion measurements and the CPMG T_2 measurement. This pulse sequence may thus help in improving the evaluation of diffusion imaging studies and thus help in clarifying and discriminating pathological processes.

Acknowledgements

This work has been supported by Philips Medical Systems (Best,The Netherlands) and by a grant (SIR 13-903) of the Dutch Organisation for Scientific Research (NWO). JBM Goense is acknowledged for helping with the Monte Carlo simulations. All experiments wer carried out at the NIH In Vivo NMR Research Center, Bethesda, USA.

References

1. C.T.W. Moonen, P.C.M. van Zijl, J.A. Frank, D. Le Bihan, E.D. Becker, Functional magnetic resonance imagingin medicine and physiology, *Science* **250**, 53-61 (1990).

2. J.P. Armspach, D. Gounot, L. Rumbach, J. Chambron, In vivo determination of multiexponential T_2 relaxation in the brain of patients with multiple sclerosis, *Magn. Reson. Imaging* **9**, 107-111 (1991).

3. R.V. Mulkern, S.T.S. Wong, P. Jakab, A.R. Bleiere, T. Sandor, F.A. Jolesz, CPMG imaging sequences for high field in vivo transverse relaxation studies, *Magn. Reson. Med.* **16**, 67-79 (1990).

4. C.S. Poon, R.M. Henkelman, Practical T_2 quantitation for clinical applications, *J. Magn. Reson. Imaging* **2**, 541-553 (1992).

5. P.R. Moran, A flow velocity zeugmatographic interlace for nmr imaging in humans, *Magn. Reson. Med.* **1**, 197-203 (1982).

6. L. Axel, Blood flow effects in magnetic resonance imaging, *AJR* **143**, 1157-1166 (1984).

7. D.A. Feinberg, L.E. Crooks, P. Sheldon, J. Hoenninger III, J. Watts, M. Arakawa, Magnetic resonance imaging the velocity vector components of fluid flow, *Magn. Reson. Med.* **12**, 555-566 (1985).

8. A. Villringer, B.R. Rosen, J.W. Belliveau, J.L. Ackerman, R.B Lauffer, R.B. Buxton, Y.S. Chao, V.J. Wedeen, T.J. Brady, Dynamic imaging with lanthanide chelates in normal brain: Contrast due to magnetic susceptibiity effects, *Magn. Reson. Med.* **6**: 164-174 (1988).

9. B.R. Rosen, J.W. Belliveau, D. Chien, Perfusion imaging by nuclear magnetic resonance, *Magn. Reson. Quart.* **5**, 263-281 (1989).

10. J.E. Tanner, Transient diffusion in a system partitioned by permeable barriers. Applications to NMR measurements, *J. Chem. Phys.* **69**, 1748-1754 (1992).

11. M.E. Moseley, Y Cohen, J. Mintorovitch, J. Kucharczyk, L. Chileuitt, H. Shimizu, J. Kucharczyk, M.F. Wendland, P.R. Weintein,Early detection of regional

cerebral ischemia in cats: comparison of diffusion- and T_2-weighted MRI and spectroscopy, *Magn. Reson. Med.* **14**, 330-346 (1990).
12.K. Minematsu, L.Li, M.Fischer, C.H. Sotak, M.A Davis, M.Fischer, Reversible focal ischemia injury demonstrated by diffusion-weighted MRI in rats, *Stroke* **23**, 1304-1310 (1992).
13. P. van Gelderen, M.H.M. de Veeschouwer, D. DesPres, J. Pekar, P.C.M. van Zijl, C.T.W. Moonen, Water diffusion and acute stroke, *Magn. Reson. Med.*. **31**, 154-163 (1994).
14. J. Pekar, C.T.W. Moonen, P.C.M. van Zijl, On the precision of diffusion/perfusion imaging by gradient sensitization, *Magn. Reson. Med.* **23**, 122-129 (1992).
15. M.D. King, N van Bruggen, A.L. Busza, J. Houseman, S.R. Williams, D.G. Gadian, Perfusion and diffusion MR imaging, *Magn. Reson. Med.* **24**, 288-301 (1992).
16. D. van Dusschoten, P.A. de Jager, H. Van As, Extracting diffusion constants from Echo-Time dependent PFG NMR data using relaxation-time information, *J. Magn Reson. A* **116**, 22-28 (1995).
17. R. Damadian, Tumor detection by nuclear magnetic resonance, *Science* **171**, 1151-1153 (1971).
18. P.A. Bottomley, C.J. Hardy, R.E. Argersinger, G. Allen-Moore, A review of ^1H nuclear magnetic resonance relaxation in pathology: are T_1 and T_2 diagnostic?, *Med. Phys.* **14**, 1-37 (1987).
19. S. Shioya, R. Christman, D.C. Ailion, An invivo NMR imaging determination of multiexponential Hahn T_2 of normal lung, *Magn. Reson. Med.* **16**, 49-56 (1990).
20. R.M. Kroeker and R.M. Henkelman, Analysis of biological NMR relaxation data with continuous distributions of relaxation times, *J. Magn. Reson.* **69**, 218-235 (1986).
21. R.J.S. Brown, Information available and unavailable from multiexponential relaxation data, *J. Magn. Reson.* **82**, 539-561 (1989).
22. R.J.S. Brown, G.C. Borgia, P. Fantazzini, E. Mesini, Problems in identifying multimodel distributions of relaxation times for NMR in porous media, *Magn. Reson. Imaging* **9**, 687-693 (1991).
23. P.T. Callaghan, "Principles of nuclear magnetic resonance microscopy", Clarendon Press, London (1991).
24. G. Bodenhausen, H. Kogler, R.R. Ernst, Selection of coherence-transfer pathways in NMR pulse experiments, *J. Magn. Reson* .**58**, 370-388 (1984).
25. A.P. Crawley, R.M. Henkelman, Errors in T_2 estimation using multislice multi-echo imaging, *Magn. Reson. Med.* **4**, 34-42 (1987).

26. G.J. Barker, T.M. Mareci, Suppresion of artefacts in multiple-echo magnetic resonance, *J. Magn. Reson.* **83**, 11-28 (1989).
27. C.T.W. Moonen, G. Sobering, P.C.M. van Zijl, J. Gillen, M.von Kienlin, A. Bizzi, Proton spectrospic imaging of human brain, *J. Magn. Reson.* **98**, 556-570 (1992).
28. C.T.W. Moonen, J. Pekar, M.H.M. de Vleeschouwer, P. van Gelderen, P.C.M. van Zijl, D. DesPres, Restricted and anisotropic displacement of water in healthy cat brain and in stroke studied by NMR diffusion imaging, *Magn. Reson. Med.* **19**, 327-332 (1991).

Chapter 4

Water mobility in heterogeneous systems investigated by PFG NMR

A nuts and bolts approach

4.1 Introduction

A fundamental problem when probing motion of water in a heterogeneous system using NMR is that little is known about the time dependent behaviour of magnetization in a microscopically inhomogeneous environment (1). The composition of, for example, a plant cell is such that the exact microscopic magnetic properties (diamagnetic susceptibility, paramagnetic ion or free radical concentration) are unknown as is the precise effect of permeable barriers in the diffusion pathway of water molecules within the cell. Several models exist which to a certain extent describe diffusion or T_2 relaxation in a heterogeneous system with connected compartments (1-6,32). No model, however, exists which describes both relaxation and diffusion processes in such a heterogeneous system simultaneously, notwithstanding that both processes are interdependent (32). Two reasons for the absence of such a model are easily pinpointed: the mathematical complexity of such a model and the lack of a suitable NMR method for determining the evolution of the magnetization in the time domain in relation with diffusion. Since T_2 relaxation and diffusion are interdependent and both influence the signal amplitude in a PFG NMR experiment (1,4,5,6) it would be best to monitor both processes in one set of experiments. Using the Diffusion Analysis by Relaxation Time Separated (DARTS) PFG CPMG sequence, which is considerable faster than the DARTS PFG MSE sequence described in Chapter 3.1, this goal can be achieved(36). This sequence monitors both T_2 relaxation and diffusion simultaneously in a set of experiments, facilitating a more robust interpretation of the effects of T_2 relaxation, diffusion and exchange of water in a heterogeneous system on the observable magnetization. Furthermore, it allows for comparison of different theoretical models which describe the time dependence of the magnetization in an NMR experiment, since such a model should correctly predict the evolution of the magnetization in two domains (TE or t and b or q) rather than in just one.

In this Chapter the results of PFG Multiple Spin Echo (MSE) CPMG measurements are compared with the predictions of four different theoretical models. Two of the more straightforward models have been used to fit the PFG CPMG data whereas the other two were used only for comparison. Monte Carlo Simulations were performed to study the reliability and the limitations of the PFG MSE CPMG experiment using a non-linear least square 2D fit routine to analyse the data in one stroke. These Monte Carlo simulations were almost exclusively applied to the case of unrestricted diffusion in a non-exchanging two compartment system. To complement the study of the potentials of the PFG MSE CPMG sequence four experimental model systems were investigated and the results of these measurements were put against the predictions of the various models. These model systems include:

(*i*) two glass tubes, filled with $CuSO_4$ doped water and ethanol, respectively

(*ii*) whole blood and transfusion blood drawn from a healthy volunteer

(*iii*) apple parenchyma tissue

(*iv*) a column with Sephadex beads with a flowing fraction.

Each of these model systems have different characteristics with regard to compartments size, exchange rate (if present), T_2 values, the size of the compartments and the diffusion constants. They therefore offer a good opportunity to investigate the potential applications of the DARTS PFG MSE CPMG and its usefulness for further testing and development of adequate models.

4.2 Diffusion and T_2 in heterogeneous samples

Non exchanging model

The signal intensity of a multi compartment system, without taking into account exchange or the effects of restricted diffusion, as acquired by a PFG CPMG sequence, can be described with (23,35)

$$S(t,b)=\Sigma_n k M_{0,n} \exp(-bD_n)\exp(-t/T_{2,n}) \qquad [4.1]$$

where n is the number of ensembles, k represents the spectrometer constant, $M_{0,n}$, D_n and $T_{2,n}$ represent the magnetization at t = 0 s, the intrinsic diffusion constant and the relaxation time of each of the ensembles, respectively. For the definition of an ensemble see (23). The results of a diffusion experiment for any value of t can be

presented in a Signal Attenuation Plot (SAP) where the ln(S(t,b))/ln(S(t,0)) is plotted versus b ($b=\gamma^2\delta^2G^2(\Delta-\delta/3)$)

Two-site exchange model

When magnetization can exchange between compartments the magnetization decay per compartment is no longer mono-exponential. For a two site exchange system the magnetization decay for the compartments a and b is given by (7):

$$dm_a/dt = - m_a(t).R_a - m_a(t)/\tau_a + m_b(t)/\tau_b \quad [4.2a]$$
$$dm_b/dt = - m_b(t).R_b - m_b(t)/\tau_b + m_a(t)/\tau_a \quad [4.2b]$$

Here $R_{a,b}$ denotes the intrinsic relaxation rate ($1/T_2$) per compartment, $\tau_{a,b}$ denotes the residence time in the respective compartments and $m_{a,b}$ denotes the magnetization amplitude $f(t)*M_{0,a/b}$ including its time dependence f(t) for each compartment. Furthermore it is important to note that

$$\tau_a/\tau_b = p_a/p_b \quad [4.3]$$

where $p_{a,b}$ equals the fractional amplitude with $p_a+p_b = 1$. Edzes and Samulski (8) have described the time dependent magnetization decay for each compartment by

$$m_a(t) = p_a^+ \exp(-tR^+)+p_a^- \exp(-tR^-) \quad [4.4a]$$
$$m_b(t) = p_b^+ \exp(-tR^+)+p_b^- \exp(-tR^-) \quad [4.4b]$$

where $p_{a/b}{}^{+/-}$ represent a mixture of the fractional amplitudes of both compartments. $R^{+/-}$ represent a mixture of the intrinsic relaxation rates of compartment a and b. In the Appendix of this Chapter the mathematical relation between $p_{a/b}$, $p_{a/b}{}^{+/-}$, $R_{a/b}$ and $R^{+/-}$ is given. Since $R^{+/-}$ of m_a and $R^{+/-}$ of m_b are indistinguishable a fit of the CPMG data yields R^+ with a fractional amplitude of $p_a^+ + p_b^+$ and R^- with a fraction amplitude of $p_a^- + p_b^-$. When a model system obeying Eq.[4.2] through Eq.[4.4] is monitored using the PFG CPMG sequence, however, the magnetization decay per compartment is no longer indistinguishable since the initial magnetization of each compartment ($p_a^+ + p_a^-$ and $p_b^+ + p_b^-$) is diffusion weighted. Thus, the magnetization decay in both the *b*-domain and the *t*- or TE-domain is given by

$$S(t,b)= k.M_0\{\exp(-bD_a).[p_a^+\exp(-tR^+)+p_a^-\exp(-tR^-)] \quad [4.5]$$

$$+\exp(-bD_b).[p_b^+\exp(-tR^+)+p_b^-\exp(tR^-)]\}$$

Now, not only $R^{+/-}$ of fraction a and $R^{+/-}$ of fraction b can be distinguished, but also $p_a^{+/-}$ and $p_b^{+/-}$ can be fitted to Eq.[4.5]. In principle it is now possible to calculate the exchange rate, intrinsic T_2's and initial amplitudes of each fraction ($M_{0,a/b}$) on the basis of the fitting results using Eq.[4.5] of a diffusion weighted T_2 experiment.

The above mentioned two-site exchange model assumes that all water molecules have an equal change of exchanging between both compartments for any time interval. Diffusion from any position within the compartment to the interface between the compartments (e.g. a membrane) is ignored. An example of a theory which describes the effect of exchange during Δ, the observation or labelling time of the PFG NMR experiment, on a diffusion measurement is given by Kärger (9) and Andrasko (2). However, this theory assumes that relaxation is constant over the sample and that the NMR diffusion constant per compartment is constant during Δ, which is not necessarily so (10). Of course, Eqs. [4.1] and [4.5] do not account for obstructions like membranes which restrict the diffusion process such that D measured by NMR becomes a function of Δ and the amplitude used for G (3,4,6) since spatial inhomogeneity is not considered. But, the principle that diffusion may be used to label the T_2 relaxation making it possible to distinguish compartments remains valid.

Multiple permeable membrane and active surface model

Two examples of models which do include diffusion to the surface of a compartment, bounded by permeable membranes at the surface, and the theoretical characteristics of these models with regard to the interpretation of the results of a diffusion experiment are discussed below. A general expression of the effect of diffusion on the NMR signal intensity in a pulsed field gradient experiment is given by (3,4,32)

$$S = \int \rho(x_0)\exp(-t/T_2(x_0))\int P(x_0|x,\Delta)\exp\left[i\gamma\delta G\bullet(x-x_0)\right]dxdx_0 \quad [4.6]$$

Here $P(x_0 \mid x,\Delta)$ is the conditional probability that a spin starting at x_0 will, after a time Δ, arrive at x. $\rho(x_0)$ is the nuclear spin density, the T_2 is assumed to be constant during Δ. In a model presented by Tanner (3), which we'll refer to as the multiple membrane model, permeable barriers are placed in an otherwise

homogeneous medium with constant T_2 and D(0), D(0) being the NMR diffusion constant for $\Delta = 0$. Snaar and Van As (4) assumed a single compartment with permeable barriers. These barriers give rise to signal loss because of surface sinks (with H, the surface sink strength density, in m/s), magnetisation penetrating the barriers enters a medium with a T_2 of 0 ms. This model, we'll refer to as the active surface model. For both models the propagator $P(x_0 | x,\Delta)$ can be found which comprises an infinite set of eigen functions (X_n) satisfying the eigen value equation based on Fick's law (4) with the eigen values α_n,

$$\delta^2 X_n/\delta x^2 + \alpha_n^2 X_n = 0 \qquad [4.7]$$

For the active surface model (4) we have the boundary condition at the surface S

$$\delta X_n/\delta x + H X_n |_S = 0 \qquad [4.8]$$

For the multiple membrane model of Tanner (3) we have

$$\delta X_{i,n}/\delta x = -\delta X_{i+1,n}/\delta x \qquad [4.9]$$

indicating the preservation of magnetisation at the boundaries and

$$\zeta(X_{i+1,n}-X_{in})=D(0)\delta X_{in}/\delta x \qquad [4.10]$$

ζ being the permeability (m/s) between the barriers of compartments i and i+1. For both these models we find that the transient diffusion constant $D(\Delta)$ is a function of the eigen values α_n

$$D(\Delta)= \Sigma_n f_n\{\alpha_n,(H \text{ or } \zeta),r,D(0)\}\exp(-D\alpha_n^2\Delta) \qquad [4.11]$$

where r denotes the radius of the compartment. The effect of an active surface on $D(\Delta)$ is, that $D(\Delta)$ reduces faster with Δ than if no active surface is present since the protons that travel over the largest distance have the highest chance of reaching the active surface thereby losing their magnetisation. In Fig. 4.1 the time (Δ) dependency of the distribution of magnetization is compared for both models.

Neither of these models includes exchange between two distinct compartments since, in fact, only one compartment is truly described. Depending on the nature of a neighbouring compartment the value derived for the radius of the compartment and the permeability of a compartment membrane under

scrutiny may be affected. For example when the T_2 outside the investigated compartment (i) is larger than that of the compartment itself the contribution of the magnetization having leaked out during Δ is underestimated in both models. To compensate for that, a higher value of the permeability is necessary when using the multiple membrane model.

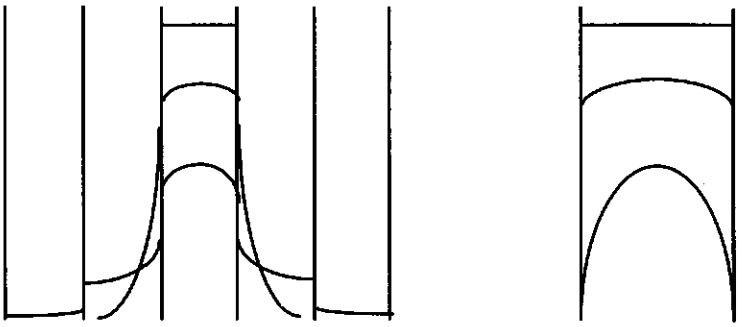

Parallel plane model of Tanner

Absorbing wall model of Snaar and Van As

Figure 4.1 Schematic representations of diffusion of magnetization in a medium with permeable parallel membranes. The figure on the left shows a schematic as presented by Tanner. The horizontal lines signifies the magnetization at Δ=0. Depending on the permebility of the membranes the magnetization can cross the membranes and diffuse into the neighbouring compartments. The displacement further depends on Δ. The curved lines represent the magnetization at longer labelling times. The right figures shows a schematic as presented by Snaar and Van As. Here magnetization penetrating the permeable membrane enters a medium with a T_2 of 0.

When using the active surface model to explain the observed diffusional behaviour this situation would have to be described by a lower or even negative H parameter or a larger compartment size.

Numerical models describing diffusion and including T_2 relaxation have been presented by Zawodzinski et al. (6) and Hills and Snaar (32). Although these models cannot be used to fit data directly they are very useful to investigate the influence of different parameters on the magnetization decay. These numerical models can also be used to generate computed PFG NMR data which can be compared with the actual experiments. In the paper of Hills and Snaar the authors note that in order to study water mobility in biological tissue the spin echo amplitude in a PFG NMR experiment should be studied as the depends of q or b, Δ and τ or TE. The PFG MSE CPMG sequence in this Chapter is doing just that. The DARTS PFG NMR method as described in (23) also measures the spin echo

amplitude in relation to both TE and b, but is time consuming because of the need to repeat the diffusion experiments at different echo times. The PFG (MSE) CPMG is one of the possible implementations of DARTS PFG NMR and is a particularly fast one.

4.3 Materials and methods

4.3.1 The PFG MSE CPMG sequence

By combining the pulsed field gradient experiment with a CPMG experiment a sequence is obtained which samples both b and TE simultaneously (36). In a previous study on a two tube sample and cat brain no precautions to prevent susceptibility artefacts were necessary (36). In apple parenchyma tissue and in whole blood susceptibility differences within the sample are expected. Therefore suppression of the artefacts caused by susceptibility differences is necessary. Also, the experiments reported here were performed on an electromagnet which causes 50 Hz and higher frequencies fluctuations of the magnetic field. Because of these fluctuations values for 2τ had to be restricted to 10 ms. Therefore additional π pulses were applied between the pair of pulsed field gradients, as is also done in the PFG MSE experiments (34).This results in a PFG MSE CPMG sequence, a schematic of which is presented in Fig. 4.2.

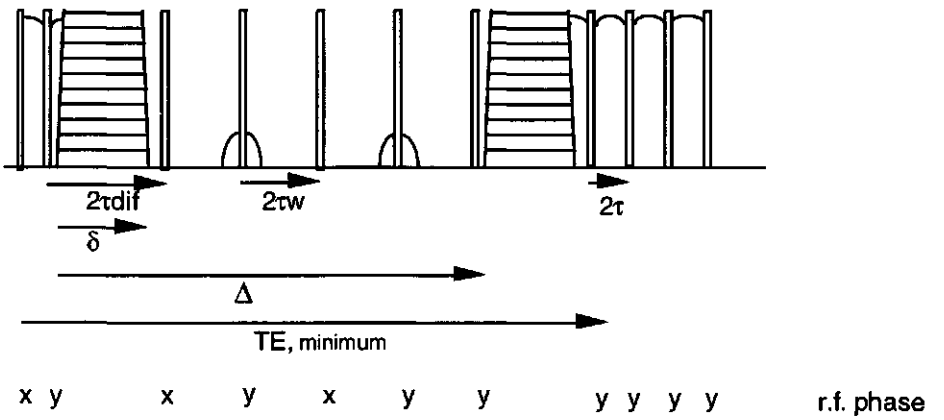

Figure 4.2 The PFG MSE CPMG sequence. The slim rectangles show the rf pulses, the curved lines the magnetization with G=0. In the period $2\tau_{dif}$ the gradient pulses with variable strength are placed.

The first echo is measured after a π pulse which is applied directly after the last gradient pulse. The initial echo time is therefore automatically coupled to Δ,

which is slightly different from the PFG MSE sequence where TE can be varied without changing Δ. The first measured echo therefore increase with Δ. PFG MSE CPMG curves sampled after a long Δ cannot directly be compared with PFG MSE CPMG curves samples with a short Δ. A solution to this problem is ignoring the first echoes of the CPMG train when shorter labelling times are used. This ensures that the same initial echo time for all Δ's is used, which can be important for the correct interpretation of the way the results fit to the model used

The value of 2τ should be kept small, in the order of 1 ms, to reduce susceptibility artefacts and sensitivity to noise on the B_0 field. Since 2τ, $2\tau_w$ and $2\tau_{dif}$ are not identical the magnetization is not refocussed in the middle between the π pulses. We found that $2\tau_w$ should not exceed $2\tau_{dif}$-τ (see Fig. 4.2 for the definition of these symbols) to prevent signal loss due to pulse imperfections even when using a XY-8 pulse phase scheme which minimises such losses (12). The signal loss becomes a real problem only when using large numbers of π-pulses, and is due to the fact that a part of the magnetisation is inadequately refocussed in between the PFG's when $2_{\tau w}$ is too short (34).

Another important point is the correction of DC artefacts caused by small field drifts, imperfect rf pulses or phase errors (glitches) of the rf pulses. A PFG MSE CPMG experiment can therefore not be performed in a single scan but requires at least two scans with DC correction. This ensures a relatively small (<0.5%) baseline which fluctuates only slightly with the different diffusion weighting steps. Also, the first scan of the experiment is not acquired with b=0 s/m^2 but with a value which is slightly larger to prevent spurious echoes.

A standard experiment takes 8 minutes using two averages and 16 *b*-steps with a TR of 15 seconds. 8000 Echoes were normally acquired with a minimum 2τ of 600 μs. This short 2τ requires that the Spectral Width was set to 200 kHz. The overall SNR, including instabilities during the experiment, of a sample of 1 cm^3 containing only water was 200.

4.3.2 Materials

As was mentioned in the introduction of this Chapter, four samples with distinct characteristics were studied. Here a more elaborate description is given of these samples.

The two tube phantom: This was a straightforward test sample consisting of two glass tubes, each filled with a different liquid; $CuSO_4$ doped water and ethanol, respectively.

The blood samples: Both Whole Blood (WB) and transfusion blood (CPD blood; Citrate, Phosphate and Dextrose were added to centrifuged blood) were used. Red Blood Cells (RBCs) are very small having a diameter of 5μm and a height of 2 μm. The membrane is very permeable to water (16) and RBC's therefore have a high exchange rate. A total of four blood samples were studied, each over a period of 24 h, to investigate the water balance in WB (stabilised with Li_2EDTA) and to investigate the degradation of the RBC over this period. For comparison CPD blood was studied, which is known to be stable over a period of three weeks. All blood samples were drawn from the same healthy, male volunteer (DvD) to ensure stable external conditions, as much as this is possible. The blood was stored at room temperature during the experiments (24 °C). The CPD blood sample was also measured after a one and a two week period, between which the blood was stored at 4 °C. The hematocrite, the volume percentage of the RBC's, was .

During the experiments the blood samples were stirred every twenty minutes. Stirring stops the sedimentation process which starts after 5 to 10 min, it also reoxygenates the blood (evident from the brightening of the blood). A high oxygen level of the blood reduces the influence of magnetic susceptibility variation on the measurements (22). In the absence of stirring the RBC's will start to form stacks (19). An essential molecule in the stack formation process is fibrinogen which is absent in CPD blood. This is the major reason why CPD blood has a very low sedimentation constant. Because of the time scale of the stack formation this process could influence diffusion measurements which typically takes about 6 minutes. Some spectroscopic data of whole blood could be explained if the stack formation is taken into account and when it does it could change the T_2^* within the RBC (20). The plasma of the Whole Blood and the CPD blood was obtained by pouring of the supernatant after half an hour without stirring. Simultaneously with the NMR experiments physiological parameters like the Na^+,K^+, glucose and lactate concentration were measured at the local hospital laboratory in Wageningen in order to combine the physiological status of the RBCs with the NMR data.

The parenchyma apple tissue: For these measurements apples of the variety 'cox' were taken. Earlier CPMG measurements performed at our lab have shown that three T_2's are found, which have been demonstrated to originate from water in the cell wall and extra cellular water, cytoplasm and vacuole (17). On average the diameter of the vacuole is 100-130 μm. The cytoplasm forms a thin layer of approximately 8 μm around the vacuole. Exchange was found to be in the intermediate time range using Mn^{2+} as a tracer molecule (17).

The Sephadex column: The selected Sephadex beads were of the type G25/300 (Signa), with an average diameter of 300 μm when swollen with water. The beads have a porous structure built up by cross-linked dextran polymers. Similar Sephadex beads suspended in water have been used as a model system for perfusion (27). In glass bead systems the relation between the pseudo diffusion coefficient, the flow rate, bead diameter and observation time has been extensively studied (28,29). The results of those studies can thus be used for comparison with the results obtained for flow through a Sephadex column. However, in a glass bead system we have only one water fraction to consider, whereas in a Sephadex column we have two fractions between which diffusive exchange takes place.

Sephadex beads were suspended in distilled and deoxygenated water and left to equilibrate in a glass pipe (diameter of 1.2 cm, length column of 18 cm) for at least one day. The ratio of the water in the interstitial spaces, the void volume, and in the beads itself, the inner volume, was determined using standard gel chromatographic techniques (30). The inner volume was found to be 63 %, the void volume 37 %. Of the total bed volume (the inner volume) 34 % was occupied by Sephadex itself, but this fraction is not observed directly with NMR because of very short T_2 of these long polymers. Standard settings were used for the PFG MSE CPMG measurements except for the number of b steps of the diffusion measurement which was set to 32. The average flow velocity, calculated for the void volume, was stepped up from 0 to 0.35, 1.05 and 1.74 mm/s.

4.3.3 Principles of fitting

There are three approaches to fitting the 2 dimensional data set which is acquired with the PFG CPMG sequence. Each has its merits and shortcomings and for 'difficult' data sets all approaches should be used to be able to discriminate between measuring artefacts and e.g. exchange or restricted diffusion. Below, the three fitting methods are listed and their characteristics discussed.

I: To determine how D_{app} develops as a function of TE, a 1D mono-exponential fit for all echoes is carried out (The number of echoes normally is 8K or more, usually this number is reduced by averaging over a number of echoes). The train of echoes at $b = 0$ is fitted to a multi-exponential function to calculate $F_n(TE)$, (see Chapter 3) and subsequently a SVD routine is used to extract D_n. The main difference between the method described in Chapter 3 and the method described here is the number of echoes which is used to measure $D_{app}(TE)$. The higher number of echoes results in a slightly higher accuracy. The improvement of

the fit is primarily limited by the accuracy of the multi-exponential fit in the time domain.

When $D_{app}(TE)$ is found to suddenly decrease near the end of the rf pulse train this indicates that not all magnetization is properly diffusion weighted; magnetization stored on the z-axis during the pulsed field gradients can leak back during the CPMG pulse train.

If the difference between the diffusion constants of the ensembles and the SNR allows a multi-exponential fit in the *b*-domain at several echo times this offers the possibility of directly monitoring the magnetization decay with TE for each ensemble since the fitted amplitude for each ensemble reflects the magnetization at each echo time (see for an example Fig.4.5.b). This method can thus serve as a tool to monitor whether the exchange obeys the two-site exchange model or that exchange should be described otherwise.

Table I. The following Table summarises the pro's and con's of the fitting method I.

Fit mode (*b*-domain)	Pro's	Con's
1 diffusion constant	-Fitting routine for $D_{app}(TE)$ is not sensitive to deviations -Check reliability of diffusion weighing possible	-With high *b*-values and high D ratios the fit conditions break down (36) -No fit corrections can be made for upward curving of the SAP due to restricted diffusion
2 diffusion constants	-Monitor magnetization decay of each ensemble with TE (e.g. exchange) -Check reliability of diffusion weighing	-Fixation of at least 1 D is necessary to overcome decrease in SNR with increasing TE. -Effects of restricted diffusion can not be detected.

II: In a PFG MSE CPMG experiment a set of relaxation curves is obtained with different initial amplitudes. Each of these T_2 curves can be analysed using a multi-exponential fitting routine. Hereby a set of T_2 values is obtained which should be identical for curves from experiments with different *b*-values when the results are fitted with the correct number of exponentials. Also, a set of initial fractional amplitudes, $S_{b,0}$, which decrease with increasing *b*-values, is obtained. The decrease of $S_{b,0}$ with increasing *b* is determined by D_n and a simple single exponential fitting routine can be used to obtain D_n and the fractional amplitudes.

In case of restricted diffusion , which causes an upward curvature of the SAP with increasing G^2, this effect can now easily be observed and analysed.

However, the upward curvature occurs only when using high pulsed field gradients and long labelling times, which results in a reduced initial amplitude. Thereby the reliability of the multi-exponential fit in the time domain reduced. Fixation of one or more of the T_2's is therefore required to overcome this problem. A high quality of the data set is required if this trick is going to work.

Table II. The following Table summarises the pro's and con's of the fitting method II.

Pro's	Con's
-Difference between effects of restricted diffusion and multi compartment diffusion become clearly evident	-Reliability reduces with SNR and thus with higher *b*-factors, fixation of T_2's necessary. -Exchange cannot be analysed

III: Finally, the 2D data set acquired with the PFG CPMG sequence may be analysed as a whole. The complete data set can be analysed to e.g. Eq.[4.1] or Eq.[4.5].The 2D fitting routine requires no special adaptations compared to conventional 1D fitting routines except for introducing educated initial guess values of the 3**n** variables, **n** being the number of fractions or ensembles to be fitted. In Chapter 3.2 two approaches were mentioned to generate these initial values. The first is to use a multi-exponential fit in both the TE-domain ($b = 0$) and the *b*-domain (minimal TE). Values for $S_{0,n}$ are taken from the fit in the TE domain because of the higher reliability of this fit. The second approach is to use a single exponential fit in both domains and generate the 3n variables using fixed ratios of these variables using pre-knowledge of the system under observation. A third approach is to use a multi exponential fit in the TE domain and a single exponential fit in the *b* domain based on the principle mentioned above.

Using single exponential fits to generate the educated initial guess values is necessary when small differences between the D and T_2 values exist. In such cases infrequent occurrences of unrealistic (or even non-values) initial guess values may prevent a smooth and accurate 2D fit. This approach was only used sporadically, however, mostly for large Δ values. The reason not to use this approach more often is the loss of a check mechanism of the reliability of the 2D fit: when fitting, one of standard outputs of the fitting routine is the goodness-of-fit parameter chi square (χ^2), given by

$$\chi^2 = \sum_{i=1}^{N}\left(\frac{y_i - y(x_i; a_i, ..., a_M)}{\sigma_i}\right)^2 * \frac{1}{(N-M)} \qquad [4.12]$$

which is a measure for how well the fitted function follows the data points. In this expression y_i are the values of the data points, σ_i is the SD for each of the data points, $y(x_i;a_1,....,a_m)$ is the fitted function, N the number of data points and M is the number of variables which are fitted. In fact Eq.[4.12] does not represent the χ^2, but the so-called reduced χ^2, which is χ^2 divided by the number of data points minus the number of variables which is fitted (N-M). Ideally, χ^2=1.0 (that is using Gaussian distributed noise with a mean of 0 and using the correct model to describe the data). It was standard practice to compare χ^2 for the 2D fit with χ^2 for the multi-exponential fit in the TE-domain which is used to generate the initial guess values. When χ^2 for the 2D fit isn't smaller than χ^2 for the TE-domain fit, this is a clear indication that either there is something wrong with the data or the model to fit the data is incorrect; additional checks, like using procedure I or II are necessary.

It should be noted that 1D fits are more sensitive to erroneous initial guess values, the outcome of the fit may even depend on it (the fit routine may find a so-called local minimum of χ^2 in stead of the true χ^2 minimum).

Table III.The following Table summarises the pro's and con's of the fitting method III.

Pro's	Con's
-Different fit models can be compared properly (e.g. exchange can be incorporated) -All data points are used, in theory reducing the required minimal SNR	-Non exponential artifacts in one domain reduce accuracy of the whole fit

Interestingly enough, we found a visual investigation of the 2D residual plot the most indicative for the reliability of a fit, despite the fact that several statistical programs can be used for that purpose.

Below a flow diagram is given which summarizes how a data set acquired by the PFG MSE CPMG sequence was analysed. Reduction of the data set was sometimes used to disregard erroneous data, but also as a means to better understand the results. This is a highly interactive and often intuitive way to see in how far the fit results are reliable and is therefore mostly not mentioned throughout the text because of the intuitive character of this procedure. However, in order to know what your data and the fit results mean, careful reduction of the data set can be a very helpful tool.

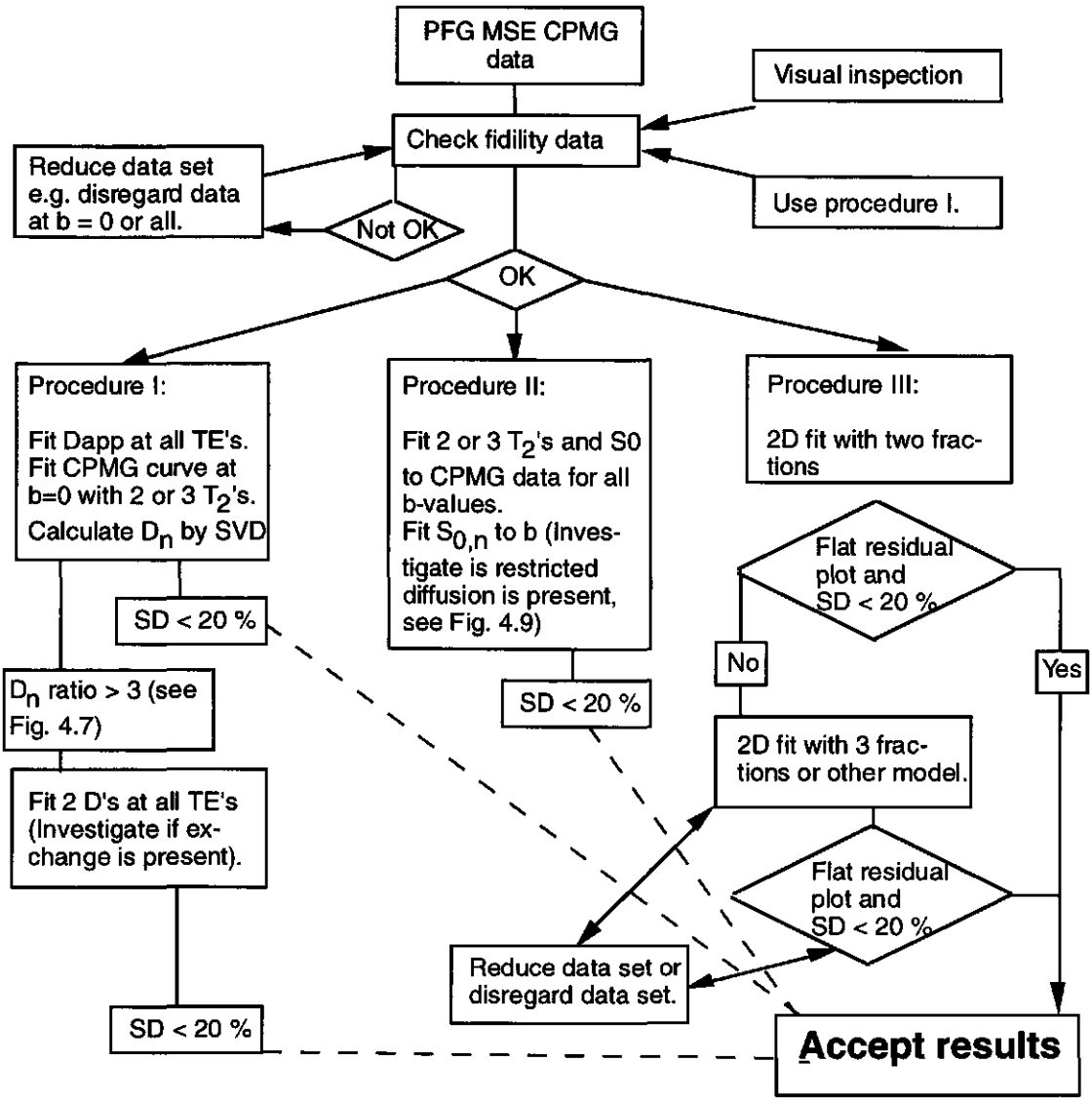

Flow diagram for fitting a data set generated by a PFG MSE CPMG experiment or by Monte Carlo Simulations.

4.3.4 Monte Carlo Simulations

Extensive Monte Carlo Simulations were performed to check how reliable the fit routine was over a wide range of T_2 values, D's and fractional ratios. MCS studies

were performed to examine whether a particular combination of NMR variables and experimental parameters (TE and *b*-values) could be reliably analysed under optimal situations (Gaussian distributed white noise and a zero baseline). Here a reliable fit is defined as yielding standard deviations below 10% for all variables. In some situations the SD was below 10% for only a few variables. Then, the fit as a whole was not considered reliable but some individual variables were. Despite the speed of current computers the number of variable inputs for 2D data sets is so large that using MCS studies may take an unjustifiable amount of time that might have been invested in optimisation of the experiments. Therefore the MCS studies were performed in such a way that the results for other experimental situations could be assessed by intra- or extrapolation of this limited number of MC Simulations. At the end of the MCS studies the effects of exchange obeying the two-site exchange model on the diffusion measurements were included as was the addition of a third fraction.

Data sets were generated on basis of Eq.[4.1], assuming two non-exchanging compartments. In the TE-domain 512 data points were used, in the *b*-domain 16. The noise was computer generated, Gaussian distributed with a mean of 0. All the programs to perform the Monte Carlo Simulations and fitting the computed or measured data sets were written under Interactive Data Language (IDL, RSI, Boulder, USA). The MCS were implemented on a 486DX2 PC , the data was generally fitted using a Silicon Graphics Indigo II workstation. The fit routines used throughout this Chapter were based on the Marquardt-Levenberg fitting method (13).

4.4 Results and discussion.

4.4.1 Monte Carlo Simulations

Two non-exchanging compartments of equal size..

To investigate differences between the 1D and 2D fit routines the diffusion curves of the first TE-domain point (TE = 4 ms) was fitted, as was the relaxation curve of the first *b*-step (b = 0 s/mm^2). Firstly, the statistics concerning the standard deviation given by the fitting program were investigated. The standard deviation was determined by taking the r.m.s. of the distribution of the fitted variables after a number of trials (e.g. 250 or 500) for one particular situation. The SD was also calculated for each fit internally, that is inside the fit routine, on basis

of the covariance matrix (13) and was compared to the r.m.s. SD. In general, the r.m.s. SD is slightly higher than the internal SD for the 2D fit. For 1D multi-exponential fits the r.m.s. SD is considerable higher than the internal SD. In the following, the r.m.s. SD is used as the standard SD further throughout this Chapter. Another parameter to verify the reliability of the fit is the average value of each of the variables of the individual MCS runs. For the 2D fit routine the deviation of the input variable from this average value was always below 0.5 %. These deviations are highly correlated with the relatively low number of runs.

In Table 4.1 the average percentile deviation of the fitted parameters and the SD values of the four fitted variables are presented in eight different columns. These were obtained using a 1D bi-exponential fitting routine on a bi-exponential data set at a single TE (TE=4 ms). The SNR was set at 1000.

	$Av(S_1)$	$SD(S_1)$	$Av(S_2)$	$SD(S_2)$	$Av(D_1)$	$SD(D_1)$	$Av(D_2)$	$SD(D_2)$	D_1/D_2
1D-fit	-0.6	4.1	+0.4	4.2	+0.5	2.7	+0.3	3.0	4.0
	-1.2	18	+1.2	19	+0.5	6.7	+0.4	7.8	2.0
	-11.2	81	+13.6	69	+15.7	23	-4.0	15	1.33

Table 4.1. The systematic error (%) of the four fitted variables (Av(..)) resulting from 1D bi-exponential fits of computed diffusion data and the standard deviation (%) of these variables as a function of D_1/D_2. 16 *b*-values (0-2048 s/mm^2), D_1=2.00. 10^{-9} m^2/s , S_1/S_2=1.0 , SNR= 1000, 500 MCS runs.

In Tables 4.2 and 4.3 the SNR was reduced to 200. In the first row of both Table 4.2. and 4.3 the SD values are given for a 1D bi-exponential fit in the TE-domain. The difference between the two Tables is the T_2 ratio which equals 4 in Table 4.2 and 2 in Table 4.3. In the lower rows the results of the 2D bi-exponential fits is given. The last column displays the ratio of the diffusion constants which were used as input for the MCS runs .

	$SD(S_1)$	$SD(S_2)$	$SD(D_1)$	$SD(D_2)$	$SD(T_{2,1})$	$SD(T_{2,2})$	D_1/D_2
1D-fit	1.1	1.2	-	-	1.5	0.75	-
2D-fit	0.32	0.36	0.59	0.35	0.35	0.20	4.0
	0.40	0.44	0.56	0.25	0.62	0.26	2.0
	0.46	0.50	0.55	0.25	0.64	0.27	1.33

Table 4.2. Standard deviation (%) of 1D bi-exponential fits of computed CPMG data (250 MCS runs) and 2D fits of computed PFG CPMG data (50 repetitions) as a function of D_1/D_2, $T_{2,1}$=125 ms, $T_{2,2}$=500 ms, TE=4,...,2048 ms in 512 steps , SNR= 200 . Other parameters as in Table 4.1.

	$SD(S_1)$	$SD(S_2)$	$SD(D_1)$	$SD(D_2)$	$SD(T_{2,1})$	$SD(T_{2,2})$	D_1/D_2
1D-fit	8.8	8.9	-	-	3.9	2.8	-
2D-fit	1.3	1.2	1.1	1.1	0.36	0.72	4.00
	2.3	2.4	1.2	1.2	0.83	0.73	2.00
	3.4	3.3	1.4	1.1	0.88	0.61	1.33

Table 4.3. Standard Deviation (%) of 1D bi-exponential fits of computed CPMG data (250 MCS runs) and 2D fits of computed PFG CPMG data (50 repetitions) as a function of D_1/D_2, $T_{2,1}$=250 ms, $T_{2,2}$= 500 ms. Other variables as in the above Tables.

The standard deviations found for the 2D fits are considerable lower than those found for the 1D fits. The improvement is lowest when a 2D fit is done for a T_2 ratio of 4 and the D ratio of 1.33. Increasing the D ratio gives a bigger reduction of the standard deviations (see Table 4.3). The decrease of the SD value of the variable with the highest SD, which largely determines the reliability of the fit (or at least the acceptable threshold SNR) is approximately 2.4 when the T_2 ratio is 4 (cf. column $SD(S_2)$ first and last points in Table 4.2). When taking a T_2 ratio of 2 the same combination gives a decrease of the SD by 2.7. Note that the average SD value in Table 4.2 is a factor 6 lower than the average SD value in Table 4.3. The best improvement occurs for a T_2 ratio of 2 combined with a $D_1/D_2 = 4$. Then, the SD reduces by a factor of 6.8. Evidently the improvement of a 2D fit over a 1D fit is considerable larger when comparing the 2D fits with the 1D fits in the *b*-domain. The reduction of the SD values (ignoring the higher SNR used for the 1D bi-exponential fits) varies between a factor of 11.7 and 176 for D_1/D_2= 4.0 and 1.33, respectively. Since the SD is linearly proportional to the SNR these factors should be multiplied by 5 to obtain the correct SD reduction factor (compare SNR for Tables 4.1 and 4.2 and 4.3). This improvement is all the more significant since more parameters are fitted in the 2D fit. In general the 1D fit with the worst SD is the one which profits most from using a 2D fit.

In conclusion, the diffusion measurements show the highest increase in reliability when using the 2D fit, but the improvement for the T_2 fits is certainly not insignificant.

The improvement of the SD values is in part caused by the increase of the number of data points used for fitting. For example, because 16 *b*-values are used with an average amplitude of half that of the first *b*-value, an SNR improvement of $0.5x\sqrt{16} = 2.0$ may be expected and $0.5x\sqrt{512} = 11.3$ as improvement for the fit in the *b*-domain when echo summation is used. Any values higher than these are caused by coupling the fit in the TE-domain and the *b*-domain. Almost all data points are coupled to four in stead of two neighbours giving a better defined

minimum of χ^2. Also, the partial derivatives used to search for the minimum of χ^2 are coupled in the two domains making the search algorithm for the χ^2 minimum more efficient and reliable.

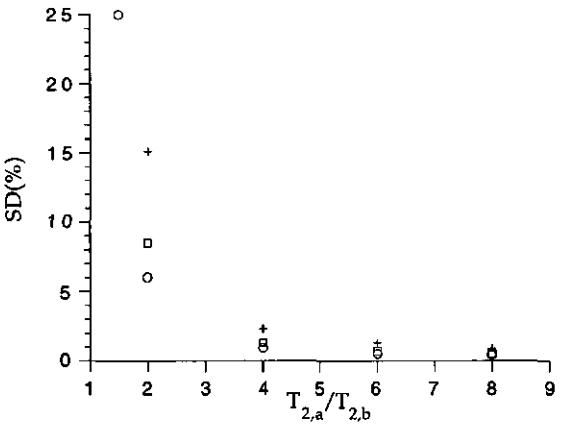

Figure 4.3 The standard deviation of the amplitude with the shortest T_2 of a 2D fit on diffusion weighted T_2 data (computer generated) versus the relaxation rate ratio. A total of 250 repetitions were used with an SNR of 200 and D_1/D_2 =2 and three different fraction ratios, o 1:1, □ 2:1 and + 3:1. The fraction with the short T_2 having the lower amplitude.

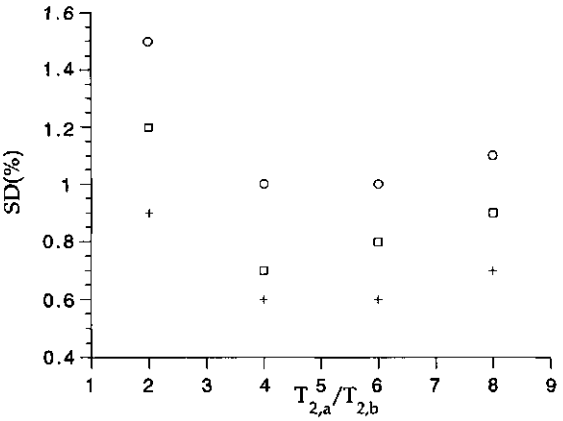

Figure 4.4 The standard deviation of the diffusion constant with the shortest T_2 of a 2D fit on diffusion weighted T_2 data versus the relaxation rate ratio. All parameters as in Figure 4.3

Two non-exchanging compartments of different size.

Not only the T_2 ratio and the D ratio determine the reliability of a fit, but also the fractional ratio. A perfusing blood fraction is a typical example of how

difficult it is to determine the fractional amplitude of only 5 to 10 % and the apparent diffusion constant associated with the perfusing blood, even though a large difference between the diffusion constants of the perfusing and non-perfusing fraction exists (14). To investigate the effects of smaller fractions on the reliability of the 2D fit a number of additional MCS studies were performed. In Fig. 4.3 the SD of $S_{0,2}$, the smallest fraction, is plotted against the T_2 ratio at different fractional ratios, whereas D_1/D_2 is kept at a fixed value of 2.0. At a T_2 ratio of 2.0 the SD of $S_{0,2}$ increases by almost a factor three when the fractional amplitude drops from 50 to 25 %. At higher T_2 ratios this increase is somewhat smaller. Not all fitted variables show a proportional relation between the T_2 ratio and the SD, as is demonstrated in Fig. 4.4 displaying the SD of the fraction with the lowest D and shortest T_2. Under these conditions the most favourable conditions for the determination of the diffusion constants exist for an intermediate (~5) T_2 ratio. Note that the SD is an order of magnitude lower than in Fig. 4.3 even for a small T_2 ratio . Still, this is not a trivial point when the sampling of the data in the *b*-domain is not optimal and the SD for the diffusion constants increases.

The above tendencies can be explained from the contribution or weighing of the partial derivative of each parameter, which determines how well the parameter is fitted (15). The contribution of the partial derivative is small for the amplitudes which are therefore the most sensitive to noise. When one of the T_2's becomes relatively short, the partial derivative of D for that component becomes small, introducing larger errors in D.

The above MCS studies indicate that, given a SNR of 200, it is theoretically possible to reliably resolve a 2D data set, acquired with a PFG CPMG sequence, with a minimum T_2 ratio of 1.9, a minimum D ratio of 1.33 and a fractional ratio of 1.

Further improvements of the fit accuracy can be achieved by optimising the distribution of the data points in the two domains (TE or *b*). The best overall result is obtained when the parameter with the lowest accuracy is sampled with more data points (35), e.g. when a parameter with a short T_2 has a high SD the fit can be improved by using shorter echo times.

Three non-exchanging compartments of unequal size.

Based on a number of initial experimental results, obtained with the PFG MSE CPMG sequence on apple tissue, a data set with three exponentials was generated (see Input row of Table 4.4) to investigate the minimum SNR required to

resolve such a data set reliably. The outcome of the 2D fit and the standard deviation are put in the lower rows.

	S_1	S_2	S_3	$T_{2,1}$	$T_{2,2}$	$T_{2,3}$	D_1	D_2	D_3
Input	100	100	100	500	250	83.3	2.00	1.00	0.75
Output	99.3	100.2	100.6	499.2	247.3	82.9	2.00	0.99	0.75
SD(%)	6.7	4.8	3.3	1.9	4.8	2.2	2.0	4.2	1.6

Table 4.4 Parameters for a three exponential 2D MCS, with T_2 values in ms and D values in 10^{-9} m^2/s. In total 50 MCS runs were used with a SNR of 225. *b*-values (0-2048 s/mm^2) in 16 steps and TE=4,...,2048 ms in 512 steps.

In Table 4.4 it can be seen that small systematic errors are present. These are partially caused by the low number of MCS runs. More MCS runs would lower the systematic errors and give a higher accuracy of the values found for the standard deviation. However, small systematic errors do exist.

Two exchanging compartments of equal size.

Small systematic errors also arise when exchange was included in the data and in the fit routine (based on Eq.[4.5], ($S_1/S_2 = 1, T_{2,1}/T_{2,2} = 4.0$, $D_1/D_2 = 4.0$)). Although fitting the data set with 8 parameters (of which 4 are amplitudes (p_a^+, p_a^-, p_b^+ and p_b^-)) in itself was not a problem, the calculation of the exchange rate based on the fit results showed a systematic deviation of 8 % even when the SD of the fitted parameters was as low as 1.5 % (SNR of 200). The error of 8 % is caused by the accumulation of the systematic errors of the fitted parameters. If exchange is ignored during the fit by purposely fitting with Eq.[4.1] whereas the data was generated with Eq.[4.12], negative diffusion constants could be found; then the residual plot showed large 2D waves. These results suggest that in the presence of exchange obeying the two-site exchange model, at least detection of this phenomenon should not meet much difficulties.

Summary of the Monte Carlo Results

The findings of the above MCS studies point out that the accuracy of a fit is determined by a wide range of variables. Despite the fact that these simulations are incomplete, since this would have to include non-Gaussian noise distributions or fitting to other models (e.g. inclusion of restricted diffusion) , it is demonstrated that 2D fitting of PFG MSE CPMG data improves the accuracy of all parameters. Especially when 1D fits render inaccurate results, because of the proximity of the decay rates, the improvement of the reliability is important.

These MCS studies also demonstrate that using higher fields to increase the SNR can be counterproductive. For example, going from 0.5 T to 2 T we gain about a factor 11 in SNR. If however, the T_2 ratio drops from 4 to 1.5 the average SD of the fit increases by a factor 25. This is not a purely hypothetical situation since T_2's tend to decrease with increasing B_0 because of chemical exchange and diffusion through *in situ* field gradients (31). A similar problem arises when combining T_2 measurements with imaging techniques. Because of diffusion during the read gradients in a CPMG train, a maximum is put to the longest T_2. At 150 µm resolution T_{2max} =1 s which reduces quadraticaly with increasing resolution to T_2 = 25 ms for 20 µm resolution ($D=1.5.10^{-9}$ m^2/s, TE=15 ms, 256 pixels). At this resolution often only one short T_2 is found despite the presence of more fractions. (36)

4.4.2 Experimental results

The two tube sample

The accuracy of the PFG MSE CPMG data acquisition and 2D fitting was first tested on the two tube test sample. Measurements were performed using 12000 echoes (SW=200 kHz, 2τ=0.6 ms) to ensure adequate sampling of the baseline. 16 *b*- values were used between 0.1 and 1360 s/mm^2. In the *b* domain the baseline is not reached, but this is of little importance since the base line is measured in the TE domain. The overall SNR was approximately 250. At 24.5 +/- 1 °C we repeated the PFG MSE CPMG measurements on the two tube sample 9 times and found D_{water} to be 2.17 +/- 0.03 10^{-9} m^2/s and $D_{ethanol}$ to be 1.02 +/- 0.02 10^{-9} m^2/s (T_{2w}=856 +/- 20 ms, T_{2eth}=1.51 +/- 0.07 s). These values compare well with values reported in literature (39). Each measurement took about 8 minutes (Number of averages = 2, TR = 15 s). The limiting parameter in this case was not the SNR but the instability of the room temperature. An increase of 1 °C causes D_{water} to increase by 1.5 %. Changing Δ did not introduce any change in D, demonstrating the absence of restricted diffusion.

Whole blood and CPD blood

First CPMG measurements were performed to analyse the relaxation behaviour of whole blood including components having short T_2's. These measurements were performed using 8000 echoes, 2τ = 0.6 ms. We found three

T_2's, in contrast to the two relaxation constants which are reported in literature (16), probably because of the large number of pulses we used, the short spacing between the pulses and the fact that the baseline was adequately sampled. The T_2's were 2.5 ms ($S_{0,1}$=9 %), 0.2 s ($S_{0,2}$=69 %) and 0.3 s ($S_{0,3}$=22 %).

	$D.10^9$ (m^2/s)	Rel. amp. (%)	T_2 (ms)
RBC in whole blood	0.21 (0.05)	32 (4)	210 (80)
plasma in whole blood	1.4 (0.2)	68 (8)	280 (110)
plasma alone	1.91 (0.02)	100	560 (560)

Table 4.5 Results of an average over 16 experiments, Δ = 6 ms, δ = 5 ms, 2τ = 0.6 ms, 8000 echoes, fitted on basis of Eq.[4.1]. The values between the brackets show the r.m.s. SD. The lowest row displays the values obtained from PFG MSE CPMG measurements on plasma alone.

The proximity of the two longest T_2's makes an accurate analysis difficult but the SD of all variables falls within the 10 % boundary. That the above mentioned T_2's are not a fit artifact is evident from the observed increase of D_{app} with TE when using the PFG MSE CPMG sequence. For identical T_2's this increase would not show up although this does not prove that the above mentioned T_2's do indeed exist. Fitting the 2D data set, assuming that exchange is absent (Eq.[4.1]), yields the results summarised in Table 4.5.

When using the PFG MSE CPMG sequence the T_2 component of 2.5 ms is not observed since the first echo which can be measured appears after 13 ms. The fractional amplitudes reported in Table 4.5 are slightly different from the ones reported in the text above. This is not caused by the absence of the first 12 ms when using the PFG MSE CPMG sequence, since an analysis of the first non-diffusion weighted curve of the PFG CPMG experiment yields two fractional amplitudes which are identical to the last two ones reported in the text above. We can think of three other explanations: *i*) The echoes are not all properly diffusion weighted. *ii*) Exchange between the RBCs and the plasma occurs. *iii)* Restricted diffusion occurs because of the RBC membranes, causing the signal amplitude to decrease non-exponentially with G^2. Point (*i*) can easily be checked by also performing the fit procedure I, described in Section 4.3.3. When insufficient diffusion weighting was found, the data set was discarded. Procedure I can also be performed using a two-exponential fit routine for all echo times (averaged over 8 echoes).

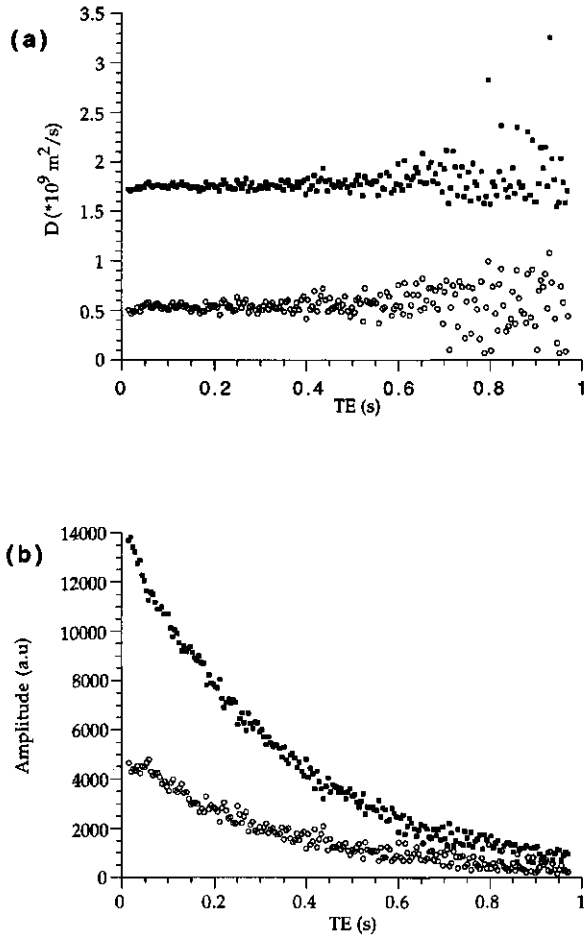

Figure 4.5 The data of a PFG MSE CPMG experiment (Δ=80 ms) was fitted using procedure I described in Section 4.3.3 using bi-exponential 1D fits at a wide range of echo times. Figure 4.5.a shows the diffusion constants at different echo times, Figure 4.5.b. shows the amplitudes stemming from the same 1D fits. The filled circles of both figures go together as are the open circles.

Fig. 4.5 a and b show the results of such a fit for Δ = 80 ms. In Fig. 4.5.a the two diffusion constants resulting from these fits for echo times between 16 ms and 1 s are shown (D_{rbc} = 0.5 10^{-9} m^2/s, D_{plasma} = 1.7 10^{-9} m^2/s). Fig. 4.5.b shows the fractional amplitude of each of the two fractions. Clearly the accuracy of the 1D fit decreases with the echo time because of the lower SNR at higher echo times. However, the diffusion constants remain constant over the whole period which indicates proper diffusion weighing. The two curves in Fig. 4.5.b show the

magnetization loss of each of the compartments and both decays are mono-exponential. Both apparent T_2's are larger than 200 ms. Results of Conlon and Outhred (16) have shown that the intrinsic T_2 of the RBC is smaller than 20 ms. By consequence, magnetization originating from the plasma leaks into the RBC during the measurement. Therefore the data was also fitted directly to Eq.[4.5], the two-site exchange model. Doing this did not result in a change of the fitted diffusion constants and only a slight change (<20%) for the fitted T_2's was observed. However, the SD sometimes increased to 40 % and no physically meaningful exchange rates could be calculated on basis of these fits. Because of the very low T_2 ratio the SD for most parameters, even when performing a normal 2D fit, was just barely below 20 %, significantly reducing the possibilities to study the degradation of the RBC's over a 24 h period. The low T_2 ratio also prevents the use of procedure II, discussed in Section 4.3.3, so the effects of restricted diffusion on the reliability of the 2D fit could not be investigated.

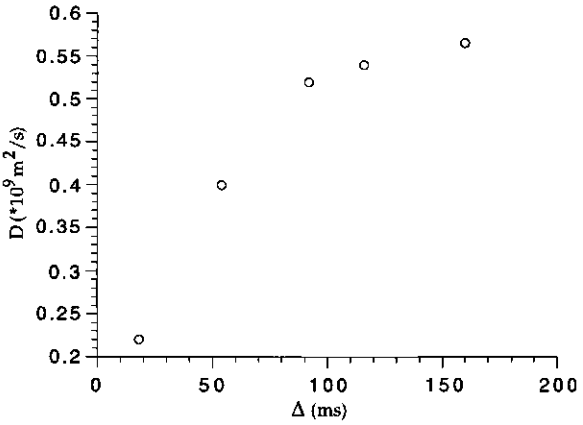

Figure 4.6 D(Δ) is plotted versus Δ, the labelling time, of magnetization residing primarily in the red blood cell as acquired by the PFG MSE CPMG sequence. A total of 8192 echoes (2τ = 0.6 ms) was acquired for all 16 diffusion steps for each of the 5 different labelling times.

When the labelling time (Δ) was increased we found that the diffusion constant of the fraction with the short T_2, which we contribute to the RBC based on the T_2 and the lower diffusion constant, increases. The results of these experiments are depicted in Fig. 4.6; the data points are an average of 16 measurements. Measurements of CPD blood resulted in an almost identical curve. At increasing Δ the difference of the diffusion constants becomes even less, D(Δ) of the RBC's increases (see Fig. 4.6), whereas that of the plasma decreases by about 20 % (D(Δ = 0.018 s) = 1.4, D(Δ = 0.164 s) = 1.1 10^{-9} m^2/s) which reduces the reliability of the 2D

fit even further (SD of 40%). Over the 24 h period no significant changes were found regarding D(Δ), the T_2's and the fractional amplitudes even though over this time span glucose in the Whole Blood was almost completely depleted (< 1mmol/L) and the K^+/Na^+ was somewhat disturbed indicating the onset of haemolysis.

An increase of D_{rbc} with increasing Δ was also found by Tanner (10) using a PFG STE sequence at 1.5 T, but in these experiments the increase only occurred with Δ > 700 ms. This author concluded that this must have been an fitting artefact. Calculations based on Tanner's data and model yielded P_d=1 10^{-4} m/s and r_{rbc} = 8 μm and , a gross overestimation of r_{rbc}. Results obtained by van der Veen et al. (21) at 7 T (using a PFG SE sequence and CPD blood) point to a different direction since in their experiments the r.m.s. displacement of the water molecules in the RBC reaches levels of at 2.2 μm, independently of Δ. A value for D_{rbc} was reported decreasing from 1.10^{-11} m^2/s to 2 10^{-12} m^2/s, a factor 20 to 100 lower than reported in our work, and a value for D_{plasma} which is lower by a factor 2 than values reported in our work and previous reports (2,10).

The T_2 of blood is known to be highly sensitive to the oxygenation level (22), 2τ and the B_0 strength because of diffusion through *in situ* field gradients within the RBC's. The very distinct divergence between the results of van der Veen et al. and the values reported in our work and in literature, can be explained invoking these internal gradients since we expect a lowering of the diffusion constant in the presence of a distribution of *in situ* field gradients, the decrease being dependent on Δ (23,24). At 0.5 T the internal gradients are significantly lower than at 7 T and because we used additional extra rf pulses between the PFG's, the effects of *in situ* field gradients are probably negligible. The internal field gradients also partly explain the increase of D_{rbc} after 700 ms in Tanner's work in stead of the much quicker rise with Δ as we have found, since Tanner performed his work at 1.5 T and made use of a sequence which was more sensitive to the internal gradients.

The multiple membrane model of Tanner (3) cannot explain the increase of D_{rbc} with Δ since in this model barriers were placed in a homogeneous solution and D_{rbc} should therefore decrease with Δ. Because $D_{plasma}(0)$ = 1.9 10^{-9} m^2/s, $D_{rbc}(0)$ = 0.6 10^{-9} m^2/s (as reported by Tanner (10)), $T_{2rbc}<T_{2plasma}$ and the exchange rate exceeds 50 s^{-1} (2,16) a proton diffuses in both fractions during the period Δ and D is an average diffusion constant of both fractions weighed by the residence time in each fraction during the period Δ, the T_2 of the respective fractions and the restrictions imposed by the RBC membrane. In the active surface model (4) a negative H parameter and a long T_2 outside the RBC should be

included to describe the behaviour of D(Δ) correctly. The results of the fit based on Eq.[4.5] do not indicate that the two-site exchange model can be used to explain the results, although it is clear from Fig.s 4.5.b and 4.6 that diffusive exchange between the RBC's and the plasma does occur. Because of the large SD values, this model should not be excluded on basis of the results presented above.

In a recent publication by Barzykin et al. (39) the boundary condition $T_2 = 0$ for spins penetrating a permeable boundary, as proposed by Snaar and Van As, was shown to be invalid for red blood cells even when the external medium was doped with a high concentration of relaxation agent. For this condition to be valid $D_{plasma}T_{2,plasma}/R^2$ should be << 1, which condition is not met for RBC's. The authors show that the eigen value problem of Eq.[4.7] can be solved analytically if a fraction outside the investigated compartment has a short, but finite value for T_2 and finite D. If the condition $D\Delta/R^2>1$ is fulfilled (the so-called long-time limit) the signal attenuation of the water molecules in the RBC is bi-exponential for small G^2 values (because spins can move into the plasma during Δ) even when only the signal originating from the RBC is measured. The fast component of the SAP originates from spins traversing the permeable membrane into a fraction with a different diffusion constant and T_2 and this component reflects the diffusion constant of the external fraction modulated by the permeability of the membrane.

Under our experimental conditions the situation is slightly more complicated since spins originating from the plasma also contribute to the NMR signal and may also exhibit a complicated diffusion behaviour. However, because of the T_2 difference between the two fractions the diffusion behaviour of both fractions should still be separable using the PFG MSE CPMG sequence. A quantitative analysis of the results should be feasible using the model proposed by Barzykin et al.

Apple parenchyma tissue

Since the T_2 of the cell wall is only 30 ms and it's fraction is only ≈ 8%, this compartment is difficult to detect directly using the PFG MSE CPMG sequence as the minimum echo time equals 18 ms. Using a Δ of 8 ms, however, three fractions could be found (Table 4.6). The origin of the first two fractions is not precisely clear but these are most likely to consist of a mixture of cytoplasm, extra cellular water and/or cell wall water. Fraction 2 is thought to reflect primarily cytoplasm water and fraction 3 originates from the vacuole water (compare with (23)). When the labelling time is increased it is no longer possible to fit three fractions. The value of

the shorter T_2's increased with Δ, which indicates that both fractions do not have a discrete T_2 but represent an average value of a spectrum of T_2's.

	$D.10^9$ (m^2/s)	T_2 (ms)	Rel. amp.(%)
Fraction 1.	1.37 (0.04)	125 (5)	10 (1)
Fraction 2.	1.20 (0.02)	650 (10)	22 (2)
Fraction 3.	1.60 (0.03)	1350 (10)	68 (2)

Table 4.6 The diffusion constants and T_2's as observed in apple parenchyma tissue using the PFG MSE CPMG sequence with a minimum echo time of 18 ms and Δ=8 ms, 2τ = 0.6 ms, TR =15 s. Between brackets the r.m.s. SD is given.

In the study of $D(\Delta)$ vs. Δ (Fig. 4.7) only 2 fractions were used for the fits. The upper points (open circles) in Fig. 4.7 stem from a fraction with a T_2 of 1.28 s (83 %), the lower points (open squares) stem from a fraction with a T_2 of 260 ms (17 %) which increases to a T_2 of 750 ms for Δ=600 ms.

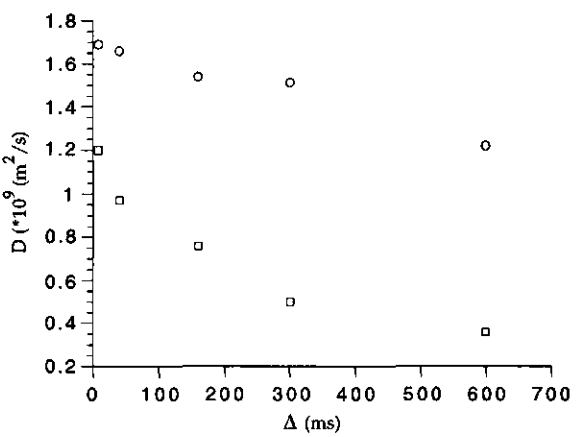

Figure 4.7 $D(\Delta)$ is plottedversus Δ for two fractions of a piece of apple acquired with the PFG MSE CPMG sequence, values for TE and G as in Figure 4.6. The top curve is thought to represent water in the vacuole, the lower curve a mixture of the cytoplasm and extra cellulair water.

With increasing Δ the minimum TE which can be used for the fit also increases. If the discrete T_2 value represent a spectrum of T_2's the significance of the shorter T_2's decreases with Δ and therefore a longer discrete T_2 may be found; a different subset of molecules determines the fitted relaxation time. In order to be able to compare the results obtained at longer labelling times with those obtained at shorter ones the minimum TE used for the 2D fits can be set to the one which is used for the longest Δ. The echoes sampled before this minimum TE are

disregarded. Results for D(Δ) of these adjusted fits are almost identical to the fits without setting the minimum TE, but give an enhanced $T_{2,2}$, namely 750 ms for all labelling times. The latter procedure gives a lower χ^2, it reduces from 6.5 to 2.4, but, since the T_2's and the D's of the two fractions become similar, the reliability of the fits with the adjusted minimum TE is less (SD of 30 % , compared to a SD of 8 % using the complete data set at short Δ).

Because the T_2 ratio with short Δ is larger than 3 it is worthwhile to investigate whether restricted diffusion effects are present. Restricted diffusion may cause a non-exponential decay of the signal with G^2, which influences the results of the 2D fit. This can be done by applying procedure II as described in Section 4.3.3. A data set with Δ= 60 ms was analysed following this procedure; the decrease of the signal of two fractions with increasing *b*, the fractions being separated based on the existing T_2 difference, is presented in Fig. 4.8. The open circles represent the SAP of the vacuolar water (longest T_2) with D=1.6 10^{-9} m^2/s, the squares represent the SAP of the cytoplasm and extra cellular water, with D=1.0 10^{-9} m^2/s. These values are within 10 % of the values determined with the 2D fit routine. In none of the experiments a non-linear decay of the SAP was found, indicating that restricted diffusion does not disturb the 2D fits of the data.

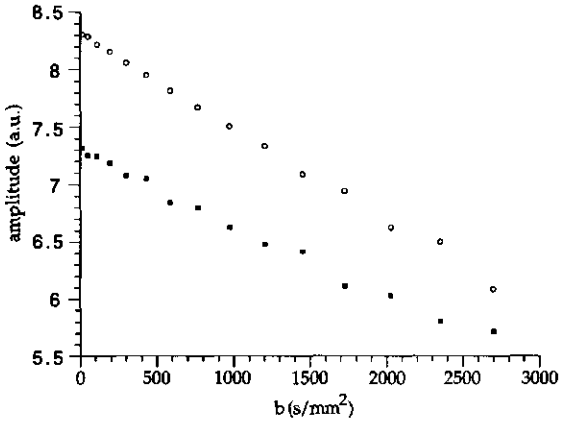

Figure 4.8 A Signal Attenuation Plot thought to represent the magnetization decay of vacuole water (upper curve) and vacuolar water (lower curve) when data acquired with the PFG MSE CPMG and analysed following procedure II described in Section 4.3.3.

To investigate the behaviour of D(Δ) at very long labelling times the PFG MSE sequence was used with an echo time of 2 s (one data point was acquired with TE= 4 s, 2τ= 4 ms). The PFG MSE sequence was used since it is programmed slightly different (34) and has a greater flexibility, so the TE at which the first (and

only) echo is measured can remain constant while changing Δ. The r.m.s. displacements calculated from the D(Δ) values are depicted in Fig. 4.9. From microscopic inspections we know the diameter of the spherical apple cells to be 100-130 μm (25). The r.m.s. displacement does not exceed this number even while using a labelling time of 4 seconds. The r.m.s. displacement of the fraction with the shorter T_2 levels is at least 22 μm ($x = \sqrt{2Dt} = 2 * 0.4.10^{-9} * 0.6 = 22\mu m$) which is considerable more than the thickness of the cytoplasm (approximately 7 μm). Part of these molecules may have spent some time in the vacuole or the extra cellular space during the labelling time, thereby enlarging the measured r.m.s. displacement. Also, some of the signal contributing to the short T_2 fraction may originate from extra cellular water, of which the diffusion pathway is unknown.

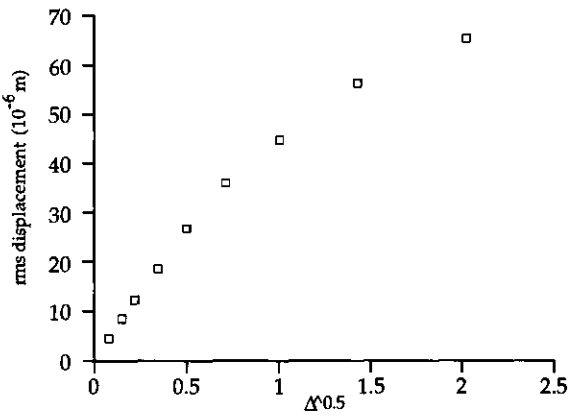

Figure 4.9 The root mean square displacement of magnetisation in apple tissue versus the square of the labelling time as acquired with the PFG MSE sequence using echo times of 2 s and 4 s for the last data point in this figure.

The results presented here show a somewhat different behaviour from other published material where the PFG SE was used (Snaar and Van As (25)). In that work D(Δ) has dropped to $10^{-9}m^2/s$ after 200 ms as compared to 1.55 $10^{-9}m^2/s$ in our work. The difference between the results of Snaar and Van As and the results presented here is due to the fact that the PFG SE is very sensitive to background gradients. Lian et al. found, using a sequence not sensitive to background gradients and working at 100 MHz, D_{app} = 1.42 10^{-9} m^2/s (26), a value identical to what we found for an average diffusion constant at an echo time of 30 ms (using the PFG MSE sequence). Lian et al. calculated that at 100 MHz the average *in situ* filed gradient, $<G_0>$, equals 89 mT/m ,which reduces to 18 mT/m at 20 MHz. The height of these internal gradients certainly affects the value of D and the slope of

$D(\Delta)$ vs. the labelling time using echo times of ~ 200 ms (τ=100 ms) as was done by Snaar and Van As. Since these gradients are highly local it is likely that the subset measured by a PFG SE sequence is also different from that using a PFG NMR sequence compensated for internal gradients.

The model of Barzykin et al. (39), discussed in the previous Section may also be useful. However, here the long-time limit is not met, causing a much more complicated set of equations with more than one eigen value (α_n).

Flow through a Sephadex column

When water is pumped through a column of stacked glass beads it is observed that the dispersion coefficient obtained from the SAP increases linearly with Δ when the flow rate is such that the vertical displacement is less than the bead diameter times the porosity (28,29). The direction of the flow is then approximately constant during the period Δ; the stationary random flow regime (31). Our measurements were performed solely in this regime because a G25/300 Sephadex column cannot sustain flow rates above 2 mm/s (in the void volume) without visible compression. Columns made of softer Sephadex beads compress at even lower flow rates.

Using the PFG MSE CPMG sequence, data sets were acquired which were all fitted to different models, e.g. two fractions each with a single value for T_2 and D, two fractions of which one (supposedly the void volume where flow occurs) has two D values, two fractions with two-site exchange and finally a model with three fractions without exchange. The model with two D values for the flowing fraction was used since Palstra et al. (28,29) have observed this phenomenon and we wished to investigate whether this could also be observed in the Sephadex column. Although the simplest model with only two non-exchanging fractions did not give the best fits (the 2D residual plot was clearly not flat), it was the only model which gave reproducible results over the whole range of flow rates and labelling times (18, 30, 42, 54, 90 and 150 ms). At flow rates of 1.05 and 1.74 mm/s, the data are best described by three relaxation rates and diffusion constants. At lower flow rates the three fraction model was used only to clarify the fit results which were obtained using the two fraction model.

Figure 4.10 a,b,c The diffusion value of the void volume and the inner volume of G25/300 Sephadex beads suspended in water, at three flow rates. a) 0.35 mm/s, b) 1.05 mm/s and c) 1.74 mm/s.

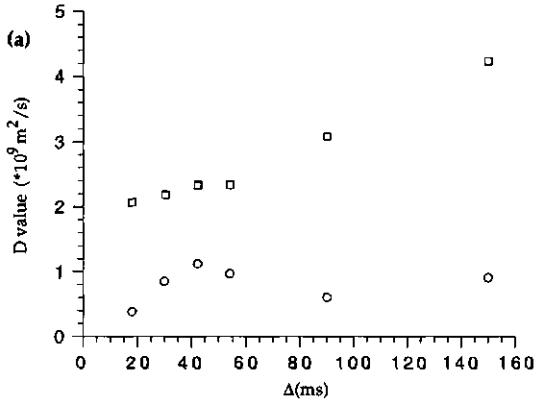
(a)
D value (*10^9 m^2/s)
0
1
2
3
4
5
0 20 40 60 80 100 120 140 160
Δ(ms)

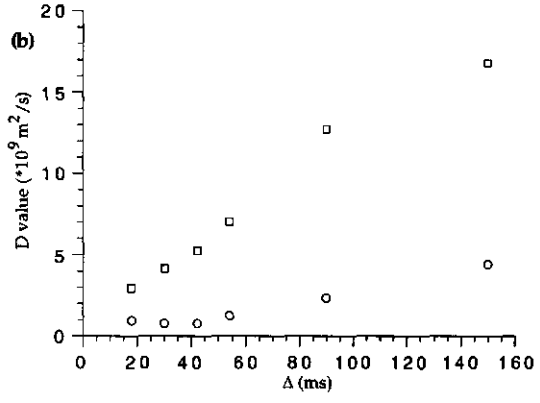
(b)
D value (*10^9 m^2/s)
0
5
10
15
20
0 20 40 60 80 100 120 140 160
Δ (ms)

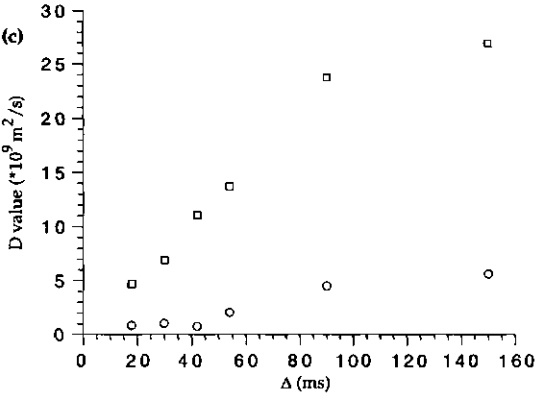
(c)
D value (*10^9 m^2/s)
0
5
10
15
20
25
30
0 20 40 60 80 100 120 140 160
Δ (ms)

At the two lower flow rates the SD of the three fraction model exceeded 30 %. The main reason for the difficulty with fitting the data to three fractions is that the long tube sticks out of the rf and gradient coils, thereby becoming relatively sensitive to noise generated by the gradients, and ambient e.m.f. noise, causing relatively slow fluctuations of the baseline of the NMR signal (2-5 times the noise level).

The values of D(Δ) for two fractions obtained by the PFG MSE CPMG are depicted in Fig. 4.10 (a,b,c) for three different flow rates. At v = 0 mm/s we find two D values, i.e. 0.7 10^{-9} m^2/s and 1.7 10^{-9} m^2/s for all Δ's. The fraction with the longest T_2 of 670 ms (41 %) is thought to represent the water in the void volume since it is this fraction of which D* increases almost linearly with Δ and the flow rate (at least for 1.05 and 1.74 mm/s). At 1.74 mm/s the T_2 of this fraction reduces to 420 ms. This cannot be explained, however, by outflow effects, since it can be calculated that after 1.5 s only 8 % of the water in the void volume disappears from the sensitive region of the r.f. coil with a length of 3 cm. At the two highest flow rates the short T_2 of 70 ms (59 %) also reduces, namely to 25-35 ms. Since both T_2's become shorter, this indicates that the Sephadex column is compressed or changed (although not visibly) at these flow rates. At the highest flow rate we find fractions which show similar relaxation behaviour to that found by Hills et al. (35). This author used centrifugation prior to the measurements at 300 MHz. In Table 4.7 the results of a three fraction fit for a flow rate of 1.74 mm/s and a Δ of 18 ms are presented.

	Rel. Amp. (%)	T_2 (ms)	$D.10^9$ (m^2/s)
Fraction 1.	51.5 (1)	25.0 (0.3)	0.99 (0.01)
Fraction 2.	6.4 (0.5)	120 (9)	1.45 (0.05)
Fraction 3.	42.1 (1)	378 (6)	2.84 (0.02)

Table 4.7 Results of a three exponential fit of 1.74 mm/s flow through a G25/300 Sephadex column with Δ =18 ms. The numbers between the brackets are the r.m.s. SD values.

It should be noted that the discrete T_2 values are likely to represent a spectrum of T_2's rather than a single discrete T_2 (18). To prevent that the results obtained at short labelling times are incomparable with those obtained at longer labelling times we disregarded all echoes sampled before the minimum TE which could be used for the longest Δ (this is an identical procedure to the one used for the apple parenchyma tissue). When the minimum TE used for the 2D fit is fixed to 160 ms for all Δ's D_{bead}(Δ = 18 ms) increases with 30 % compared to results obtained without adjusting the minimum TE for the 2D fit. At the highest flow rate the apparent increase of D_{bead}(Δ) is over 400 %. This would indicate that there is

some flow in the Sephadex beads. However, when three exponentials are used to fit the data obtained at the highest flow rate, $D(\Delta)$ of the fraction with a T_2 of 30 ms remains constant at about 0.9 10^{-9} m^2/s. The diffusion constant coupled to the middle T_2 rises with Δ from 1.2 to 8 10^{-9} m^2/s. $D(\Delta)$ of the fraction coupled to the longest T_2 follows the same trend as depicted in Fig. 4.10c, with a 10 % higher value for D.

The fraction with the middle T_2 (fraction 2) is likely to represent a component which experiences both relaxation in the beads and in the void volume, a tentative conclusion also reached by Hills (35). Convection in Sephadex beads is not likely to exist in a Sephadex bead (38) and should be ruled out to explain the increase of $D_{bead}(\Delta)$ with Δ when using the two fraction model. The most likely explanation of the rise of $D(\Delta)$ coupled to the short T_2 therefore lies in water protons experiencing two domains during Δ and/or the time after the gradient pulses. In the two fraction model the fraction with the lowest D is probably a mixture of fraction 1 and 2 from Table 4.7.

4.5 Conclusions

We have demonstrated in both Chapters 3 and 4 that small differences between diffusion constants need not prevent an accurate analysis of these diffusion constants as long as the relaxation times of the ensembles are distinguished. Using the PFG MSE CPMG sequence and the subsequent analysis of the 2D data set is not fundamentally different from using the PFG MSE sequence at different echo times. The difference is mainly a practical one, where the PFG CPMG is superior in experimental time expenditure, overall SNR and stability. The resolution limit as determined by MCS studies is close to the experimentally determined resolution, that is, a T_2 ratio of 2 and a D ratio of 1.33 (fractional ratio of 1) determined by the MCS studies and a T_2 ratio of 2 and a D ratio of 1.5 as the experimental limit. This limit can be reduced further by increasing the stability of the sample and the spectrometer during the measurements. Discrimination of three fractions has been demonstrated in this work also but then the relatively low SNR limits the accuracy of the fits. However, fitting with three fractions or a distribution of relaxation times holds much promise for further improvement in the understanding of diffusion in heterogeneous samples. Minimising artefacts like susceptibility differences are essential to achieve this goal so the approach of using additional rf pulses between the PFG's is essential.

In three of the samples mentioned in this Chapter not only multi-exponential decay in the *b*-domain and TE-domain play a major role, but also diffusive exchange between the ensembles or compartments (either restricted or non restricted), which are the building blocks of these samples, is present. (Restricted) diffusive exchange between compartments is best studied by changing the labelling time of the diffusion experiments (32). In whole blood we found an increase of D_{rbc} and a decrease of D_{plasma} with Δ. For these samples diffusive exchange is not much affected by the membrane of the RBC's. In apple parenchyma tissue the membranes seem to reduce the diffusive exchange more severely, although water in the cytoplasm seems capable of traversing the tonoplast and penetrating into the vacuole, since the average r.m.s. displacement during Δ exceeds the thickness of the cytoplasm. Because $D(\Delta)$ still decreases with Δ the tonoplast membrane is more restrictive than the RBC membrane; the ratio of the residence time of water in the cytoplasm and the vacuole is much larger than the ratio of the residence time of water in the RBC and the plasma. In the Sephadex column with flow in the void volume a third fraction seems to exist which is not as clear an ensemble as the vacuole or the RBC, but more likely an intermediate region between two ensembles, the Sephadex bead and the void volume, respectively. The layer is detected by PFG NMR because diffusive exchange occurs between two physically distinct regions (bead and void volume).

A theoretical framework for diffusional behaviour, either rotational or translational, has not been presented in this Chapter. Most data, however, can be understood by an intuitive approach. For a quantitative analysis of the 2D data sets acquired with the PFG MSE CPMG sequence with variable Δ, related to T_2, D, q,TE and Δ, such a theoretical framework is certainly required for an accurate fit of the data. The models of Tanner and Snaar/Van As could not be used in the three samples discussed before because the boundary conditions of these models are not valid for these samples. Numerical models of Hills and Snaar (32) and Zawodzinski (6) do offer the opportunity to get a more reliable interpretation of the data, certainly when these models are modified to include PFG MSE CPMG measurements. Combination of theory and experiment can thus be helpful to understand the dynamics of water in heterogeneous samples.

Appendix 4.a

The solution of the two coupled differential equations (4.2,a,b) is

$$m_a(t) = p_a^+ \exp(-R^+t) + p_a^- \exp(-R^-t) \qquad [4.13a]$$

$$m_b(t) = p_b^+ \exp(-R^+t) + p_b^- \exp(-R^-t) \qquad [4..13b]$$

with

$$p^+_{a,b} = \frac{R_{a,b} - R^-}{R^+ - R^-} \cdot p_{a,b} \qquad [4.14a]$$

$$p^-_{a,b} = \frac{R_{a,b} - R^+}{R^+ - R^-} \cdot p_{a,b} \qquad [4.14b]$$

The decay of the total magnetisation is described by $m_a(t)+m_b(t)$. Thus, the magnetization decay is given by

$$M(t) = M_0\{p^+\exp(-R^+t) + p^-\exp(-R^-t)\} \qquad [4.15]$$

where p^+ is a sum of p_a^+ and p_b^+ and p^- is a sum of p_a^- and p_b^-. The relaxation rates R^+ and R^- of Eqs. 4.13, 4.14 and 4.15 are given by

$$R^{\pm} = \frac{1}{2}\left(R_a + R_b + \frac{1}{\tau_a} + \frac{1}{\tau_b} \pm \sqrt{\left(R_a - R_b + \frac{1}{\tau_a} - \frac{1}{\tau_b} \right)^2 + \frac{4}{\tau_a \tau_b}} \right) \qquad [4.14]$$

Based on Eq.[4.12,a,b] the true fractional amplitudes and relaxation rates can be calculated. The exchange rate can be calculated on basis of Eq.[4.14].

References.

1. P.S. Belton and B.P. Hills, Molecular Physics **6**, 999 (1987).
2. J. Andrasko, Biochim. Biophys. Acta **428**, 304 (1976).
3. J.E. Tanner, J. Chem.Phys **69**, 1748 (1978).
4. J.E.M. Snaar and H.Van As, J. Magn. Res. **A 102**, 318 (1993).
5. K.R. Brownstein and C.E. Tarr, J. Magn. Res **26**, 17 (1977).
6. T.A. Zawodzinski, T.E. Springer, M. Neeman and L.O. Sillerud, Israel J. Chem **32**, 281 (1992).
7. J.R. Zimmerman and E.O.Brittin, J. Phys Chem. **61**, 1328 (1957).
8. H.T. Edzes and E.T. Samulski, J. Magn. Reson. **31**, 207 (1978).
9. J. Kärger, Ann. Phys. **24**, 1 (1969).
10. J.E. Tanner, Arch. Biochem. and Biophys. **224**, 416 (1983).
11. J. Kärger, H. Pfeifer and W. Heink, Advances in Magn. Reson. **12**, 1 (1988).
12. T. Gullion, D.B. Baker and M.S. Conradi, J. Mag. Reson. **89**, 479 (1990).
13. W.H. Press, S.A. Teukolsky, W.T. Vetterling and B.P. Flannery,' Numerical Recipes in C, second edition', Cambridge University Press (1992).
14. J. Pekar, C.T.W. Moonen and P.C.M. van Zijl, Magn. Reson. Med **23**, 122 (1992).
15. M.D. King, N. van Bruggen, A.L. Busza, J. Houseman, S.R. Williams and D.G. Gadian, Magn. Reson. Med. **24**, 288 (1992).
16. T. Conlon and R. Outhred, Biochim. Biophys. Acta **288**, 354 (1972).
17. J.E.M. Snaar and H. Van As, Biophys. J. **63**, 1654 (1992).
18. B.P. Hills, K.M. Wright and P.S. Belton, Molecular Phys. **67**, 193 (1989).
19. J.A. Dormandy, Viscositas **1**,1 (1979).
20. J.K. Nicholson, M.J. Buckingham and P.J. Sadler, Biochem. J. **211**, 605 (1983).
21. J.W.C. van der Veen, P. van Gelderen, J.H.N. Creyghton and W.M.M.J. Bovée, J. Magn. Reson. **29**, 571 (1993).
22. K.R. Thurlborn, J.C. Waterton, P.M. Matthews and G.K. Radda, Biochim. Biophys Acta **714**, 265, (1982).
23. D. van Dusschoten, P.A. de Jager and H. Van As, J. Magn. Reson. A **116**, 22 (1995).
24. J Zhong, R.P. Kennan and J.C. Gore, J. Magn. Reson. **95**, 267 (1991).
25. J.E.M. Snaar and H. Van As, pers. communication.
26. J. Lian, D.S. Williams and I.J. Lowe, J. Magn. Res. **A 106**, 65 (1994).
27. D. Le Bihan E. Breton, D. Lallemand, M.L. Aubin, J. Vignaus and M. Laval-Jeantet, Radiology **168**, 497, (1988).
28. W. Palstra, H. Van As and T.J. Schaafsma, pers. communication
29. W. Palstra, H. Van As and T.J. Schaafsma, pers. communication

30. L. Fischer,' Gel Filtration Chromatography', Elsevier/North-Holland (1980).
31. B.P. Hills and S.L. Duce, Magn. Reson. Imaging **8**, 321 (1990).
32. B.P. Hills and J.E.M Snaar, Molecular Phys. **76**, 979 (1992).
33. P.T. Callaghan,' Principles of Nuclear Magnetic Resonance Microscopy', Clarendon Press, Oxford, 1992.
34. D. van Dusschoten, P.A. de Jager and H. Van As, J. Magn. Reson. **A 112**, 237 (1995).
35. D. van Dusschoten, C.T.W. Moonen, P.A. de Jager and H. Van As, submitted to Magn. Reson. in Med.
36. J.S. Veres, G.A. Johnson and P.J. Kramer, A. J. Botany **78**, 80 (1991).
37. A.V. Barzykin, K. Hayamizu, W.S. Price and M. Tachiya, J. Magn. Reson. **A 114**, 39 (1995).
38. S.B. Libicki, P.M. Salmon and C.R. Robertson, Biotechn. and Bioeng. **32**, 68 (1988).
39. M. Holz and H. Weingärtner, J. Magn. Reson. **92**, 115 (1991).

Netherlands Journal of Zoology
45 (3-4): 338-346 (1995)

Chapter 5

5.1 VISUALISING THE WATER FLOW IN A BREATHING CARP USING NMRi

by

COEN VAN DEN BERG*#, DAGMAR VAN DUSSCHOTEN†, HENK VAN AS†, ARIE TERLOUW*, TJEERD J. SCHAAFSMA† and JAN W.M. OSSE*

(**Department of Experimental Animal Morphology and Cell Biology, Agricultural University of Wageningen, Marijkeweg 40, 6709 PG, Wageningen, the Netherlands; †Department of Molecular Physics, Agricultural University of Wageningen, Dreijenlaan 3, 6703 HA, Wageningen, the Netherlands*)

ABSTRACT

The study of water flow inside the fish mouth and opercular cavities has been hampered by the lack of a non-invasive measuring device. Measurements of the water flow during breathing of a carp are presented here, using a non-invasive technique, Nuclear Magnetic Resonance imaging (NMRi). Using NMRi, velocity profiles in a whole slice of the fish can be measured at once. The present results, which represent the average flow pattern during a breathing cycle, confirm literature data of an elongated volume of moving water in front of the mouth of the fish. Furthermore, it is observed that in the narrow spaces between the hemibranchs the water flow remains fast. Suggestions are given for improvement of the experimental set-up, such that more detailed and complete data of the flow in the fish mouth and opercular cavities may be obtained.

KEY WORDS: NMR imaging, flow visualisation, *Cyprinus carpio*.

INTRODUCTION

During breathing and suction feeding fish expand and compress their head, generating water flow through their buccal and opercular cavities (BALLINTIJN, 1968). Detailed knowledge of the water flow pattern generated by this expansion/compression pump is needed for the study of this pump, the gas exchange processes in the gills and the filter-feeding mechanism of the branchial sieve (HOOGENBOEZEM *et al.*, 1991).

There are three approaches to study flow patterns: hydrodynamic modelling, physical modelling and experimental measurement. Since the system 'fish head' is instationary both in time (it is a rhythmical pump) and in shape and dimensions (expansion/compression of the head) it is very difficult to make a hydrodynamic model of water flow in the fish head. Even a comparatively simple model, describing the mouth cavity as an expanding truncated cone, leads to highly complicated hydrodynamics (MULLER *et al.*, 1982). Furthermore, too little is known of the complex shape and shape changes of the buccal and

Present address (= address for correspondence): Department of Zoology, University of Cambridge, Downing street, CB2 3EJ, Cambridge, United Kingdom.

opercular cavities during a breathing cycle to construct an adequate physical model of the fish head.

The water flow outside the fish head has been measured accurately using neutrally buoyant polystyrene spheres (MULLER *et al.*, 1982; VAN LEEUWEN, 1984). The pressures in the buccal and opercular cavities during breathing and feeding have been recorded with pressure transducers (*e.g.* HUGHES & SHELTON, 1958; HOLETON & JONES, 1975; ALEXANDER, 1967, 1983; LAUDER, 1980; VAN LEEUWEN & MULLER, 1983; SIBBING *et al.*, 1986) and local velocities have been measured using a hot-film anemometer (MULLER & OSSE, 1984). Disadvantages of these techniques are that only point measurements are made and that the measuring device interferes with normal functioning of the fish and possibly with the flow pattern itself, since it needs to be placed inside the fish head. In a study of the buccal flow velocity in the paddlefish, SANDERSON *et al.* (1994) overcame the second of these problems by inserting the probe through a hole in the hyomandibula.

The above problems may be overcome using NMR (Nuclear Magnetic Resonance) flow imaging. NMR sequences are available to measure flow in rhythmically moving organs, like the heart (*e.g.* DIESBOURG *et al.*, 1992). NMR imaging is non-invasive, hence it does not interfere with the flow pattern. Furthermore, the flow profile in a whole slice of the object can be measured in a single experiment. A disadvantage of the technique is the total duration of the measurements, which necessitates the object to be immobilised (partly anaesthetised). Also, the echo time (see materials and methods) must be short compared to the length of one cycle, *i.e.* in case of fish respiration preferably less than 50 ms, to avoid artefacts caused by breathing movements.

This paper presents for the first time NMRi measurement of the water flow pattern in a breathing carp. Although the biological relevance of the present data is limited, the results clearly show the potential of NMRi in this novel field of application.

MATERIALS AND METHODS

Carp and anaesthesia

The carp (*Cyprinus carpio* L.) of 15-25 cm standard length were laboratory bred at the Dept. of Experimental Animal Morphology and Cell Biology in Wageningen. They were transported to the measurement site in buckets, sedated in 20-25 mg per litre MS222 (Crescent Research Chemicals, Phoenix, USA). We found that a stabile, deep state of anaesthesia could not be achieved with MS222, given the fact that the fish cannot be observed when it is in the NMR machine.

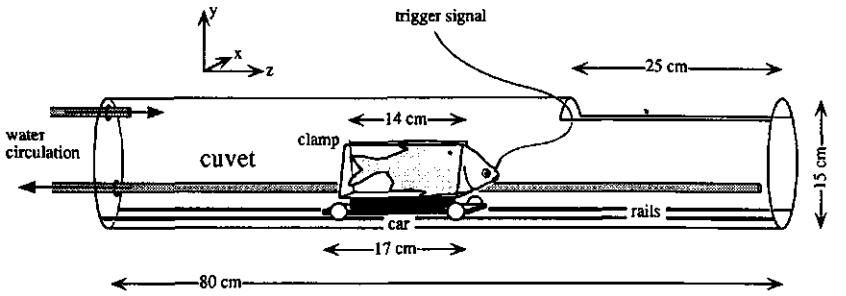

Fig. 1. Cylindrical cuvette designed for the NMR experiments, with the anaesthetised carp in a clamp on a cart, as described in the text.

Instead, we used intra-peritoneal injections of Nembutal (Abbot, SA, France), which took about an hour to take full effect. Since Nembutal has never before been used in fish, its effect was tested prior to the experiments. The dose required to get a carp in a stabile, deep state of anaesthesia turned out to be very critical and somewhat dependent on the specimen (on average 60 mg/kg). Some habituation was observed. At the NMR measurement site several injections of Nembutal were given, carefully increasing the total dose until the carp just kept breathing quietly (breathing frequency 0.5-1 Hz) but stopped responding to being picked up. Usually, the carp would remain in this state for over two hours.

Cuvette and fish immobilisation

The fish was put in a cylindrical cuvette (fig. 1), containing no iron or other ferro-magnetic materials. A total volume of 18 litre of water could be circulated through the cuvette by means of a pump at more than three meters from the magnet (in view of the strong magnetic stray fields). During measurements the pump was stopped, to ensure that water flow is caused exclusively by the fish. The anaesthetised, breathing fish was fixed in a plastic clamp, leaving the head free. A wet cloth protected the clamped body. The clamp was fixed on a cart, which could slide on rails attached to the bottom of the cuvette (fig. 1). Once the fish was placed in the cuvette, a lid was put on the opening and sealed with waterproof adhesive tape. By twisting the cart handle, the height of the clamp could be altered, using a construction of plastic cogs and axles (technical Lego). Thus, both the vertical and axial position of the fish could be adjusted while it was in the cuvette, hence

the measuring area (the mouth cavity of the fish) could be positioned in the centre of the r.f. coil and the magnet.

NMR techniques

The general principles of NMR imaging are treated in several recent textbooks on this subject (*e.g.* CALLAGHAN, 1991), but for clarity some of the aspects of NMR are mentioned here. NMR is based on the fact that the atomic nuclei in an object behave as tiny magnets. The nuclei will tend to align to a strong magnetic field (H_0); the object will thus get a net magnetic vector in the direction of H_0. The magnetic axis of each nucleus rotates around the direction of H_0 (= precession; similarly, a spinning top precesses in the gravitational field), but since all nuclei precess out of phase this does not affect the orientation of the net magnetic vector of the object. The precession frequency is dependent (a/o) on the type of nucleus; hydrogen nuclei (= protons) are used for NMR imaging. By applying a second magnetic field (H_1) at right angles to H_0 and rotating at the precession frequency (a so-called r.f. (= radio frequency) pulse), the hydrogen nuclei can be excited (made to precess in phase) and the net magnetic vector of the object will start to precess and move out of the direction of H_0. When the r.f. pulse is stopped the vector will return to its original position. The time constants of this decay are called T_1 (decay in the direction of H_0) and T_2 (decay perpendicular to H_0). The decay is measured as the electric signal which is induced by the rotating magnetic vector (the 'echo'). The time delay between excitation by the r.f. pulse and measurement is called the echo time (TE). By using gradients in the magnetic field strength a well defined slice can be selected, with adjustable angles with respect to the magnet coordinate frame. To obtain the full spatial information within such a slice several measurements need to be done, *e.g.* for a 128×128 image 128 measurements have to be done. The time delay between measurements of the same slice is called the repetition time (TR). Due to the large number of scans required for imaging, it is essential that the object remains immobile. For regular, pulsatile flow best results are obtained by triggered data acquisition, yielding flow data at a particular phase of the cycle.

For the present NMR measurements a so-called Fast Field Echo (= FFE) sequence (VAN DER MEULEN *et al.*, 1988) was used. This r.f. pulse sequence can acquire a 128×128 image within 400 ms depending on the available hardware and is considered to be relatively fast. It consists of a burst of low intensity, equally spaced, narrow bandwidth r.f. pulses. Since the TR in these experiments is comparatively short, the water protons in the slice get saturated and the signal intensity dimin-

ishes. However, if non-excited water protons enter the slice during the scan the signal reduction is less. This happens when flow perpendicular to the slice exists. Regions with such flow brighten up, the increase of signal being proportional to the flow speed. Unfortunately, this relation is non-linear, since it also depends on the T_1, T_2, TR and TE; calibrations have to be extensive. It has been shown in medical applications that with some adjustments FFE can be used to quantitatively measure flow (BOESINGER *et al.*, 1992). A few other NMR techniques ('single shot sequences') allow faster data acquisition, sometimes within 100 ms. Using such sequences, like EPI and GRASE, quantitative flow measurements can be done in short time intervals (*e.g.* COHEN & WEISSHOFF, 1991).

All measurements presented here were performed on a standard 1.5 T Whole Body Imager of Philips Medical Systems at its test facility in Best, the Netherlands. The r.f. pulse frequency was 64 MHz. The repetition time (TR) was 24 ms, the total scan time per slice was 2.8 s (*i.e.* 116 scans per slice) and the echo time (TE) was 10 ms. The slice thickness was 2 mm. Slices were selected in three orthogonal directions.

RESULTS AND DISCUSSION

The present results were obtained without triggering by the breathing signal, hence the *average* water flow pattern during a number of breathing cycles was measured (116 scans in 2.8 s; with a breathing frequency of between 0.5 and 1 Hz this means 1.5 to 3 breathing cycles). Despite this averaging the motion artefacts are small, most likely because the breathing movements of the anaesthetised carp are small compared to normal breathing movements. All data are from one carp, during one session, with identical experimental conditions throughout. Figure 2A, B and C show transversal, horizontal and sagittal slices of the breathing carp; figure 2D shows the orientation of these slices with respect to the fish. The signal intensity (brightness) in the cross section of the fish body is related to the magnetic properties of each tissue. The signal intensity of the water is related to the water flow component *perpendicular* to the plane of the slice. The signal intensity of the water increases with the magnitude of this flow component. The relation between these parameters has not been quantified, but it is the same for each of the three slice directions.

Both in front of the mouth and behind and beneath the opercular slits the water flow has strong components in all directions (Fig. 2A-C). Interestingly, the smoke-like volume of moving water in front of the mouth (Fig. 2B, C) is similar to the water flow patterns measured and

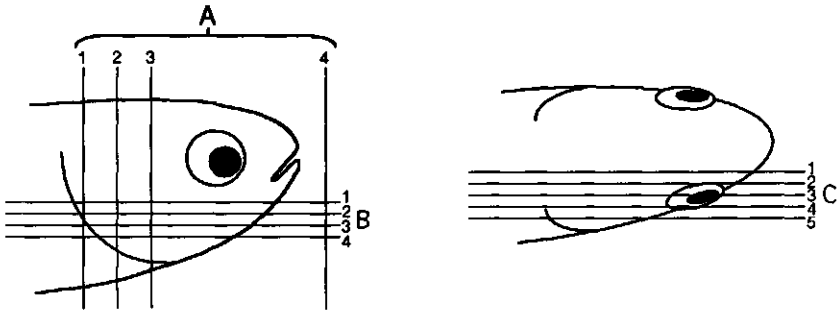

Fig. 2. A) Transversal slices. The water flow component in the z-direction (rostro-caudal) is measured here. The slices of picture 1-3 show cross sections of the branchial apparatus from back to front, with 6 mm spacing between the slices (from left to right). Picture 4 is a slice 5 mm in front of the mouth. B) Horizontal slices. The water flow component in the y-direction (dorso-ventral) is measured here. The slices show the gills from top to bottom with 2 mm spacing between the slices (from left to right). The black arrows indicate the flow in the narrow slit between the hemibranchs of the first and second gill arch. Note the smoke-like volume of water flow in front of the mouth. C) Sagittal slices. The water flow component in the x-direction (left-right) is measured here. The slices show the right side of the fish from inside to outside, with 2 mm spacing between the slices. Note the smoke-like volume of water flow in front of the mouth and the downward oriented water flow through the opercular slit. The black arrow indicates the flow in the narrow slit between the hemibranchs of the fourth gill arch. D) This scheme shows the positions of the numbered slices in fig. 2A-C with respect to the fish. Note that the fish orientation is not exactly in line with the NMR frame of reference. a = anterior, d = dorsal, ga = gill arch, p = posterior, ps = pharyngeal slit, sb = swim bladder, v = ventral.

predicted by VAN LEEUWEN (1984; figures 7 and 14 of this reference). The water flow through the opercular slits is largely oriented downwards. The flow signal inside the mouth tube, the pharyngeal slit, the gill slits and between the hemibranchs is white (comparatively high velocity). Moreover, these high velocities occur in all directions (x, y and z). It cannot be decided from the present experiments whether this is due to turbulent flow or to averaging of the flow patterns. The images clearly show that water flows through each gill slit. Furthermore, the signal remains bright (fast flow) even in the narrow slits between the hemibranchs (arrows in fig. 2B, C). The clear image of the hemibranchs in the present averaged flow data suggests that the gill arches are essentially motionless during quiet breathing.

Several aspects of the present experimental set-up can be optimised:
— Triggering: we tried to use the pressure fluctuations in the buccal cavity of the fish as trigger signal (*c.f.* VAN LEEUWEN & MULLER, 1983). A long tube (Ø 2 mm), filled with water, was surgically inserted

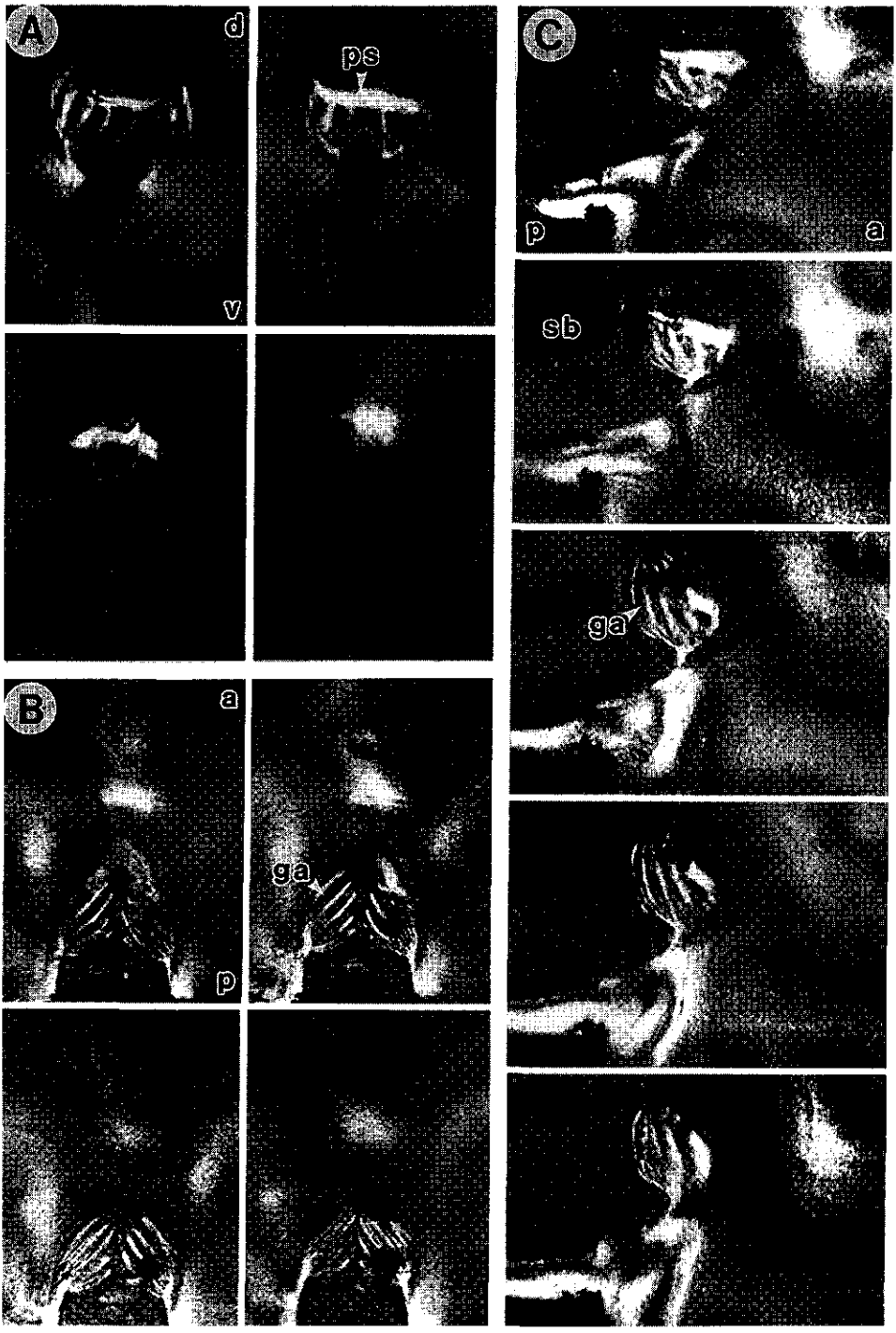
A
d
v
ps
B
a
p
ga
C
p
a
sb
ga

through the carp nose into the mouth cavity and connected to a pressure transducer. Unfortunately, the resulting trigger signal was disturbed by drift of the electrical signal and by irregularities in the pressure amplitude, due to irregularities in the breathing movements of the fish. Hence, it could not be used in the present experiments.
— A fast working sedative with antagonist should be applied for accurate control of the breathing amplitude during each experiment. The design of the clamp can be improved.
— The settings of the NMR sequence should be optimised to show the whole range of velocities within the buccal and opercular cavities. Using a phantom (a flow tube with accurately known flow speed) the relation between signal brightness and flow speed should be calibrated.
— The speed with which scans are made should be increased by using a magnet with higher gradient strengths (the maximum gradient in the present experiments was 10 mT/m) and/or by using faster sequences. It should be possible to obtain quantitative flow profiles within the mouth of the fish with a spatial resolution of about $0.5 \times 0.5 \times 2$ mm within 150 ms (*e.g.* DIESBOURG *et al.*, 1992).

CONCLUSION

The present pilot study is the first attempt to use NMR imaging to study the water flow in a breathing fish. Our study indicates that this technique is potentially very useful for the study of such pulsatile flows, since it is non-invasive; furthermore, quantitative measurements can be made.

ACKNOWLEDGEMENTS

Philips Medical Systems is acknowledged for providing the NMR facilities to perform the experiments. We are indebted to Jan Groen for operating the NMRi equipment. Jos van den Boogaart and four anonymous referees are acknowledged for their valuable comments on the manuscript.

REFERENCES

ALEXANDER, R.McN., 1967. *Functional design in fishes.* Hutchinson and Co Ltd., London.

ALEXANDER, R.McN., 1983. *Animal mechanics.* Packard Publishing Ltd., Funtington, Chichester, U.K.

BALLINTIJN, C.M., 1968. *The respiratory pumping mechanism of the carp Cyrpinus carpio (L).* Doctoral thesis, University of Groningen, Groningen.

BOESINGER, P., S.E. MAIER, L. KECHENG, M.B. SCHEIDEGGER & D. MEIER, 1992. Visualization and quantification of the human blood flow by magnetic resonance imaging. J. Biomech. **25**: 55-67.

CALLAGHAN, P.T., 1991. *Principles of Nuclear Magnetic Resonance Microscopy*. Clarendon Press, London.

COHEN, M.S. & R.M. WEISSHOFF, 1991. Ultra-fast imaging. Magn. Res. Imaging **9**: 1-37.

DIESBOURG, L.D., F.S. PRATO, G. WISENBERG, D.J. DROST, T.P. MARSHALL, S.E. CARROLL & B. O'NEILL, 1992. Quantification of myocardial blood flow in extracellular volumes using bolus injections of Gd-DTPA: kinetic modelling in canine ischemic disease. Magn. Res. in Med. **23**: 239-253.

HOLETON, G.F. & D.R. JONES, 1975. Water flow dynamics in the respiratory tract of the carp (*Cyprinus carpio* L.). J. Exp. Biol. **63**: 537-549.

HOOGENBOEZEM, W., J.G.M. VAN DEN BOOGAART, F.A. SIBBING, E.H.R.R. LAMMENS, A. TERLOUW & J.W.M. OSSE, 1991. A new model of particle retention and branchial sieve adjustment in filter-feeding bream (*Abramis brama* (L.), Cyprinidae). Can. J. Fish. Aquat. Sci. **48**: 7-18.

HUGHES, G.M. & G. SHELTON, 1958. The mechanism of gill ventilation in three freshwater teleosts. J. Exp. Biol. **35**: 807-823.

LAUDER, G.V., 1980. The suction feeding mechanism in sunfishes (*Lepomis*): an experimental analysis. J. Exp. Biol. **88**: 49-72.

MULLER, M. & J.W.M. OSSE, 1984. Hydrodynamics of suction-feeding in fish. Trans. Zool. Soc. Lond. **37**: 51-135.

MULLER, M., J.W.M. OSSE & J.H.G. VERHAGEN, 1982. A quantitative hydrodynamical model of suction feeding in fish. J. Theor. Biol. **95**: 49-79.

SANDERSON, S.L., J.J. CECH & A.Y. CHEER, 1994. Paddlefish buccal flow velocity during ram suspension feeding and ram ventilation. J. Exp. Biol. **186**: 145-156.

SIBBING, F.A., J.W.M. OSSE & A. TERLOUW, 1986. Food handling in the carp (*Cyprinus carpio*): its movement patterns, mechanisms and limitations. J. Zool. Lond. (A) **210**: 161-203.

VAN DER MEULEN, P., J.P. GROEN, A.M.C. TINUS & G. BRUNTINK, 1988. Fast Field Echo Imaging: an overview and contrast calculations. Magn. Res. Imaging **6**: 355-363.

VAN LEEUWEN, J.L., 1984. A quantitative study of flow in prey capture by Rainbow trout, *Salmo gairdneri*, with general consideration of the actinopterygian feeding mechanism. Trans. Zool. Soc. Lond. **37**: 171-227.

VAN LEEUWEN, J.L. & M. MULLER, 1983. The recording and interpretation of pressures in prey-sucking fish. Neth. J. Zool. **33**: 425-475.

5.2 Line scan flow measurements

5.2.1 Introduction

The results presented in section 5.1 can hardly be quantified. There is no single cause for this, but several phenomena can be identified which hamper the quantitative data analysis. In sequences based on build-up of steady state magnetization the intensity of the signal is a complex function of T_1, T_2, TE and TR (1-4), which is further complicated by flow. For steady flow NMR measurements of the flow rate can be calibrated and thus quantified (2). Unfortunately, the flow velocity in the buccal cavity of fish, but also in many other situations, is pulsatile. When the build up of magnetization is slow compared to the change of the flow velocity the signal intensity cannot be coupled to a flow rate. Furthermore motional artefacts arise within the image (5). Two solutions can be brought up to avoid these artefacts; *i*) triggering and *ii*) reduction of the scan time. The first solution requires that the frequency of the pulsatile flow is constant during the measurement, the second solution is limited by hardware or by the desired resolution. Even when these difficulties can be tackled the non-linear relation between the signal intensity and the flow rate remains. For these reasons it was necessary to investigate whether other pulse sequences could be used or developed to enable fast and reliable flow measurements.

Instead of using inflow or outflow as a means of measuring the flow rate the phase of an echo can be used to quantify the flow velocity (6,7). Employing pulsed field gradients in a pulse sequence not only attenuates the signal intensity when diffusion takes place, but also alters the phase of the signal in the presence of flow (8). Combination of pulsed field gradients with the fastest imaging sequence Echo Planar Imaging (EPI) or forms derived from this sequence has led to relatively fast, single shot, flow measurement techniques (9-11). The EPI sequences require fast switching gradients, especially for flow measurements, since flow which is not perpendicular to the slice introduces large image artefacts (10). The rise and fall time of the gradients is very important for an EPI sequence since it determines the minimum echo time and the total period during which the ADC samples data points. Using a 32x32 imaging matrix Kose was capable of reducing the echo time to 24 ms and constraining the acquisition window down to 21 ms (10). Even this short acquisition window of 21 ms is only appropriate with samples showing little magnetic susceptibility differences. More 'standard' scan times are in the order of 100-150 ms, sequences like GRadient And Spin Echo (GRASE) or Field echo Low Angle SHot (FLASH) have longer scan times (4,12,35), and the acquisition window is in the order of 50 ms. During a scan changes in the

flow velocity occur when investigating the breathing cycle of a live fish even when these cycles take about 1 second, corresponding to a base frequency of 1Hz. Coupled to the base frequency higher harmonics, derived from the base frequency, exist and can be as high as 20 Hz, the highest frequency thought to be relevant for flow in arteries. These higher harmonics may be found during one heart cycle (13); changes of the flow rate in the buccal cavity of a fish may occur within 50 ms (14,15). It would therefore be advantageous to use shorter echo and scan times . There are a number of options:

a) use a Fast Field Echo (FFE) or FLASH sequence without the phase encoding step, Real time ACquisition and Evaluation (RACE), whereby a projection of a slice is obtained (16). In this manner pulsatile flow can be followed. However, the data is hard to quantify since the phase of the signal is not only related to flow but also to *in situ* field gradients within the slice. Data manipulation, whereby the constant vector of the non-flowing water is subtracted from the total signal vector, allows a more reliable flow measurement. This has been demonstrated by Bock *et al.*(16) for flow in the aorta, but plug flow had to be assumed in order to arrive at their results. It is questionable whether this assumption is valid.

b) As another option the Modified Repetitive Pulse method (17) could be used. However, implementation of this sequence on a normal (medical) imager is very complicated, and the linear relation between the out-of-phase signal and the flow velocity breaks down with flow rates exceeding 4 cm/s (17,18).

c) Finally, a line scan sequence can be modified to obtain flow sensitive phase information. Only a few changes of the line scan sequence are necessary to enable these flow measurements. Since the line scan sequence can be implemented on standard equipment (19,20) and is not so sensitive to *in situ* field gradients it is preferable compared to EPI or FFE sequences.

A problem which cannot be circumvented by fast NMR sequences is the spread of flow velocities which may exist within a voxel because of the size of the voxels. For faster sequences this problem is enhanced since resolution is sacrificed for speed. If the complete flow profile is to be known, e.g. flow through the gills of a fish or close to a bifurcation, both of which exceed the spatial resolution, a special form of flow encoding is required and possible (21,36). Several authors have proposed a name for 2D or 3D imaging or mapping the flow velocity (21-25), e.g. "q-space", "Fourier flow imaging" and "velocity imaging", but there is no universally agreed name in literature for encoding flow, or in general motion (e.g. body motion or diffusion). We use the term "displacement imaging" for the remaining part of this Chapter. Displacement imaging measurements using the

line scan sequence thus renders a 2D data set,: one is the spatial axis (r), the other the displacement (σ).

5.2.2 The flow sensitised line scan sequence

Line scan sequences belong to the older NMR imaging sequences being capable of selecting unique voxels in 3D space (19,20). Their main advantage is a fast (< 20 ms) 1D acquisition of a selected line through a sample. Therefore (irregular) motion has little effect and images can be acquired without the artefacts inherent to 2D FT imaging (26). The procedure of selecting lines is depicted in Fig. 5.3. By using a narrow bandwidth r.f. pulse to excite magnetization while applying magnetic field gradients a plane is selected. During the 180° pulse magnetic field gradients perpendicular to ones used for the 90° pulse are used which yields a plane with inverted magnetization. Where both planes cross (see Fig. 5.4), the selected line, a spin echo is generated. Localisation of spins within the line is achieved by using a so-called read out gradient during the spin echo. A dephasing gradient is used before that to ensure that an approximately symmetric echo can be acquired. When Line Scan Imaging is used to quickly generate 2D images by selecting and imaging parallel lines for every subsequent scan (using off-resonance r.f. pulses), the procedure of selecting individual lines must be such that no information of any of the selected lines is misplaced into that of others. That is, one has to prevent spurious echoes. If done properly, fast imaging of motional regions of the body where homogeneity is too poor for other fast NMR sequences (e.g. near the lungs) is feasible (26). Since line scan imaging is a straightforward modification of a spin echo sequence it can therefore, in principle, easily be modified to be sensitive to flow. By accurate implementation the line scan sequence facilitates quantitative, phase sensitive, flow measurements. An example of such a flow sensitive line scan sequence is given in Fig. 5.3. In this figure the hatched blocks represent pulsed field gradients which are used to encode for flow. To obtain reliable phase information only related to flow several phenomena require special attention. These are (*i*) in- and outflow, (*ii*) phase coherence during the pulse sequence and (*iii*) the prevention of spurious echoes.

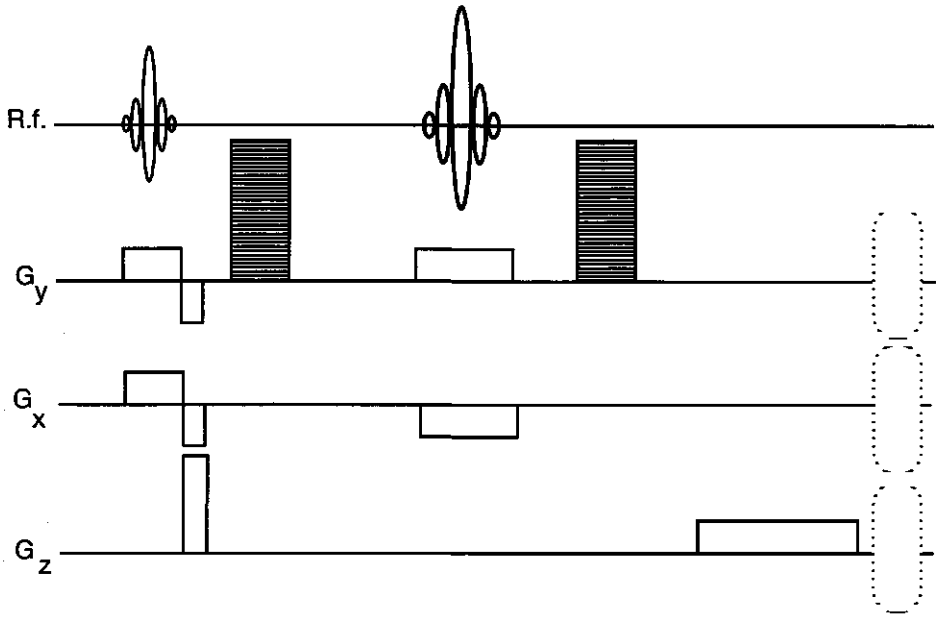

Figure 5.3 A schematic representation of the flow sensitised line scan sequence. The hatched blocks show the pulsed field gradients, which can either remain constant during real time measurements or be stepwise varied for displacement imaging. The dotted shapes are crusher gradients.

Ad (*i*): Relatively high repetition rates (TR << T_1) using spin echo sequences are only applicable when sufficiently fast inflow of non saturated magnetization occurs. Spins which experience several 90° pulses during T_1 get saturated which results in a reduced signal amplitude. If one of the slices or planes excited by the 90° or the 180° pulse overlap with the flowing fluid saturation follows and the *inflow effect* is reduced. The optimum inflow effect is reached when the 90° and 180° pulses make an 45° angle with the flow direction, both slices being perpendicular to one another. Off-centre selection of lines is obtained by applying frequency offsets for both the 90° and 180° pulses (see Fig. 5.4). As mentioned above the optimum inflow effect is reached when using a 45° angle of the excited slices with regard to the flow direction. The disadvantage of scanning with this angle is that an enhanced *outflow effect* is observed. This outflow effect does not result in a reduced signal however, but instead it shows up as a shift of the selected line. Since the flowing part of the tilted slice moves during τ (the 90°-180° spacing) the refocussing pulse 'selects' a different, shifted, line. The shift Δr is given by

$$\Delta r = v.\tau.\sin\varphi.\cos\varphi \qquad [5.1]$$

for plug flow. The angle φ is defined in Fig. 5.4 and can be varied by adjusting the relative strength of the slice selection gradients. In how far the shift of the selected lines by the amount Δr causes a problem depends on the flow velocity relative to the radius of the tube. By reducing the echo time (2τ) or φ (sacrificing some inflow signal enhancement) this line shift is minimised.

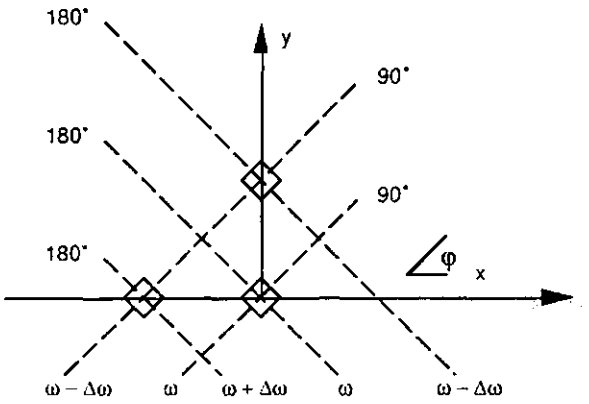

Figure 5.4 The selection of the line through a sample is achieved by selecting two slices perpendicular to each other and with an angle ϕ with respect to the x axis. The position of the line is controlled by the frequency offset Δω.

Ad(*ii*): The most difficult part in obtaining accurate phase information of flowing fluids is conserving the correct phase of the spin echo, independently of the spatial offset of the line by using off-resonance r.f. pulses. This requires *phase coherence* during the scan, but also precise tweaking of the gradients. Phase coherence was maintained by taking two precautions; the duration of the frequency offset during each scan was set to 1 ms, whereas the frequency offset for the r.f. pulses themselves was set to multiples of 1 kHz. In addition, the offset was identical in magnitude for the 90° and 180° pulses, but opposite in sign. One of the slice selection gradients during the 180° pulse was inverted to select the correct line (Fig. 5.3). For our experiments exact timing is critical down to 100 ns, the clock frequency of our pulse programmer, and a phase continuous synthesiser. If these precautions are ignored a phase image of a sample will show first order phase artefacts in the direction perpendicular to the scanned lines. Inappropriate tweaking of the read gradient leads to first order phase artefacts in the direction of the lines whereas incorrectly tweaking of the slice selection gradient leads to signal loss and to small phase artefacts. With proper implementation quantitative real time flow measurements, which are performed with fixed values of the pulsed field

gradient during an experiment with several line scans, are within reach. For displacement imaging the pulsed field gradients in the flow direction should be stepped instead of fixed.

Ad (*iii*): *Spurious echoes* are prevented by placing crusher gradients after each scan (dotted lines in Fig. 5.3). By continuously changing the net direction of the crusher gradient refocussing of the magnetisation from earlier excitations can be prevented (28). None of the combinations of crusher gradients should reappear within the T_2 of the flowing liquid since the recurrence of identical crushers may reverse the effect of earlier gradient crushers (28).

5.2.3 Displacement imaging

Fourier transformation of an echo obtained by the line scan sequence results in a 1D spin density matrix $\rho(r)$ modulated by T_2, T_1, TR and TE. Since the line scan sequence is a modification of a spin echo sequence a pair of pulsed field gradients around the 180° pulse can be used to induce a phase shift of the magnetization resulting from flowing spins. The induced phase shift is proportional to the flow velocity v and is given by (6):

$$\phi(r,t) = \gamma\delta g\Delta v(r,t) \qquad [5.2]$$

,with **g** the strength, δ the duration and Δ the separation of the gradient pulses, also denoted as observation or labelling time. The profile v(r) is influenced by several conditions, e.g. the flow velocity, tube diameter, dynamic viscosity, shape of the tube and smoothness of the tube wall. The flow profile in a straight, smooth tube is parabolic (laminar) if the Reynolds number, Re= r.v/v (v being the dynamic viscosity, r the radius of the tube) is below 2000 (10,13).

For stable flow, or period flow which can be precisely triggered, velocity imaging can be used to resolve differences of the flow velocity within a voxel. These differences arise when the spatial resolution is insufficient to resolve all flow velocities within the sample. When laminar flow is disturbed (30) by obstructions, or by irregular flow rates, displacement imaging may yield exact information about the effects of these irregularities on the flow pattern.

The NMR echo amplitude S(g) and -phase of a moving fluid depend on **g** or q (q=$(1/2\pi)\gamma g\delta$) as follows (31):

$$S(g) = \int \rho(r) \int P_S(r \mid r', \Delta) \exp(i\gamma\delta g \bullet (r - r'))dr'\, dr \qquad [5.3]$$

$$= \int \rho(r) E(g, r, \Delta) dr$$

In this equation, $P_s(r \mid r', \Delta)$, is the conditional probability function averaged over a voxel, describing the probability that a spin which, at the beginning of the first gradient pulse at t = 0, is at **r** will be at **r'** at t = Δ. E(g,r,Δ) is the Fourier transformation of the displacement. In the presence of a flow gradient within a voxel E(g,r,Δ) is described by ,

$$E(g, r, \Delta) = \int_{v_{min}}^{v_{max}} P(v) \exp(i\gamma \delta g \bullet v\Delta) dv \qquad [5.4]$$

In Eq.[5.4] the effect of diffusion is ignored. The flow profile P(v) is the same as $P_s(r \mid r', \Delta)$, except for diffusion, and can be recovered after Fourier transformation (FFT) in the *q*-domain and subsequent division by Δ. Thus, the characteristics of the flow profile can be obtained by displacement imaging. When one voxel covers the complete laminar flow profile the conditional probability P(v) is constant from 0 to v_{max}, with a amplitude of $1/(2\overline{v})$, Here, $\overline{v}$ is the average flow velocity within the voxel.

More complicated patterns arise as a result of turbulence or pulsatile flow . Water flowing through a glass bead bed in a cylindrical tube is an example of such complex flow. The net motion in the direction of the tube axis is superimposed on a more random motion, both in amplitude and direction. When the displacement during Δ is short compared to the pore diameter the average displacement increases linearly with the observation time, even for the rms displacement perpendicular to the flow direction. For longer observation times, the perpendicular flow becomes more chaotic and the nature of the average displacement becomes similar to that of diffusion (32,33). When the displacement increases linearly with the observation time we may speak of 'stationary random flow' (SRF), for the diffusion-like displacement we may speak of 'pseudo diffusion' (31).

Time dependent flow can be expressed by a series of sines and cosines (13),

$$v(t) = \frac{v_0}{2} + \sum_{k=0}^{k=\infty} \left\{ A_k \sin(k\omega t) + B_k \cos(k\omega t) \right\} \qquad [5.5]$$

When repeating a spin echo sequence including imaging gradients and gradient pulses with fixed values to encode flow, two time domain signals are acquired. During the read gradient *k-space*, the reciprocal image space, is sampled in the first time domain, which is repeated at a repetition frequency of 1/TR in the second

time domain. Each separate scan can be Fourier transformed, yielding a profile of ρ, including the effects of relaxation, as well as in- and outflow effects and with a phase defined by Eq.[5.2]. When the phase of each voxel in the second time domain is Fourier transformed, a FFT of Eq.[5.5] is obtained, since phase and flow velocity are related by Eq.[5.2]. For pulsatile flow, an FFT yields the frequency ω_0 of the pulsatile flow period and higher harmonics. These higher harmonics are related to the original periodic modulation (e.g. the heart beat rate (ω_0) or the breathing rate of a fish), the elasticity of walls which surround the flowing medium and the presence of obstructions in the flow path (13). When changes in the flow rate are not nicely periodic a Fourier transformation in the second time domain yields additional harmonics which do not have to be related to ω_0. As mentioned in section 5.2.1, for the heart beat cycle higher harmonics with frequencies up to 20 Hz have been found and are thought to be relevant for describing the pulsatile flow in the arteries. When the line scan sequence is used, irregular repetitions of pulsatile flow do not present a problem because each scan is separate from and independent of its predecessor. For 2D FT imaging this does not apply since each phase encoding step is related to its predecessor by the FFT in the second *k-space* domain, even when triggering is used.

Note that the NMR signal resulting from the line scan sequence is also affected by T_2, susceptibility and several NMR scan parameters. Poor spatial resolution, which occurs when using the line scan sequence, may result in merging of the NMR signal arising from several fractions being present in one voxel, each with its own $P_s(r|r',\Delta)$ and T_2. These fractions should be separated in an accurate flow measurement. Displacement imaging can achieve this goal, but the TE dependency of $P_s(r|r',\Delta)$ should be investigated to see whether more fractions contribute to the NMR signal (34).

5.2.4 Experimental setup

The NMR spectrometer hardware used to perform the experiments described in the remainder of this Chapter was identical to the one described in Chapter 2. The open structure of the rf and gradient coils allow long tubes to be introduced in the rf coil. To ensure laminar flow in the r.f. region, glass tubes with a length of at least 20 centimetres, were used with the inlet as far as possible from the measuring area. Because flow velocities below 50 mm/s were used in a tube with an internal diameter of 6 mm, the Reynolds number did not exceed 80. Free, elastic tubes were used to connect the glass tube and the pump. To generate stable flow a Masterflex 7550-62 pump was used. Pulsatile flow was generated by a

Verder VRX200 pump, normally equipped with 3 rollers, which was modified to perform experiments with only one or two rollers.

The soft rf pulses used in the line scan sequence had a duration of 800 μs. Together with the fast switching gradients, echo times of 6 ms could be achieved, so that in principle repetition times of 10 ms could be used. Normally the TR was set to 33 ms and the TE to 16 ms; these short TE and TR values can also be used on more standard NMR spectrometers with a maximum gradient strength of 20 mT/m. A TE-value of 16 ms is certainly feasible when the flow velocity exceeds a few centimetres per second and rf pulses of 2 ms are used, because then the flow-induced phase shift due to the slice selection gradients is sufficiently large to measure flow (7). In the experiments described below the bipolar slice selection gradient was too short, so a pair of pulsed field gradients were necessary to induce a sufficiently large phase shift in the presence of flow. All data was analysed using IDL software (RSI, Boulder, USA).

5.2.5 Results

In one set of experiments the relation between the phase shift and the flow velocity in the middle of the tube was determined by simply using the line scan sequence in real time mode, a stopwatch and a balance and assuming laminar flow (Fig. 5.5). The phase shift, calculated using Eq.[5.2] with δ = 0.75 ms, Δ = 3.45 ms, G = 175 mT/m and variable v, should be 0.199xv radians. The relation between v and the phase shift was fitted to be 0.194xv radians, a deviation of only 2.5 % from the correct value. This deviation can be explained by the fact that the velocity within a pixel is an average over a small cube and the there is some uncertainty in the exact position of this cube. Also the calibration of the gradients could give rise to a small systematic error.

In the same set of experiments the flow profile was determined. In Fig. 5.6 an example of a flow profile is given in a line through the middle of a tube, measured by the phase shift ϕ, is given. The solid line represents the calculated laminar flow profile. As can be seen in Fig. 5.6, the agreement between theory and experiment is quite satisfactory. The flow profile was also verified using a standard 2D FT spin echo sequence and was found to be very similar to the one determined with the line scan sequence.

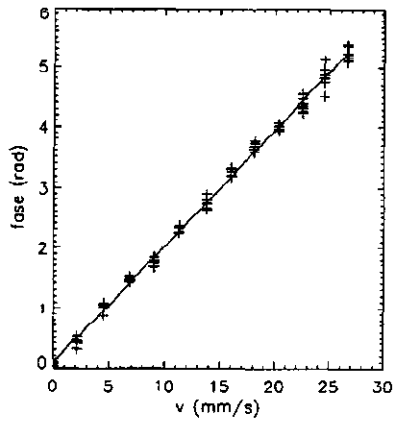

Figure 5.5 The dependence of the echo phase and the flow velocity in the middle of a 6 mm glass tube. *Scan parameters: slice thickness* = 3 mm, field of view (fov) = 40 mm, te = 8 ms, Δ = 3.45 ms, δ = 0.75 ms and G = 175 mT/m.

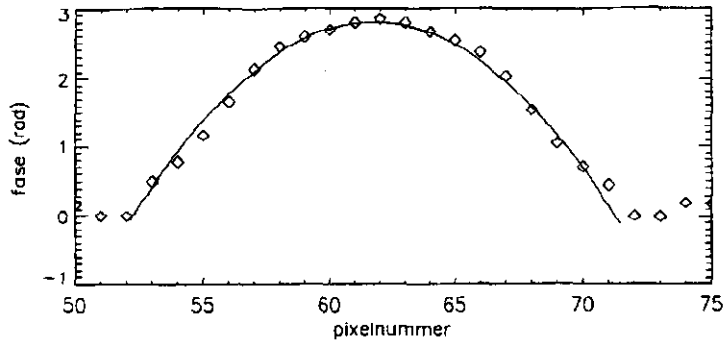

Figure 5.6 The flow profile through the centre of a 12 mm diameter glass tube as obtained by a line scan measurement. The same scan parameters were used as for Figure 5.5

By using the roller pump with a single roller, oscillatory flow was procured. The frequency of these oscillations (3.2 Hz using a single roller, 2.5 Hz using two rollers) was simply determined by counting the revolutions per minute. Following the water meniscus by eye no flow reversions were observed. Because only a very low, average, flow velocity of approximately 1 cm/s was possible, the inflow effect during the 33 ms repetition time (TR) was very small necessitating a large slice

thickness of 7 mm. The flow velocity monitored in the centre of a 12 mm diameter glass tube is depicted in Fig. 5.7.a (measurement at constant G).

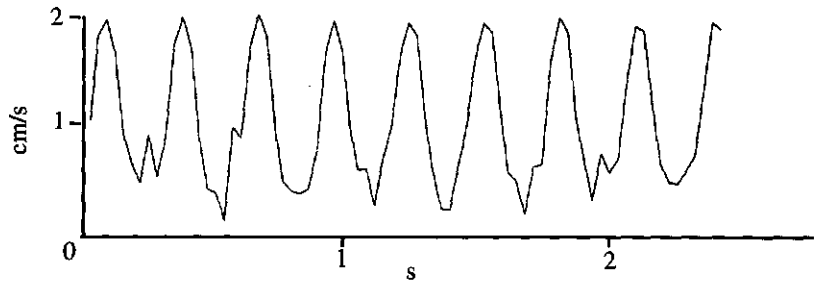

Figure 5.7.a Oscillatory flow monitored with the flow sensitised line scan sequence. Flow in the middle of the tube was selected. Scan parameters: slice thickness = 7 mm, fov = 30 mm, te = 16 ms, tr = 33 ms, Δ = 7.45 ms, δ = 0.75 ms and G = 175 mT/m.

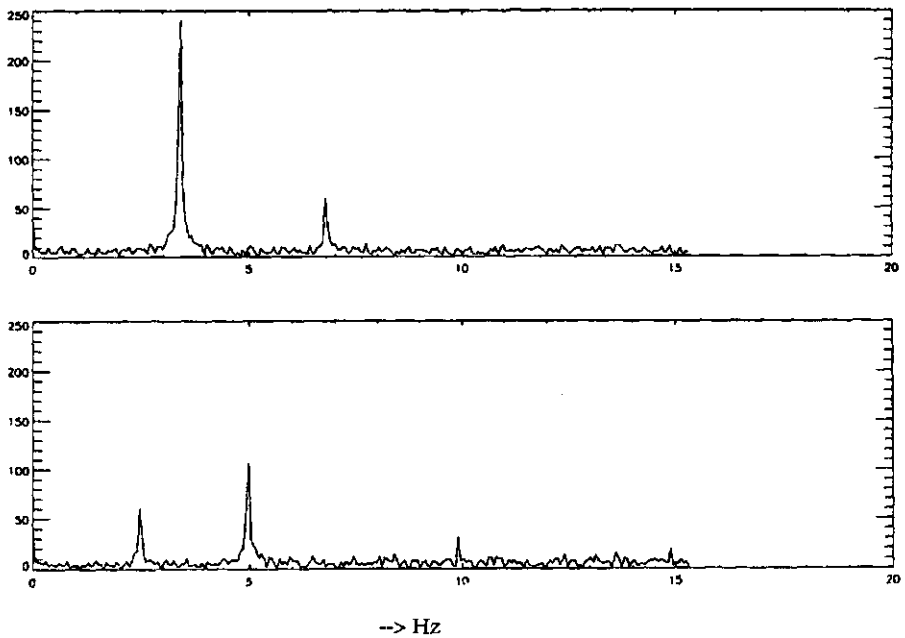

Figure 5.7.b The Fourier Transformation of the signal presented in Figure 5.7.a. with one roller (top figure) and the Fourier Transformation of the signal resulting from a pump equipped with two rollers (bottom figure). Scan parameters as in Figure 5.7.a.

The Fourier transform of the time domain data shows two frequencies (Fig. 5.7.b) at the base frequency of 3.2 Hz and at the first harmonic at a frequency of 6.4 Hz. Remounting one of the other rollers results in four peaks in the Fourier transformed spectrum at 2.5, 4.9, 9.9 and 14.9 Hz, where the last two have a relative

amplitude of only 5 %. The decrease of the higher order harmonics amplitude results from the elastic tubes connecting the pump and the glass tube. Higher order harmonics have a shorter wave length and therefore are more subject to damping than lower order harmonics (13). Since frequencies of at least 15 Hz (higher frequencies can not be measured when using a TR of 33 ms) are present and can be measured when two rollers are mounted, this indicates that the presence of a single roller, harmonics above the first were absent or have a very low amplitude.

To investigate to what extend linescan displacement imaging is feasible in a heterogeneous sample, flow through a glass bead bed in a 12 mm diameter tube was studied. The glass bead system was chosen in view of the broad experience exists with this system (32,33) at our department. Two glass bead beds were investigated, one with beads between 400 and 500 μm, and one with beads between 1.2 and 1.3 mm. The column height of the bed was 15 cm to stabilise flow with a velocity of 7.5 mm/s within the glass bead bed with a porosity of ≈ 0.4. To encode for displacement 64 gradient steps were used; in the read out direction 64 data points were acquired for each echo. To construct NMR images the data matrix was zero filled to 128x128 prior to Fourier transformation. The product $\Delta.\delta$ was kept at a fixed value to ensure comparable displacement encoding. Since the T_1 of water is long (~ 2.5 s) and inflow effects are relatively small, the TR was set to 600 ms resulting in a complete velocity image within 40 seconds. Despite the fact that the T_2 of the glass bead systems exceeds 800 ms (determined by a separate CPMG measurement with 2τ = 0.6 ms) it was not possible to use echo times exceeding 40 ms. For the glass beads of 450 μm it was necessary to limit the TE to 30 ms. The TE range is limited by *in situ* field gradients (see Chapter 2.) causing an increased loss of phase coherence at longer TE values, but this loss is not as severe as that of the 80 μm glass bead system. This can be understood noting that*in situ* field gradients are proportional to the radius of the glass beads (31).

Fig. 5.8 represents velocity images of the 450 μm beads. Figures A-D represent the rms displacement ($\sigma_{\perp}$) perpendicular to the flow direction, the images E-H represent the displacement in the flow direction ($\sigma_{//}$). The labelling time decreases from top to bottom, i.e. from 18 ms to 7 ms.

Figure 5.8 Displacement of water (displayed vertically) in the direction of the flow through a glass bead bed (ϕ(bead) = 450 μm) (A, C and E) and of the displacement perpendicular to the flow direction (B, D and F) using displacement imaging in combination with a line scan sequence. Scan parameters: slice thickness = 5 mm, fov =3 0 mm, te = 30 ms and G_{max} = 175 mT/m. $\overline{v}$ = 7.5 mm/s.

A and B. Δ = 18 ms, δ = 2 ms, C and D. Δ = 11 ms, δ = 3 ms, E and F. Δ = 7 ms, δ=5 ms.

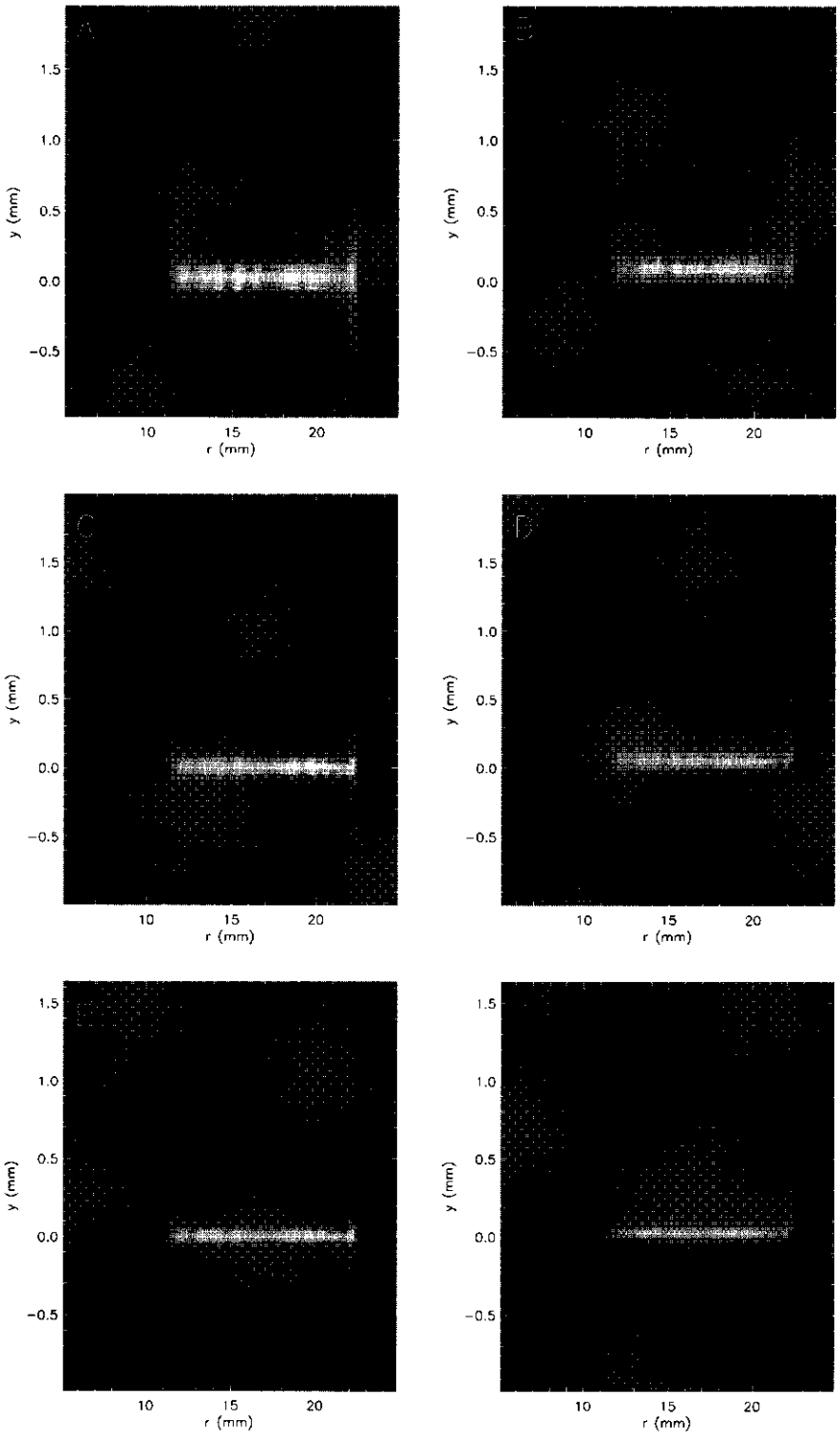
A
B
C
D
1.5
1.0
0.5
0.0
−0.5
y (mm)
10
15
20
r (mm)

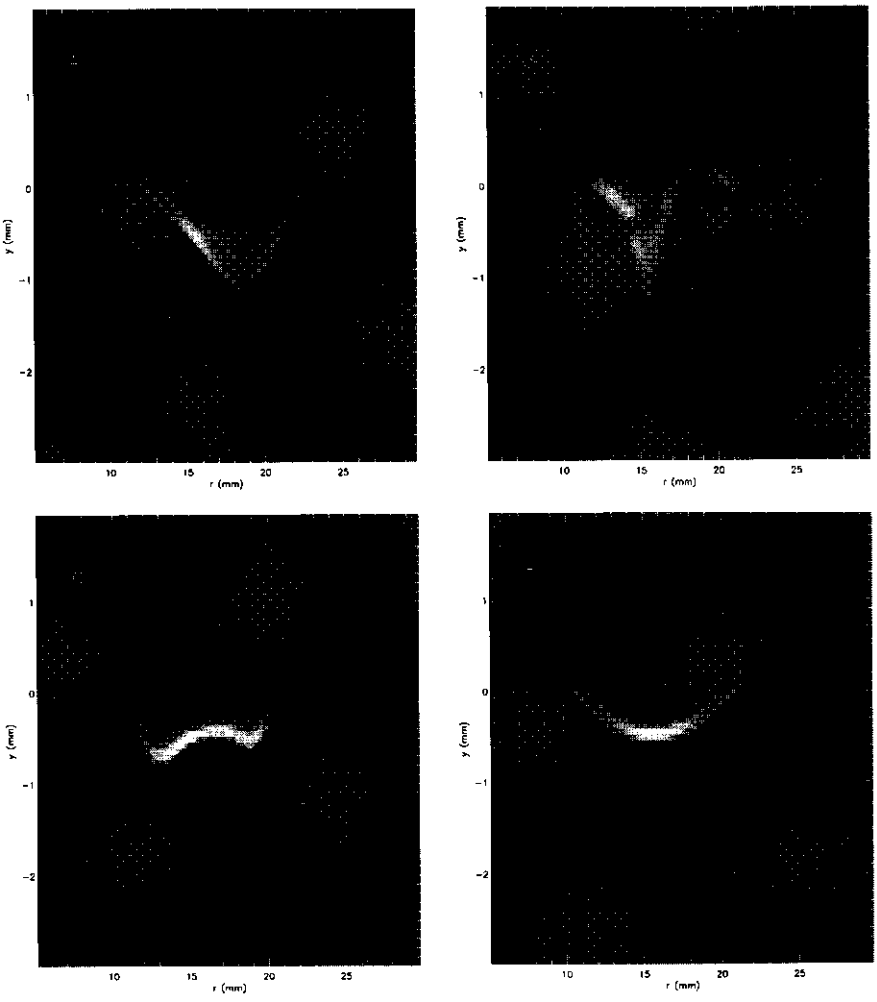
y (mm)
r (mm)
10
15
20
25
1
0
−1
−2

All images show an increased displacement near the tube wall and also an enhanced amplitude in this region. Because the tube wall distorts the glass bead bed geometry the porosity near the wall is larger than farther away from the wall and so fewer beads obstruct the water flow near the wall. At the wall the flow velocity is 2.5 times higher (for the 1.3 mm beads 2 times higher) and the signal intensity a factor 1.1. Similar enhancement of flow near the tube wall was found for the larger beads. The values for $\sigma_{\perp}$, and $\sigma_{//}$ are comparable to those found by Palstra et al. (32,33). Integrating the vertical displacement and dividing by Δ yields a velocity which is 10 % higher than the value of 7.5 mm/s which can be calculated using the measured flow rate and assuming a porosity of 0.4.

Since the flow pattern in the buccal cavity of a fish or near an artery bifurcation is not constant and is often turbulent, examining the change of the flow pattern along the flow direction itself is of interest. To demonstrate this change we used a cylindrical glass tube with a glass filter. The flow pattern below and above the glass filter was measured with the line scan sequence in the displacement imaging mode, the results of which are displayed in Fig. 5.9.A-D. The vertical, upward, flow had an average velocity of 3 cm/s. For these measurements a line thickness of 4 mm was used, the line being parallel to the filter and perpendicular to the flow direction. For all experiments a line through the middle of the glass tube was selected. Fig. 5.9.A shows the spread of displacement during Δ of a line 1 cm below the filter, Fig. 5.9.B shows that of a line through the filter. the filter being approximately 3 mm thick Fig.5.9.C shows that of a line 2 cm above the filter and Fig. 5.9.D shows that of a line 4 cm above the glass filter. Image D shows a parabolic flow profile, which indicates that the flow profile has recovered within 4 times the tube diameter (12 mm). Such a fast recovery is only possible when the Reynolds number is rather low, in this case it was calculated to be 50 (29,30). The flow profiles in and near the glass filter are depicted in Figures 5.9.B and C and are not truly turbulent since the Reynolds number is so much below 2000 and flow disturbances are therefore not sustained throughout the pipe (10). The indication that Fig. C depicts distorted, non turbulent, flow is further supported by the observation that repetition of the experiment yields almost identical flow profiles.

Figure 5.9 Vertical displacement (displayed vertically) monitored before, in and after a glass filter within a 12 mm glass tube. Scan parameters: slice thickness = 4 mm, fov = 30 mm, te = 30 ms, Δ = 10 ms, δ = 2 ms and G_{max} = 140 mT/m. Flow was upward through the filter ($\overline{v}$ = 3 mm/s). A. 1 cm below the filter, B. inside the glass filter, C 2 cm above the filter and D 4 cm above the filter

Also, displacement imaging perpendicular to the flow shows regulars patterns (data not shown), supporting this hypothesis. It should be noted that the depicted flow profiles are averaged over 26 seconds (TR=0.4 s) and may therefore suffer from the same problem as the flow measurements in the fish, i.e. temporal variations of the flow pattern and velocity are averaged over the scanning period. If these variations are truly periodic, additional lines would show up in the images, very similar to the ones obtained with the line scan sequence in real time mode. Non-periodic variations would cause blurring of P(v). Reduction of TR to 10 ms could remedy such an artefact but this requires higher flow rates and possibly thicker scan lines.

5.2.6 Discussion and conclusions

Precise acquisition of irregular pulsatile flow requires a measurement technique which is fast compared to the repetition rate of flow oscillations. NMR sequences employing 2D acquisition of a plane are limited to frequencies up to about 8 Hz. This time resolution requires highly specialised hardware. When frequencies above 10 Hz need to be considered 2D acquisition using normal hardware is insufficiently fast. We have demonstrated that a 1D acquisition sequence is capable of sampling frequencies up to 15 Hz. With more specialised hardware it is expected that sampling frequencies up to 50 Hz become feasible. With these high repetition rates the flow sensitised line scan sequence can be considered to perform real time flow measurements. By selecting a line instead of a whole slice, as in the RACE sequence, accurate flow velocities can be measured at any voxel in 3D space within the detection range of the r.f. coil. The real time character of these measurements is only impeded by the SNR which decreases with TR but increases again at increasing flow velocity. Even on standard NMR equipment the above mentioned time resolution should be attainable (35).

If only the average flow velocity is detected, as in the line scan flow measurement in real time mode, and the spread of velocities within a voxel is important, displacement imaging is a solution. This technique, however, destroys the real time flow character of the sequence. The results in this Chapter show that within 30 seconds the displacement distributions of flow within a pixel of a line can be resolved. Theoretically this can be performed in 1 second. These short acquisition times are interesting when observing physiological changes in the order of seconds or minutes. Then, flow sensitised line scan measurements offer a good alternative to EPI and FLASH velocity imaging. Furthermore, the imaging of flow through a glass bead bed shows an additional advantage of the line scan sequence,

i.e. its ability to produce images within regions with *in situ* field gradients. To improve this capability a modified STE line scan sequence (36) should give the required flexibility in changing the observation time. One could also combine the line scan sequence with a MSE sequence, similar to what has been shown in Chapter 2. By such a combination the degenerative effects of *in situ* magnetic field gradients can be cancelled and longer echo times become again feasible.

In conclusion, fast and accurate displacement measurements can be performed using a line scan sequence which is sensitive to displacement. Accurate (real-time) flow measurements in complex, biological, structures, such as the buccal cavity of a fish or a beating heart are no longer out of reach.

References

1. P. van der Meulen, J.P. Groen, A.M.C. Tinus and G. Bruntink, Magn. Res. Imaging **6**, 355 (1988).
2. R.C. Hawkes and S. Patz, Magn. Res. Med **4**, 9 (1987).
3. P. Boesinger, S.E. Maier, L. Kecheng, B. Scheidegger and D. Meier, J. Biomechanics **1**, 55 (1992).
4. A. Haase, Magn. Reson. Med. **13**, 77 (1990).
5. W.H. Perman, P.R. Moran, R.A. Moran and M.A. Bernstein, J. Comp. Ass. Tom. **10**, 473 (1986).
6. P.R. Moran, Magn. Reson. Imaging **1**, 197 (1982).
7. D.G. Nishimura, A. Macovski and J. M. Pauly, IEEE Trans. Med. Imaging **MI-5**, 140, (1986).
8. H. Van As and T.J. Schaafsma, in 'An Introduction to Biomedical Nuclear Magnetic Resonance', edited by S.B. Petersen et al., Georg Thieme Verlag, Stuttgart (1985).
9. M.S. Cohen and R.M Weisskopf, Magn. Res. Imagin **9**, 1 (1991).
10. K. Kose, Phys. Rev. A **44**, 2495 (1991).
11. D.N. Guilfoyle, P. Gibbs, R.J. Ordidge and P. Mansfield, Magn. Res. Med. **18**, 1 (1991).
12. K. Oshio and D.A. Feinberg, Magn. Reson. Med. **20**, 344 (1991).
13. A. MacDonald, Blood flow in arteries, Edward Arnold, London (1974).
14. M.R. Drost, M. Muller and J.W.M. Osse, Porc. R Soc. Lond. B **234**, 263 (1988).
15. C. van den Berg, Ph. D. thesis, Wageningen (1993).
16. M. Bock, L.R. Schad, E. Müller and W.J. Lorenz, Mag. Reson. Imaging **13**, 21 (1995).

17. H. Van As, A.A.M. Brouwers and J.E.M. Snaar, Proceedings of the 2nd symposium on progress of NMR in medicine, **87** (1986).
18. D. van Dusschoten, non published data.
19. P. Mansfield and A.A. Maudsley, Phys. Med. Biol. **21**, 847 (1976).
20. J. Pauly S. Conolly, D.G. Nishimura and A. Macovski, Book of Abstracts 9th SMRM, 28 (1990).
21. P.T. Callaghan and Y. Xia, J. Magn. Reson. **91**, 326 (1991).
22. D.A. Feinberg, L.E. Crooks, P. Sheldon, J. Hoenninger III, J. Watts and M. Arakawa, Magn. Reson. Med. **2**, 555 (1985).
23. D.N. Firmin, R.H. Klipstein, G.L. Hounsfield, M.P. Paley and D.B. Longmore, Magn. Reson. Med. **12**, 316 (1989).
24. R.E. Wendt III, W. Nitz, P.H. Mruphy and R.N. Bryan, Magn. Res. Med **9**, (1989).
25. P.T. Callaghan, A. Coy, D. MacGowan, K.J. Packer and F.O. Zelaya, Nature **351**, 467 (1991).
26. D.C. Ailion, K. Ganesan, T.A. Case and R.A. Christman, Magn. Reson. Imaging **10**, 747 (1992).
27. G.T. Gullberg, M.A. Simons and F.W. Wehrli, Magn. Reson. Imaging **6**, 437, (1988).
28. C.T.W. Moonen, G. Sobering, P.C.M. van Zijl, J. Gillen, M. von Kielin and A. Bizzi, J. Magn. Reson. **98**, 556 (1992).
29. S.E. Rittgers, D. Fei, K.a. Kraft, P.P. Fatouros and P.R.S. Kishore, J. Biomech. Eng. **110**, 180 (1988).
30. J.K.B. Krijger, B. Hillen, H.W. Hoogstraten and M.P.M.G. Van den Raadt, Appl. Sci. Research **47**, 233 (1990).
31. P.T. Callaghan, Principles of Nuclear Magnetic Resonance Microscopy, Clarendon Press, Oxford (1991).
32. W. Palstra, H. Van As and T.J. Schaafsma, pers. communication
33. W. Palstra and H. Van As, pers. communication.
34. D. van Dusschoten, P.A. de Jager and H. Van As, J Mag. Reson. **A 116**, 22 (1995).
35. K.D. Merboldt, W. Hänicke and J. Frahm, Magn. Reson. in Med. and Biology **1**, 137 (1988).
36. R. Turner, M. von Kienlin, C.T.W. Moonen and P.C.M. van Zijl, Magn. Reson. Med **14**, 401 (1990).

Summary

In this Thesis a practical approach is presented to study water mobility in heterogeneous systems by a number of novel NMR sequences. The major part of this Thesis describes how the reliability of diffusion measurements can be improved using some of the novel NMR sequences. The reliability of the data can be further enhanced by combining different NMR characteristics in a single fit routine. In addition, a fast NMR sequence for flow measurements is shown. A wide variety of samples is used to demonstrate how the NMR sequences and the subsequent analysis work.

Throughout this Thesis the term *heterogeneous system* is used whenever a sample contains different physical or chemical environments or compositions, each of which influence the NMR signal in a distinguishable way. One of the effects of such a heterogeneous system is the variation of the magnetic susceptibility within the sample causing so-called *in situ* magnetic field gradients. These gradients lower the NMR signal amplitude and may cause a substantial deviation of the real diffusion constant from the one measured by NMR using pulsed field gradient spin echo or stimulated echo sequences. In the second half of Chapter 2 an improved version of the PFG multiple spin echo sequence is introduced which minimises the degrading effects of *in situ* field gradients. While using additional r.f. pulses between the pulsed field gradients to reach the desired reliability no compromises with regard to flexibility were necessary.

This flexibility is important to study the change of the apparent diffusion constant with the echo time. This phenomenon, superficially appearing as an artefact, arises because compartments, as for example a vacuole, not only have a characteristic diffusion constant but also a T_2 which may significantly differ from other T_2's in the sample. In Chapter 3 it is shown how a T_2 difference can be used to separate diffusion constants (D) even if these have a similar magnitude. Using Diffusion Analysis by Relaxation Time Separation the diffusion constant for water in the vacuole, the cytoplasm and the extra cellular space, respectively, can be distinguished in apple parenchyma tissue. In the second half of Chapter 3 a fast implementation of DARTS PFG NMR is presented which is combined with NMR imaging. Here, spatially localised T_2 measurements are preceded by pulsed field gradients for diffusion weighting.

In this way the diffusion constant and fractional amplitude of cerebral spinal fluid (CSF) and white and grey matter in cat brain can be measured. The validity of these measurements are supported by Monte Carlo simulations of computer generated 2D data sets.

Chapter 4 deals primarily with improving the DARTS technique without imaging (DARTS PFG MSE Carr Purcell Meiboom Gill) and determining the best resolution (for discriminating diffusion constants) which can be obtained, using Monte Carlo simulations on 2D data sets. The use of the 2D fitting routine is extensively studied. Furthermore, existing theoretical models are mutually compared and confronted with the results obtained by the PFG MSE CPMG sequence for different samples. Four heterogeneous samples with different complexity are studied, i.e.:

a- A sample consisting of two tubes with different fluids, between which exchange can be ignored.

b- Whole Blood where diffusive exchange between the red blood cells (RBC's) and the plasma causes the apparent D of the RBC's to increase with increasing observation time.

c-Apple parenchyma tissue where the membrane between the vacuole and the cytoplasm (the tonoplast) is shown to severely restrict, but not prevent, diffusive exchange between these compartments.

d- A column with Sephadex beads (porous beads) where flow is introduced. The effect of this flow on the water displacement outside and inside the beads is described. Experiments demonstrated exchange between the flowing fraction and the stationary water in the beads.

In all instances it is profitable to combine the diffusion and T_2 measurements and analyse the resulting 2D data set as a whole. In this way an intuitive understanding is obtained of diffusion in complex systems measured by NMR. By using the T_2 as a label, the resolving power of NMR to distinguish diffusion constants is greatly improved and a difference between the diffusion constants as small as 30 % is demonstrated to be resolvable. None of the presented theories can be used to quantitatively describe the data.

In Chapter 5 the subject of flow in heterogeneous systems is studied in further detail. In the first half of this Chapter novel flow measurements in and around the buccal cavity of a Carp are described. These measurements are performed on a standard medical imager without special, fast NMR sequences. The described data can therefore only be used in a qualitative manner. In the

second half the line scan flow measurement is introduced. A temporal resolution of 16 ms can be obtained with this sequence allowing accurate, real time flow measurements. The combination of this line scan sequence with displacement imaging yields NMR images which picture the distribution of flow velocities over a line. Demonstrations of displacement imaging are performed in a tube with glass beads and in a pipe with a glass bead filter. The presented data can be used quantitatively.

The diffusion and flow measurements described in the Thesis all employ pulsed field gradients to encode for motion. Despite the obvious similarities between the measurements, the optimisation of the NMR sequences results in sequences which can be rather distinct. By careful tuning of the NMR sequences the range of displacements which can thus be measured lies between 5 μm and about 5 cm. This range and the fact that small differences in flow velocities and diffusion constants can be resolved, if necessary using other NMR characteristics, makes NMR a powerful tool to study water mobility in heterogeneous systems.

Samenvatting

In dit proefschrift wordt een praktische aanpak voor het meten van de water mobiliteit in heterogene systemen met behulp van NMR gepresenteerd. Enkele nieuwe NMR sequenties en toepassingen hiervan worden beschreven. Het grootste deel van dit proefschrift wordt besteed aan de verbetering van diffusie metingen met behulp van de nieuwe sequenties. De betrouwbaarheid wordt verder verhoogd door verschillende NMR kenmerken met elkaar te combineren in één fit routine. Tevens wordt een NMR sequentie geïntroduceerd waarmee snel stromingsmetingen kunnen worden uitgevoerd. Een breed spectrum van monsters is gebruikt om de werking van de sequenties te demonstreren en ook van de daaropvolgende analyse methode.

Door het proefschrift wordt de term *heterogene systemen* gebruikt telkens wanneer een monster uit verschillende fysiche of chemische omgevingen of composities bestaat welke ieder het NMR signaal op een kenmerkende manier beïnvloeden. Een van deze kenmerken is de variatie van de magnetische susceptibiliteit binnen het monster, wat resulteert in zogenaamde *in situ* magnetische veld gradiënten. Deze gradiënten reduceren de signaal amplitude en kunnen verder een wezenlijke afwijking tussen de werkelijke diffusie constante en de met NMR gemeten diffusie constante veroorzaken, wanneer gebruikt gemaakt wordt van de pulsed field gradient spin echo of stimulated echo sequenties. In de tweede helft van Hoofdstuk 2 wordt een verbeterde versie van de PFG multiple spin echo sequentie getoond welke de negatieve effecten van de *in situ* veld gradiënten minimaliseert. Terwijl er extra r.f. pulsen tussen de gepulseerde gradiënten geplaatst om de gewenste betrouwbaarheid te verkrijgen is er geen kompromis nodig om de flexibititeit van de metingen te behouden.

Deze flexibiliteit is belangrijk om de verandering van de schijnbare diffusie constante met de echo tijd te bestuderen. Dit fenomeen, dat bij oppervlakkige beschouwing als een artefact optreedt, wordt veroorzaakt doordat een compartiment zoals de vacuole niet alleen een karakteristieke diffusie constante heeft maar ook een T_2 welke onderscheidbaar kan

verschillen met die van andere fracties. In Hoofdstuk 3 wordt getoond hoe dit T_2 verschil tussen fracties gebruikt kan worden om de verschillende diffusie constantes (D) van elkaar te onderscheiden, zelfs wanneer hun onderlinge verschil klein is. Gebruik makend van Diffusion Analysis by Relaxation Time Separation kan de diffusie constante van respectivelijk water in de vacuole, het cytoplasma en de extracellulaire ruimte van appel parenchiemweefsel onderscheiden worden. In de tweede helft van Hoofdstuk 3 wordt een snelle implementatie van DARTS PFG NMR besproken welke gecombineerd wordt met NMR imaging. Hier worden gelokaliseerde T_2 metingen voorafgegaan door diffusie weging. Op deze wijze kunnen de diffusie constante en de fractie amplitude van cerebral spinal fluid (CSF) en witte en grijze hersenen worden gemeten. De betrouwheid van de metingen wordt ondersteund door Monte Carlo simulaties toegepsast op computer gegenereerde 2D data sets.

Hoofdstuk 4 gaat hoofdzakelijk over de verbetering van de DARTS techniek zonder imaging (DARTS PFG MSE Carr Purcell Meiboom Gill) en het bepalen van de hoogste resolutie (wat betreft het onderscheiden van diffusie constantes), via bestudering van de Monte Carlo simulaties op 2D data sets. Het gebruik van de 2D data analyse wordt uitgebreid besproken. Verder worden vier theoretische modellen onderling met elkaar vergeleken en ook met resultaten verkregen met de PFG MSE CPMG sequentie van verschillende monsters. Vier heterogene systemen met verschillende complexiteit worden bestudeerd, namelijk:

a- Een monster met twee buisjes met verschillende vloeistoffen waartussen geen uitwisseling kan plaatsvinden.

b- Compleet bloed, waar diffusive exchange tussen de rode bloedcellen en het plasma de waargenomen diffusie constante doet toenemen met toenemende observatietijd.

c- Appel parenchiemweefsel waar de membraan tussen de vacuole en het cytoplasma (de tonoplast) de uitwisseling t.g.v. diffusive tussen deze compartimenten beperkt maar niet verhindert.

d- Een kolom van poreuse Sephadex bolletjes waarin stroming wordt geïntroduceerd. Het effect van deze stroming op de water verplaatsing binnen en buiten deze bolletjes is met NMR bestudeerd. De stationaire waterfase in de bolletjes en de stromende waterfase tussen de bolletjes blijken uitwisseling te vertonen.

In alle gevallen biedt het voordelen om de diffusie en T_2 metingen met elkaar te combineren en de resulterende 2D data set in zijn geheel te analyseren. Op deze manier wordt intuïtief inzicht in de resultaten van de NMR diffusie metingen verkregen. Door de T_2 als een label te gebruiken kunnen diffusie constantes onderscheiden worden die slechts 30 % van elkaar verschillen. Geen van de gepresenteerde theorieën kan gebruikt worden om de data geheel quantitatief te beschrijven.

In Hoofdstuk 5 wordt de bestudering stroming in heterogene systemen verder uitgebreid. In de eerste helft van dit Hoofdstuk wordt de stroming in en rond de mondholte van een karper beschreven. Deze metingen zijn uitgevoerd op een standaard medische imager die niet met speciale, snelle NMR sequenties is uitgerust. De beschreven data set kan daardoor niet quantitatief gebruikt worden. In de tweede helft wordt de line scan stromings meting geïntroduceerd. Een tijdsresolutie van 16 ms kan worden verkregen met deze sequentie waardoor er nauwkeurige, snelle stromings metingen mogelijk zijn. De combinatie van de line scan sequentie met verplaatsings imaging levert NMR beelden op die de distributie van stromingssnelheden op één lijn weergeven. Verplaatsingsimaging wordt gedemonstreerd aan de hand van een buis met een glasfilter en een buis gevuld met glaskorrels. Deze resultaten kunnen worden omgezet in quantitatieve gegevens over de optredende stroming.

De diffusie- en stromingsmetingen die in dit proefschrift beschreven worden gebruiken alle pulsed field gradients voor het z.g. coderen van de beweging. Ondanks duidelijke overeenkomsten tussen deze metingen, veroorzaakt de optimalisatie van de NMR sequenties een aanmerkelijk verschil tussen de verschillende NMR sequenties. Door een goede afstemming van de NMR sequenties op de eigenschappen van het object is het mogelijk om verplaatsingen tussen 5 μm en ongeveer 5 cm te meten. Dit brede resolutietraject, en het feit dat ook kleine verschillen in verplaatsingssnelheden kunnen worden opgelost, eventueel gebruik makend van andere NMR karakteristieken, maken NMR een buitengewoon krachtige methode om de water mobiliteit in heterogene systemen te meten.

Curriculum vitae

Dagmar van Dusschoten werd geboren op 24 mei 1967 te Emmen. In 1985 legde hij het eindexamen af aan de GSG te Emmen, waarna hij de studie Moleculaire Wetenschappen begon aan de Landbouw Universiteit Wageningen. Bij de vakgroep Moleculaire Fysica werd een 5-maands afstudeervak voltooid betreffende een NMR studie aan de waterbalans van sporen van de schimmel Aspergilus Nidulans. Een stage bij Philips Medical Systems aangaande NMR metingen van pulsatiele stroming diende als afronding van de studie in 1989. Hierna werkte hij tot in 1994 als aio aan de vakgroep Moleculaire Fysica. Sinds juli 1994 is hij als universitair docent bij de vakgroep Molecularie Fysica bezig met de wetenschappelijke coördinatie van het Wageningen NMR Centrum.